

Theoretical Studies of Properties of Low-Dimensional Systems: Clusters and Conjugated Polymers

Dissertation

zur Erlangung des Grades des Doktors der Naturwissenschaften der
Naturwissenschaftlich-Technischen Fakultät III Chemie, Pharmazie, Bio- und
Werkstoffwissenschaften der Universität des Saarlandes

vorgelegt von

Yi Dong

Saarbrücken, September 2006

DATUM DES KOLLOQUIUMS: 21. DEZEMBER 2006

DEKAN: PROF. DR. KASPAR HEGETSCHWEILER

MITGLIEDER DES PROMOTIONS-AUSSCHUSSES:

PROF. DR. CHRISTIAN HUBER

PROF. DR. VOLKHARD HELMS

PROF. DR.-ING. OLIVER KOHLBACHER

DR. ANDREAS RAMMO

Chapter 1

Abstract

This thesis consists of two parts of which one is dedicated to global structure-optimization of clusters and the other part to conjugated polymers in the presence of an external DC field.

Clusters are intermediates between smaller molecules and extended, macroscopic solid. Often, only for very few cluster sizes the structure is known. However, due to their size and low symmetry it is a far from trivial task to perform a global structure optimization. In the present work, new global optimization methods, i.e., the "Aufbau" and the genetic algorithms have been developed. These structure-optimization methods are combined with density-functional tight-binding calculations for the determination of the total energy for a given structure. The approach is applied to study HAIO, AIO, Au, and Al clusters.

In the study on electronic and structural properties of nanostructured HAIO clusters, we have considered isolated $(\text{HAIO})_n$ clusters, the interactions between two such clusters, and two-dimensional layers of HAIO. In the calculations we used a parameterized density-functional tight-binding method in the calculation of the electronic properties for a given structure, combined with two different unbiased approaches, i.e., a "Aufbau" and a genetic-algorithm method, for optimizing the structure for clusters with n up to 26. The results for the isolated clusters are analyzed by means of similarity, stability, and shape parameters.

The optimized HAIO clusters were found to contain a core of AlO where, moreover, mainly heteroatomic bonds exist. The H atoms are found only on the surface of the core and are only bonded to Al. From additional parameter-free density-functional calculations we could see that there is a strong energetic driving force for creating systems with Al–O bonds and, moreover, the clusters would prefer to have one Al–H bond per unit. The cluster with $n=4$ has a very high symmetry. Moreover, with increasing n the total energy per unit decreases monotonously. The combined clusters $n_1 + n_2$ are slightly more stable than the two isolated clusters of n_1 and n_2 units, but significantly less stable than the optimized $n_1 + n_2$ cluster. We also found that infinite layered HAIO can be stable, in particular for a system consisting of two AlO layers bonded via Al–O bonds and with additional H atoms attached to the Al atoms. It turned out, however, that this system was only marginally more stable than the most stable cluster of our study.

In the study of Au clusters, the geometries and electronic properties of the most stable Au_N clusters with N from 2 up to 58 are presented. An intensive search for low-energy minima of Au_N clusters was carried through using DFTB method combined with genetic algorithms for an unbiased global structure optimization. Various descriptors are used in analysing the results, including stability, shape, and similarity functions, as well as radial distances of the atoms and the orbital energies, all as functions of N . Also dissociation patterns and the symmetry of the clusters are analysed. By comparing with results of jellium calculations, it is demonstrated that for gold clusters, electronic effects are very important, leading to a partly suppression of the occurrence of magic numbers, as well as to low-symmetry and less compact clusters.

This study represents the first such one where also electronic degrees of freedom explicitly are included, which indeed turns out to be important. When including orbital interactions, not only packing but also directional interactions determine the optimal structure and, therefore, in most cases our optimized structures do not have a very high symmetry, i.e., the occurrence of magic numbers becomes much less pronounced. In this respect, gold seems to be special. For other metals, packing effects are often dominating, whereas for covalently bonded elements, the effects due to directional bonds are dominating. We suggest that for gold there is a competition between the two leading to the low-symmetry, although quite compact structures of the Au_N clusters.

Admittedly, by using a parameterized (and not first-principles) method, our results may be connected with some uncertainty. Thus, the fact that we find the transition from planar to three-dimensional structures for a much too small N may be explained from this. On the other hand, low-symmetry structures have been found in other, more accurate studies on selected clusters.

The fact that electronic effects are important was indicated by the results of the calculations for the spherical-jellium model. In particular the stability function from these calculations had a somewhat larger amplitude than was the case for the DFTB results. Once again, the lowering of the symmetry is one reason for this difference. Furthermore, in some cases we could correlate the occurrence of particularly stable clusters with large gaps of the electronic orbitals around the Fermi level.

We observed a number of consequences of the occurrence of structures that are less compact and with low symmetries. Thus, the existence of magic numbers was not particularly pronounced, and for dissociation processes of clusters with more than around 20 atoms it was energetically favored to split off a larger part. Moreover, the structures showed hardly any resemblance with fragments of either crystalline gold or an icosahedron. Nevertheless, the structures did show some regular patterns like the building up of an atomic shells for clusters smaller than around 20 atoms.

In a second part we studied infinite, periodic chains in the presence of an external electrostatic field parallel to the chain direction. We used different approaches. In a first approach we approximated the external potential through a potential with a periodicity of the Born von Kármán zone. This approach was used both for a simple Hückel-like Hamiltonian with one orbital and electron per atom. With this approach the approximations could be studied in some details. The same approach was also used in combination with our own parameter-free density-functional method and applied to conjugated polymers.

However, ultimately we were able to prove that this approach is inaccurate. Approximating the system as being infinite and periodic has consequences for how the dipole moment (or, equivalently, the polarization) shall be defined. Whereas the dipole moment for any finite system, independently of its size, contains only contributions from the static charge distribution,

an additional current contribution has to be included in the case that the system is assumed being infinite and periodic. Since the response of the system to an external electrostatic field is described through the additional term $\vec{P} \cdot \vec{E}$, with \vec{P} and \vec{E} being the polarization and the electric field vector, respectively, our finding made it necessary to modify the approach of how to include electric fields in the calculations.

Chapter 2

Zusammenfassung

Die vorliegende Arbeit gliedert sich in zwei Teile: zum Einen wurde sich mit global strukturoptimierten Cluster befasst, während im zweiten Teil der Einfluss eines externen Potentialfeldes auf konjugierte Polymere untersucht wurde.

Cluster bilden das Verbindungsglied zwischen kleinen Molekülen und makroskopischen Festkörpern. Lediglich für eine unbedeutende Anzahl von ihnen ist überhaupt eine Struktur bekannt. Aufgrund ihrer geringen Größe und niedrigen Symmetrie gestalten sich globale Strukturoptimierungen der Cluster alles andere als trivial. In der vorliegenden Arbeit wurden neue Methoden zur Optimierung entwickelt, wie die "Aufbau" Methode oder der Genetische Algorithmus. Zur Bestimmung der Gesamtenergie einer gegebenen Struktur wurden diese Entwicklungen zusammen mit einer Tight-Bindung-Dichtefunktionaltheorie verwendet. Dies wurde auf HAIO, AlO, Au und Al Cluster angewandt.

Bei den Studien zu den elektronischen und strukturellen Eigenschaften der nanostrukturierten HAIO Cluster wurden isolierte $(\text{HAIO})_n$ Cluster, die Wechselwirkung zwischen zweier solcher Cluster und zwei-dimensionale Schichten von HAIO betrachtet. In den Berechnungen zu den elektronischen Eigenschaften für eine gegebene Struktur wurde eine parametrisierte Tight-binding Dichtefunktionalmethode verwendet, welche mit den zwei unterschiedlichen

vorbedingungsfreien Anwendungen, "Aufbau" Methode und genetischer Algorithmus, kombiniert wurde, um eine Strukturoptimierung von Cluster mit n bis zu 26 durchzuführen. Die Ergebnisse für die isolierten Cluster wurden mit Hilfe der Parameter Ähnlichkeit, Stabilität und Form analysiert.

Die optimierten HAIO Cluster enthalten einen AIO-Kern welcher hauptsächlich heteroatomar gebunden ist. Die Wasserstoffatome wurden ausschließlich an der Kernoberfläche lokalisiert und binden nur an Aluminiumatome. Zusätzliche parameterfreie Dichtefunktionalberechnungen zeigten, dass eine starke energetisch treibende Kraft existiert, die die Bildung von Al-O-Bindungen begünstigt und die Cluster lediglich eine Al-H-Bindung pro Einheit bevorzugen. Für den Cluster mit $n = 4$ wurde eine hohe Symmetrie gefunden. Mit steigendem n nimmt die Gesamtenergie pro Einheit monoton ab. Die kombinierten Cluster $n_1 + n_2$ sind geringfügig stabiler als die isolierten Cluster n_1 und n_2 , aber bedeutend instabiler als der optimierte $n_1 + n_2$ Cluster. Ebenso wurde stabiles unendlich geschichtetes HAIO gefunden, insbesondere für Systeme aus zwei AIO-Schichten, gebunden über Al-O-Bindungen und mit zusätzlichen H-Atomen angelagert an die Al-Atome. Es stellte sich heraus, dass dieser Cluster nur geringfügig instabiler war, als der stabilste Cluster innerhalb dieser Untersuchungen.

Zu den Betrachtungen der Au-Cluster werden die geometrischen und elektronischen Eigenschaften der stabilsten Au_N - Cluster mit N von 2 bis 58 gezeigt. Für die intensive Suche nach Energieminima der Au_N -Cluster wurde die DFTB-Methode mit dem Genetischen Algorithmus kombiniert um eine vorbedingungsfreie globale Strukturoptimierung zu ermöglichen. Die umfangreiche Analyse der Ergebnisse umfasst die Stabilitäts-, Form- und Ähnlichkeitsfunktionen ebenso wie die radialen Atomentfernungen und die Orbitalenergien als Funktionen von N dargestellt. Zusätzlich wurde das Dissoziationsverhalten und die Symmetrie der Cluster untersucht. Im Vergleich zu Jellium-Rechnungen wurde gezeigt, dass für Au-Cluster elektronische Effekte von Bedeutung sind und teilweise das Auftreten der magischen Zahlen unterdrücken, ebenso wie Cluster niedriger Symmetrie und nur gering kompakte Cluster.

Dies sind die ersten Studien, die ebenfalls elektronische Freiheitsgrade berücksichtigen, was sich als wichtig herausgestellt hat. Bei der Beachtung der Orbitalwechselwirkung bestimmen nicht nur die Packung, sondern auch die richtungsbezogenen Wechselwirkungen die

optimale Struktur und daher besitzen in den meisten Fällen unsere optimierten Strukturen keine hohe Symmetrie, wodurch das Auftreten der magischen Zahlen weniger ausgeprägt erscheint. Vor diesem Hintergrund scheint Gold ein Spezialfall zu sein. Bei anderen Metallen spielen die Packungseffekte die bedeutende Rolle, wohingegen für kovalent bindende Elemente die Effekte auf Basis der gerichteten Bindungen dominieren. Wir gehen daher davon aus, dass der Wettstreit zwischen den beiden zuvor beschriebenen Effekten zu der gering symmetrischen, aber dennoch ziemlich kompakten Struktur der Au_N -Cluster führt.

Zugegebenermaßen führt die Verwendung einer parametrisierten (und nicht first-principles) Methode bei unseren Ergebnissen zu einer gewissen Unsicherheit. Damit kann der Umstand, dass wir einen Übergang von einer planaren zu einer drei-dimensionalen Struktur für viel zu kleine N gefunden haben, erklärt werden. Auf der anderen Seite wurden aber gering symmetrische Strukturen in anderen genaueren Untersuchungen zu ausgewählten Clustern gefunden.

Die Tatsache, dass elektronische Effekte eine Rolle spielen, wurde durch die Ergebnisse der sphärischen Jellium-Modell-Rechnungen aufgezeigt. Insbesondere die Stabilitätsfunktion dieser Berechnungen hatte eine größere Amplitude als im Falle der DFTB Ergebnisse. An dieser Stelle sei noch einmal erwähnt, dass die Erniedrigung der Symmetrie hierfür eine Erklärung sein kann. Außerdem korrelieren wir in manchen Fällen das Auftreten teilweise stabiler Cluster mit grossen Lücken der elektronischen Orbitale um das Fermi-Niveau herum.

Wir beobachteten zahlreiche Konsequenzen aus dem Auftreten von Strukturen geringer Kompaktheit und niedriger Symmetrie. Folglich war die Existenz der Magischen Zahlen nicht besonders ausgeprägt und, für die Dissoziation von Clustern mit mehr als 20 Atomen, war es energetisch günstiger, einen großen Teil abzuspalten. Die Strukturen zeigten kaum Ähnlichkeiten mit Fragmenten von kristallinem oder ikosaedrischem Gold. Trotzdem zeigten die Strukturen regelmäßiges Verhalten, wie den Aufbau von atomaren Schalen für Cluster mit weniger als 20 Atomen.

Im zweiten Teil dieser Arbeit wurden unendliche periodische Ketten in einem externen

elektrostatischen Feld, welches sich parallel zur Kette ausbreitet, untersucht. Zur Verwendung kamen verschiedene Modelle. In einem ersten Ansatz wurde das externe Feld mit einem Potential angenähert, welches die Periodizität der Born von Kármán Zone aufweist. Dieser Ansatz wurde für einfache hüchel-ähnliche Hamiltonoperatoren mit einem Orbital und einem Elektron je Atom verwendet. Mit Hilfe dieser Methode konnten die Näherungen in gewissem Umfang durchgeführt werden. Der gleiche Ansatz wurde mit unserer eigenen parameter freien Dichtefunktionalmethode auf konjugierte Polymere angewandt.

Allerdings konnten wir recht schnell zeigen, dass dies der falsche Weg war. Das System als unendlich und periodisch anzunähern hat Auswirkungen auf das Dipolmoment (bzw. die Polarisation). Während für das Dipolmoment für endliche Systeme, unabhängig von ihrer Größe, lediglich Beiträge der statischen Ladungsverteilung zu berücksichtigen sind, muss für unendliche periodische Systeme noch ein Beitrag des Stroms berücksichtigt werden. Da die Antwort des Systems auf ein externes elektrostatisches Feld durch den zusätzlichen Ausdruck $\vec{P} \cdot \vec{E}$, mit \vec{P} und \vec{E} als Polarisations- und elektrischem Feldvektor beschrieben wird, führte unsere Erkenntnis dazu, den Ansatz dahingehend zu ändern, auf welche Art und Weise elektrische Felder in den Berechnungen zu berücksichtigen sind.

Chapter 3

Preface

In this thesis, the results of two separate, independent, fields of work will be presented. The first part is devoted to the development of global structure optimization methods with special application to clusters. The second part describes our study of electronic properties of infinite, periodic, conjugated polymers exposed to external DC fields.

In the first part, two new algorithms, i.e., "aufbau" method and genetic algorithms, have been developed and combined with density-functional tight-binding methods. The new algorithms are unbiased, and a global search of the structure of the lowest total energy can be carried out without making any approximation. In the study, not only the global structures of the clusters are searched unbiasedly, but also the electronic properties of the clusters are included in the calculation, making our studies more detailed than those of most other structure optimization studies. The new algorithms were applied to clusters with three, two, or one types of atoms, for example HAIO, AIO, Au-Cu, Cu-Ni, Al, Au, and Na clusters. The results show that the new unbiased global optimization methods are reliable, and that they are good tools to study the electronic and structural properties of the clusters

In the second part, different theoretical methods for treating external DC fields for infinite polymers are compared. Both results of model calculations and those of ab initio, density-functional calculations are reported.

The thesis consists of an introductory part, describing the background to the studies, followed by publications that have been either published or submitted for publication in international scientific journals. The articles, included in this thesis, are:

1. Y. Dong and M. Springborg: "Infinite Polymers and Electrostatic Fields", *Synth. Met.* **135-136** (2003) 349-350.
2. M. Springborg, B. Kirtman, and Y. Dong: "Electronic polarization in quasilinear chains", *Chem. Phys. Lett.* **396** (2004) 404-409.
3. M. Springborg, Y. Dong: "Conjugated Polymers in External DC Fields" in *Advances in Quantum Chemistry*, **47** (2004) 369-392.
4. Y. Dong and M. Springborg: "Theoretical study of nanostructured HAIO" in *Advances in Science and Technology*, **44** (2004) 167-174.
5. Y. Dong, M. Springborg, M. Burkhart and M. Veith: "Structural and electronic properties of nanostructured HAIO and AIO", *Advances in Computational Methods in Science and Engineering* **4A** (2005) 1010-1013.
6. Y. Dong, M. Burkhart, M. Veith and M. Springborg: "Structural and electronic properties of nanostructured HAIO", *J. Phys. Chem. B* **109** (2005) 22820-22829.
7. Y. Dong and M. Springborg: "Properties of Au_N clusters", submitted for publication.
8. Y. Dong and M. Springborg: "Global structure optimization study on Au_{2-20} Clusters", submitted for publication.
9. Y. Dong and M. Springborg: "Unbiased determination of structural and electronic properties of gold clusters with up to 58 atoms", submitted for publication.

The first three articles contain the study of electronic properties of infinite, periodic, conjugated polymers exposed to external DC fields. The articles from 4 to 9 contain studies on global structure optimization methods with application to HAIO, AIO and Au clusters. Article 4, article 5 and article 6 are the study on HAIO and AIO clusters, article 7 to 9 devoted to Au clusters study, which have been submitted to the publication. For

all articles, they were written as a collaboration among all involved scientists. In articles 1-3, the density functional code had been developed by others, whereas I applied it to the problems of interest. I developed the Hückel method and accompanying program myself and applied it too. For article 2, I carried through some of the calculations. For articles 4-6, I developed the methods and applied them. All calculations and a major part of the analysis of the results were my work, the only exception is the DFT calculation by Markus Burkhardt on the clusters with n from 2 to 6 units. All the calculations, all the program development and major of the analysis of the results for articles 7-9 are my work,

Chapter 4

Acknowledgements

This work has been completed under supervision of Prof. Dr. Michael Springborg at the Physical and Theoretical Chemistry, University of Saarland.

My special thanks to Prof. Dr. Michael Springborg.

My thanks go to

Mr. Michael Bauer for all the helps, Dr. Sudip Roy, and Dr. Jan-ole Joswig for fruitful discussions.

Ms. violina Tevekeliyska and Ingolf Warnke for nice cooperation.

Mrs. Ingelore Weidenfeld for her general help.

Mrs. Sylvia Kuhn for her extraordinary help during my foreign life.

My group members.

All my relatives for all the supports.

Contents

1	Abstract	i
2	Zusammenfassung	v
3	Preface	ix
4	Acknowledgements	xiii
5	Clusters	1
5.1	Random Number Generator	4
5.2	Aufbau method	5
5.3	Genetic Algorithms	5
5.4	Message-Passing Interface (MPI)	10
5.5	Density Functional Tight-Binding Method	10
6	Conjugated Polymers in External DC Fields	15

6.1	A simple Hückel-like model	18
6.2	LMTOs	20
6.3	The Breakdown of the Approach	22
7	List of Talks	27
8	List of Publications	29

Chapter 5

Clusters

It is well known that materials properties depend sensitively on their structure and composition, and actually the development of our society is to a large extent a consequence of our capability to exploit this fact, although precise prediction of the materials properties for a given system not yet has become possible. During the last quarter of a century another approach for controlling and varying materials properties has been intensively studied and partly also exploited in practical applications. Thus, when the materials dimensions are reduced to the nm range, their properties change markedly from those of their macroscopic counterparts.

One class of such systems is provided by clusters that typically contain between some 10s and some 100 000s of atoms, and most often only a few type of atoms (with, however, the possible exception of surfactants that saturate dangling bonds on the surface of the clusters). Quantum-size effects combined with the fact that the number of surface atoms relative to the total number of atoms is far from vanishing may be held responsible for the unique, size-dependent properties of those materials and they have, accordingly, been the subject of many experimental and theoretical studies (see, e.g., [1]). The precise determination of the relation between size and property is, however, not easy for clusters. In experimental studies the clusters are rarely isolated, but instead they often interact with some other medium like a solvent or a supporting surface, possess surfactants, or their precise size is only approximately known. On

the other hand, theoretical studies most often deal with isolated clusters of a well-defined size and often without ligands for which it is overwhelmingly complicated to determine the structure. Without any further information the identification of the structure of the lowest total energy for a cluster of N atoms requires searching in a geometry space of $3N - 6$ dimensions, which for any but the smallest values of N hardly is possible.

Since most of the structures of the clusters are unknown. Determination of the geometric ground state of the clusters is the work that faces to scientists. But, global structure optimization is very difficult, this is because of the omnipresence of local minima, and the number of which tends to increase exponentially with the size of the problem. For example, there are at least 1506 distinct local minima for the 13-atom Lennard-Jones clusters and good reasons to expect roughly as many local minima for more realistic potentials modeling various elements. The number of minima of n atom clusters of most elements should be in the thousands for $n = 13-15$ and probably on the order of $10^4 - 10^6$ for $15 \leq n \leq 25$. On the other hand, the computer cost of reliable relaxation for the individual optimization is also other problem. Global optimization is a hard task because it has two contradictory requirements: the search has to explore the entire space of potential surface so that the searching will not miss the lowest total energy minimum, and simultaneously every individual relaxation has been done enough.

Numerous approaches to solving the global optimization problem have been suggested, among them, Simulated Annealing (SA), Basin - Hopping(BH), Genetic Algorithms (GA) are the most often used methods, there are also other methods: minima hopping [2, 3], and multi-canonical algorithms [4], conformational space annealing (CSA) [5] *et al.* [9, 10, 11]. Detailed comparisons of different approaches are rare. Wales and Scheraga [6] reported global optimization of clusters, crystals, and biomolecules by basin hopping method. Simulated annealing [26] probably provided the first generally applicable technique for global optimization, in this approach the state of the system is followed by simulation as the temperature is decreased slowly from a high value, in the hope that it will eventually come to rest at the global potential energy minimum. Simulated annealing has several merits: (1) it does not get suck in local minima as do classical gradient searches; (2) it is derivative-free, trivial to program (and maintain), and can be easily applied to a wide class of optimization problems. The technique has been shown in a variety of applications [7, 8]. Another global optimization method is Basin - Hop-

ping, in essence the BH method is Monte Carlo minimization, which removes relatively low barriers separating local minima of the potential energy hypersurface and thus effectively converts portions of the potential energy surface into a multidimensional staircase, each accepted Monte Carlo move is associated with an energy minimization[12, 13]. With the exception of GA, most standard algorithms are based on thermodynamic principles. At sufficiently low temperature the ground state configuration will be the dominant configuration and hence the search is solved in principle. Unfortunately thermodynamics does not tell us anything about how fast the thermodynamic equilibrium distribution is obtained and as a matter of fact it can be extremely slow. Consequently, global optimization strategies based on thermodynamic may be of questionable value.

On top of the global optimization methods, one may add extra features in order to speed up the calculation, like the taboo search [21, 22]. The basic idea of the taboo search is quite simple: avoid trying the same solution more than once. The problem of repeated visits of certain configurations has already been recognized by many researchers. one remedy that was proposed is flooding [24], and other is history operators [25] by defining an order parameter, and building the history path in the space of the parameter itself, or in the cluster configuration space [23].

It is the purpose of the present work to develop, and subsequently apply, new global optimization methods. Initial structures will be generated using random-number generators, but since a search based purely on random numbers will converge extremely slowly (essentially, approaching the lowest total energy as $M^{-1/3}$, where M is the number of structures that have been studied), we combine this initial guess with more intelligent structure-optimization methods. are developed in this work by using random operator, aufbau methods and genetic algorithms.

It turned out that the most effective approach was obtained by combining genetic operators with density-functional tight binding methods. Before discussing these methods in detail, we emphasize the following aspects about clusters.

First, small atomic clusters (roughly $n \leq 100$) are different from bulk and show specific size effects. These properties can be very sensitive to structure, but little is known about the

structure of small clusters apart from a few very small clusters ($n \leq 10$). Second the lowest-energy structures are usually the most abundant in experiments on clusters, and the number of the distinct minima on the potential-energy surface of clusters grows exponentially with the size of the clusters, so mathematically the calculations are costly. Third, also the single total-energy evaluation for one structure grows rapidly with systems size.

5.1 Random Number Generator

It may seem perverse to use a computer to produce "random" number since any program, after all, will produce output that is entirely predictable, hence not truly "random". The meaning randomness is to generate a diversity of numbers that satisfy the programmer. In other words, any two different random number generators ought to produce statistically the same results when coupled to your particular applications program. A pragmatic point of view, then is that randomness is in the eye of the programmer. Uniform deviates are just random numbers that lie within a specified range (typically 0 to 1). Other sorts of deviates are almost always generated by performing appropriated operations on one or more uniform deviates. We are dealing with structure optimization problem, in other words, we want to have very many different initial structures that we hope that they could cover entire space and later leading to relaxed structures, so we need the random generator that generates as many divities as possible. One of system-supplied random number generators is called a "random number generator," named like "ran," and a calling sequence like `x=ran(iseed)`. You initialize `iseed` to a arbitrary value before the first call to run. Each initializing value will typically return a different subsequent random sequence, or at least a different subsequence of some one enormously long sequence. The same initializing value of `iseed` will always return to the same random sequence. The system-supplied random number generator `ran(iseed)` can supply random number from 0 to 1, and since the same initializing value of `iseed` can always give the same random sequences, there is one advantage that we can trace back to the structures that were generated.

In the present work we shall use random numbers to generate initial structures that subsequently will be improved by using one of the two methods below.

5.2 Aufbau method

Once we have chosen the method for calculating the total energy for a given structure (in our work it is the density-functional tight-binding method that will be described below), the next question is how do we perform a structure optimization, particularly when we do have little information about the systems that we are about to study, which is the case for HAIO clusters, AlO clusters, Au clusters, and Al clusters. "Aufbau" method was also developed to study HAIO, AlO, Au and Al clusters. In the present work the "Aufbau" method was mainly used to study HAIO clusters and, therefore, we shall describe the method only for this system. For the HAIO clusters it was important that it was known from experiment that the clusters are stoichiometric, i.e., are of the form $(\text{HAIO})_n$. We start out optimizing the structure of a single HAIO molecule (i.e., $n=1$) by choosing the structure of the lowest total energy from a very large number of calculations on randomly constructed structures that were allowed to relax to their closest total-energy minimum. Subsequently, we only assume that the structure of the cluster with $n+1$ units can be obtained by randomly adding one Al, one O, and one H atom to the cluster with n units. Thus, out of very many calculations where we randomly add those three atoms to the optimized structure of the cluster with n units (imposing only the constraints that the extra atoms should not be too close to any other atom or too far from all the other ones, and subsequently allowed to relax) we obtain an optimized structure of the system with $n+1$ units. The resulting cluster of such calculation is not with absolute certainty that of the global total-energy minimum, but, hopefully, a very good approximation to it.

5.3 Genetic Algorithms

Calculations on $(\text{HAIO})_n$ clusters showed that although the "Aufbau" method is efficient, even more efficient were methods based on genetic algorithms. Therefore, in further studies we shifted to these methods that shall be described here.

Physics, chemistry, biology or economy often have to deal with the classical problem of optimization, Generally speaking, a large part of mathematical development dealt with that

topic. Purely analytical methods widely proved their efficiency, they nevertheless suffer from an insurmountable weakness. Other methods, combining mathematical analysis and random search have appeared, but although these methods are very efficient, there is no proof that the optimum will be found.

Genetic algorithms inspired by Darwinian evolution process were formally introduced in the United States in the 1970s by John Holland at University of Michigan. His achievements were presented in the publication of 'Adaptation in Natural and Artificial System' in 1975. Holland had a double aim: to improve the understanding of natural adaption process, and to design artificial systems having properties similar to natural systems[58, 59].

The continuing price/performance improvements of computational systems has made genetic algorithms attractive for some types of optimization. In particular, genetic algorithms work very well on mixed (continuous and discrete), combinatorial problems. They are less susceptible to getting 'stuck' at local optima than gradient search methods. But they tend to be computationally expensive. To use a genetic algorithm, you must represent a solution to your problem as a *genome* (or *chromosome*). The genetic algorithm then creates a population of solutions and applies genetic operators such as mutation and crossover to evolve the solutions in order to find the best one(s).

Under these conditions, genetic algorithms are increasingly being used in a number of global optimization problems in chemistry ranging from crystal structure prediction and protein folding in biomolecules to parameter development for empirical and semi-empirical quantum mechanical calculation. And when used to study atomic clusters, they are called Cluster Genetic Algorithms (CGA). The cluster genetic algorithm works by randomly selecting and mating the more fit individuals in a generation to produce the next generation of offsprings, where the fitness is some measure of the energetic stability for an individual cluster structure. The global minimum is eventually located because some of the new cluster conformations created by the genetic algorithm have lower energies than the structures in previous generations. A good mating operator causes good structural features in a cluster to be passed to next generation while maintaining structural diversity in the overall population.

Until to now, different genetic operators have been used to optimize the structure of clus-

ters. Deaven and Ho [14, 15, 16] first proposed that the most important mating operator is the cut-and-paste method in a GA for global optimization of atomic clusters. Wolf and Landman [17] used the add/etch operations in their global optimization studies of large Lennard-Jones cluster. Ge and Head [18, 19] used four mating methods to study Si passivated by H atoms: one is to take the arithmetic mean of the cartesian coordinates from two parent geometries. The second method is to take a fragment of Si atoms from one parent and replace it with the fragment of the other parent with the same number of atoms, and also cut a fragment of H atoms in one parent and replace it with a fragment of H atoms in the other parent with the same number of atoms. The third method is to cut each parent into halves and then recombine one half from each parent to generate the offsprings. and the fourth method is to use basic CGA as the above-mentioned three methods, but by modifying the genetic operators which produce new offsprings from the parent clusters. Joswig and Springborg [20] used a parent-children, cutting and mating method to study Al clusters.

Global optimization faces two contradictory requirements: i) the search has to explore the entire space in order to not miss the global minimum, ii) a local relaxation shall be sufficiently accurate in order to provide an accurate total energy for that initial structure. Furthermore, one has to remember, that there is no guarantee that any method will identify the structure of the global total-energy minimum. In order to arrive at a sufficiently efficient method, we developed our own versions of genetic operators to search for the global-energy-minimum for different sizes of clusters.

- A) Operator 1: Suppose that we have optimized the structure of the cluster with n units. From this structure we construct a first generation consisting of M independent clusters for the $(n + 1)$ -unit system by randomly adding one unit (or atom) and letting these structures relax to their nearest total-energy minima. Subsequently, a new set of clusters is constructed by cutting each of the original ones randomly into two parts that are interchanged (under the constraints mentioned above) and, afterwards, allowed to relax. Out of the total set of $2M$ structures, the M ones of the lowest total energy are kept as the next generation. This procedure is repeated until the lowest total energy is unchanged for a large number of generations.

- B) Operator 2: Based on the "Aufbau" method and GA method, operator 2 was developed by combining the two methods together. First the "Aufbau" method is applied to generate many initial configurations (for example 200). Then from the 200 relaxed structures, seeds are selected as the initial structures for GA operator 1. Afterwards, GA operator 1 is used to carry out structure optimization.
- C) Operator 3: As we mentioned above that the computing cost for one energy evaluation is extremely large compared to that of all other operations in global optimization, i.e., the generation of random numbers, the generation of initial structures, the cutting and interchanging the structures, and the sorting and selection of clusters for the next generation.... In order to make the global optimization realistic, there are two things that we can do to reduce the computing time. One is to reduce the time of the local optimization, another is to reduce the number of the initial structures that later will be relaxed. Local optimization is relatively simple and there are many good algorithms. Here we used methods based on the energy gradients. In the optimization, the energy gradients are used to update the geometry. Another way of reducing the time of optimization is to reduce the number of generations. As we mentioned above a single energy evaluation is extremely costly, so compared with the first factor to reduce the computation time, the second factor is of paramount importance. In the first operator 1, after cutting the optimized structures, we form new clusters by pasting the halves. However, it is possible that the new clusters are similar to the clusters that we have studied before. Therefore, in order to make sure that the clusters of the next generation are different from the ones of the present generation, we compare the structures directly. If the two structures are found to be similar, the structure of the new generation is discarded and a new structure constructed.

In order to quantify similarity between two structures we proceed as follows. For each structure we consider either the radial distances of the interatomic distances. E.g., for a $(\text{HAIO})_n$ cluster, the radial distance for each of the $3n$ atoms is

$$r_i = |\vec{R}_i - \vec{R}_0| \quad (5.1)$$

SYSTEM	Δ_{str}	ΔE
SO1 – SM1	0.759	0.1971
SO1 – SM2	3.333	0.08588
SO2 – SM2	3.3726	0.084146
SM1 – SM2	3.6051	0.1112
SM1 – SO2	1.4262	0.19535

which \vec{R}_0 is the center of the cluster,

$$\vec{R}_0 = \frac{1}{3n} \sum_{i=1}^{3n} \vec{R}_i, \quad (5.2)$$

defined from the positions \vec{R}_i of the atoms.

Two structures of the same number of atoms are then compared by sorting these radial distances for each structure, separately, and subsequently calculate

$$\Delta_{\vec{r}} = \left(\frac{1}{3n} \sum_{i=1}^{3n} (r_i^1 - r_i^2)^2 \right)^{\frac{1}{2}}. \quad (5.3)$$

Alternatively, the sorted interatomic distances, $\{d_i\}$, can be used in defining a structural difference

$$\Delta_d = \left(\frac{2}{3n(3n-1)} \sum_{i=1}^{\frac{3n(3n-1)}{2}} (d_i^1 - d_i^2)^2 \right)^{\frac{1}{2}} \quad (5.4)$$

Finally, the upper indices "1" and "2" refer to the two different structures.

Using these concepts we can actually illustrate the problem of identifying the structure of the global total-energy minimum. Thus, in Table I we show the total-energy difference between some different structures together with their structural difference as defined above. SO1, SO2 are old structures, whereas SM1, SM2 are new structures obtained in a next generation. The table shows clearly that different structures may have comparable total energies, whereas similar structures may have quite different total energies, i.e., the total energy is indeed a complicated function of structure.

In particular the genetic algorithms are based on studying several structures in parallel (i.e., all the members of a generation). This suggests that the calculations with advantage can

be carried through using several CPUs in parallel. As a part of this present work we therefore implemented the possibility of performing parallel computing, although it ultimately was not used.

5.4 Message-Passing Interface (MPI)

MPI makes it possible to perform parallel computations. For either "aufbau" or genetic algorithms methods that we have described above, the program handles more than one clusters at the same time. This makes it possible to use MPI assuming that a cluster of computers that can handle this is available. MPI (message-passing interface) was defined in 1994 by a broadly-based group of parallel computer vendors, computer scientists, and applications developers after 2 years of intensive process. MPI is not a new computer language, but is instead a library. According to the number of instruction and data, one may use either SIMD (Single-Instruction Multiple-Data) or MIMD (Multiple-Instruction Multiple-Data). Yet another possibility is SPMD (Single-program Multiple-Data) and MPMD (multiple-Program Multiple-Data).

5.5 Density Functional Tight-Binding Method

In the sections above, we have discussed in some detail the problem of minimizing the total energy as a function of structure, without, however, discussing how the total energy is being calculated. In the present work we used a parameterized density-functional tight-binding method that now shall be described.

The tight-binding method lies between very accurate, very expensive, *ab initio* methods and the fast, but less accurate, empirical methods. When compared with *ab initio* methods, a tight-binding method is typically two to three orders of magnitude faster, but suffers from a reduction in transferability due to the approximations made; when compared with empirical methods, the tight-binding method is two to three orders of magnitude slower, but the quantum mechanical nature of bonding is retained, ensuring that the angular nature of bonding is

correctly described far from equilibrium structures. Tight-Binding is therefore useful for the large number of situations in which quantum-mechanical effects are significant and unknown for systems like cluster, but for which the system size makes *ab initio* calculations impractical.

The calculations of the electronic properties for a given structure were performed using the parameterized density functional tight-binding (DFTB) method of Seifert *et al.* [27, 28, 29].

According to this method, the single-particle eigenfunctions $\Psi_i(\mathbf{r})$ to the Kohn-Sham equations are expanded in a set of atomic-like basis functions ϕ_m :

$$\Psi_i(\mathbf{r}) = \sum_m c_{im} \phi_m(\mathbf{r}) \quad (5.5)$$

Here, m is a compound index that describes the atom at which the function is centered, the angular dependence of the function, as well as its radial dependence. These functions are obtained from self-consistent density functional calculations on the isolated atoms employing a large set of Slater-type basis functions.

The Hamiltonian is defined as

$$\hat{h} = \hat{t} + V_{eff}(\mathbf{r}) \quad (5.6)$$

Here, \hat{t} is the kinetic-energy operator, and the effective Kohn-Sham potential $V_{eff}(\mathbf{r})$ is approximated as a simple superposition of the potentials of the neutral atoms:

$$V_{eff}(\mathbf{r}) = \sum_j V_j^0(|\mathbf{r} - \mathbf{R}_j|) \quad (5.7)$$

Furthermore, we make use of a tight-binding approximation, so that

$$h_{mn} = \langle \phi_m | \hat{t} + \sum_j V_j^0 | \phi_n \rangle = \langle \phi_m | \hat{t} + V_{j_m}^0 + (1 - \delta_{j_n, j_m}) V_{j_n}^0 | \phi_n \rangle \quad (5.8)$$

where \mathbf{R}_{j_m} and \mathbf{R}_{j_n} are the positions of the atoms at which the m th and n th basis functions are centered, respectively. The Kronecker- δ is included in order to assure that the potential is not double counted for $j_n = j_m$. Through this approximation, only two center terms in the Hamiltonian matrix are considered, but all two-center terms ($h_{mn} = \langle \phi_m | \hat{h} | \phi_n \rangle$, $S_{mn} = \langle \phi_m | \phi_n \rangle$) are calculated exactly within the Kohn-Sham basis. These approximations lead to the secular equation

$$\sum_m c_{nm} (h_{mn} - \epsilon_n S_{mn}) = 0. \quad (5.9)$$

Using the Kohn-Sham eigenvalues ϵ_i , the total energy $E[\rho(\mathbf{r})]$ may be written as

$$E[\rho(\mathbf{r})] = \sum_i^{occ} \epsilon_i - \frac{1}{2} \left[\int V_{eff}(\mathbf{r})\rho(\mathbf{r})d\mathbf{r} - \int V_{ext}(\mathbf{r})\rho(\mathbf{r})d\mathbf{r} \right] + E_{XC} - \frac{1}{2} \int V_{XC}(\mathbf{r})\rho(\mathbf{r})d\mathbf{r} + E_N. \quad (5.10)$$

The external potential V_{ext} is the electrostatic potential from the nuclei, E_{XC} is the exchange-correlation energy, V_{XC} the corresponding potential and E_N the nuclear repulsion energy. Since the difference between superposed atomic electron densities and the true electron density of the system of interest is only small and since by far the largest parts of the interatomic interactions are of fairly short range, the major part of the total energy is contained in the difference of the single particle energies of the system of interest, $\{\epsilon_i\}$, and of the isolated atoms, $\{\epsilon_{jm}\}$ (ϵ_{jm} is the j th eigenvalue of the m th atom), i.e.,

$$\epsilon_B = \sum_i^{occ} \epsilon_i - \sum_j \sum_m \epsilon_{jm} \quad (5.11)$$

The short-ranged interactions can be approximated by simple pair-potentials, so that the expression for total energy becomes

$$E_B \approx \sum_i^{occ} \epsilon_i - \sum_j \sum_m \epsilon_{jm} + \frac{1}{2} \sum_{j \neq j'} U_{jj'}(|\mathbf{R}_j - \mathbf{R}_{j'}|) \quad (5.12)$$

$U_{jj'}(|\mathbf{R}_j - \mathbf{R}_{j'}|)$ is determined as the difference of ϵ_B and ϵ_B^{SCF} for diatomic molecules (with E_B^{SCF} being the total energy from exact density-functional calculations). Finally we will consider only valence electrons for our calculation, whereas the others will be treated as frozen-core.

With these approximations all relevant information on the above-mentioned matrix elements can be extracted from calculations on isolated two-atomic systems, in our cases on these two-atomic systems shown in the table.

The local total-energy minimization is performed by using the forces. Here, the force \mathbf{F}_j that acts on the j -th atom of the system of interest can be calculated using the Hellmann-Feynman theorem.

$$\mathbf{F}_j = -\frac{\partial E}{\partial \mathbf{R}_j} \quad (5.13)$$

Compound	Diatomics	Valence Electrons
<i>HAlO</i>	<i>Al₂, O₂, H₂, AlO, OAl, OH, HO, AlH, HAl</i>	<i>Al : 3s, 3p; O : 2p; H : 1s</i>
<i>AlO</i>	<i>Al₂, O₂, AlO, OAl</i>	<i>Al : 3s, 3p; O : 2p</i>
<i>Al</i>	<i>Al₂</i>	<i>Al : 3s, 3p</i>
<i>Au</i>	<i>Au₂</i>	<i>Au : 5d, 6s</i>

The forces can be split up into two parts, one acting on the electrons only (\mathbf{F}_j^e), the another one acting exclusively on the nuclei (\mathbf{F}_j^N),

$$\mathbf{F}_j = \mathbf{F}_j^e + \mathbf{F}_j^N \quad (5.14)$$

The nuclear part consists of the sum of the derivatives of the repulsive energies of the nuclei,

$$\mathbf{F}_j^N = \sum_{j \neq j'} \frac{\partial}{\partial \mathbf{R}_j} \left(\frac{Z_j Z_{j'}}{|\mathbf{R}_j - \mathbf{R}_{j'}|} \right) \quad (5.15)$$

whereas the electronic part can be written as the sum of the orbital contributions,

$$\mathbf{F}_j^e = \sum_i n_i \mathbf{F}_{ji} = - \frac{\partial}{\partial \mathbf{R}_j} \left(\sum_i n_i \langle \phi_i | \hat{h} | \phi_i \rangle \right) \quad (5.16)$$

Here, n_i is the occupation number of the i -th orbital (either being $n_i=0$, or $n_i=1$), and as a consequence we sum only over the occupied orbitals ($n_i=1, i=1, \dots, \text{occ}$). \mathbf{F}_{ji} can be written as

$$\mathbf{F}_{ji} = \sum_{m,n} c_{im} c_{in} \left(- \frac{\partial H_{mn}}{\partial \mathbf{R}_j} + \epsilon_i \frac{\partial S_{mn}}{\partial \mathbf{R}_j} + \frac{\partial V_{mn}^{ee}}{\partial \mathbf{R}_j} \right) \quad (5.17)$$

V_{mn}^{ee} are the matrix elements of the electron-electron potential ($V^{ee} = V_H + V_{xc}$). The component of the potential is compensated by the nuclear part \mathbf{F}_j^N ,

$$\mathbf{F}_j^N \approx \sum_{m,n} c_{im} c_{in} \frac{\partial V_{mn}^{ee}}{\partial \mathbf{R}_j} \quad (5.18)$$

These two terms are approximated by the repulsive term $U(R)$,

$$U(R) = \begin{cases} \sum_n a_n (R - R_1)^n & \text{for } R < R_1 \\ 0 & \text{for } R \geq R_1 \end{cases} \quad (5.19)$$

The forces that are acting on an atom positioned at \mathbf{R}_j can finally be calculated as,

$$\mathbf{F}_j = -\nabla_j E_{tot} = \sum_i \sum_{m,n}^{occ} \left(- \frac{\partial H_{mn}}{\partial \mathbf{R}_j} + \epsilon_i \frac{\partial S_{mn}}{\partial \mathbf{R}_j} \right) + \frac{1}{2} \sum_{j \neq j'} \frac{\partial}{\partial \mathbf{R}_j} U(|\mathbf{R}_j - \mathbf{R}_{j'}|). \quad (5.20)$$

Chapter 6

Conjugated Polymers in External DC Fields

Conjugated polymers have been at the focus of a large research activity over more than a quarter of century (see, e.g., [33, 34, 35, 36]). Compared with more traditional plastics, the conjugated polymers contain a backbone with sp^2 - and sp -bonded (and not sp^3 -bonded) carbon atoms. The last valence electron(s) per carbon atom occupy p orbitals and participate in π bonds between the carbon atoms. This has two consequences: the polymers are essentially planar, and the energy gap between occupied and unoccupied orbitals is small (i.e., corresponds to that of conventional semiconductors) with π orbitals appearing closest to the Fermi level.

There is a strong coupling between electrons and phonons (structure) which leads to a lowest-energy structure with alternating C–C bond lengths and to the occurrence of structural defects (i.e., solitons and polarons) when the chains are charged. Both finite oligomers and essentially infinite polymers can be synthesized, and a special class of oligomers is the finite, so-called push-pull systems where the two end-groups are different, so that an excitation involves an internal charge transfer from one end to the other.

Due to the combination of mechanical properties as plastics and electronic properties as

crystalline semiconductors, these materials are been considered interesting for many special-purpose applications, including light-emitting diodes, transistors, and sensors. For the present purpose it is, however, most important to observe that the π electrons that are somewhat loosely bound to the backbone, but not so loosely bound that they are free-electron-like, give rise to very large linear and, in particular, non-linear responses to external electric fields. The responses can be quantified through the polarizabilities (α) and hyperpolarizabilities (β, γ, \dots) by expanding either the dipole moment

$$\mu_i = \mu_i^{(0)} + \sum_{j=x,y,z} \alpha_{ij} E_j + \sum_{j,k=x,y,z} \beta_{ijk} E_j E_k + \sum_{j,k,l=x,y,z} \gamma_{ijkl} E_j E_k E_l + \dots \quad (6.1)$$

or the total energy

$$\begin{aligned} E_{\text{tot}} = E_{\text{tot}}^{(0)} - \sum_{i=x,y,z} \mu_i^{(0)} E_i - \frac{1}{2} \sum_{i,j=x,y,z} \alpha_{ij} E_i E_j - \frac{1}{3} \sum_{i,j,k=x,y,z} \beta_{ijk} E_i E_j E_k \\ - \frac{1}{4} \sum_{i,j,k,l=x,y,z} \gamma_{ijkl} E_i E_j E_k E_l + \dots \end{aligned} \quad (6.2)$$

in the electric-field components. When AC fields are applied, the (hyper)polarizabilities become frequency dependent,

$$p_{i,j,k,\dots,m}(\omega_i, \omega_j, \omega_k, \dots, \omega_m) \quad \text{with } \omega_i = |\omega_j \pm \omega_k \pm \dots \pm \omega_m| \quad (6.3)$$

with p being $\alpha, \beta, \gamma, \dots$. Non-zero values of β and γ lead to effects like second- and third-harmonic generation, four-wave mixing, electric-field-induced second harmonic, the Kerr effects, and the Pockels effect, which are interesting both for basic and for applied science. Accordingly, much effort is put into obtaining maximally large values of these parameters.

In the thermodynamic limit any property Z for a finite system A-(X) $_n$ -D will be either independent of or proportional to n . Experimental [37] and theoretical [38, 39, 40, 41, 42] studies have, however, shown that when Z is the polarizability α or the hyperpolarizability γ , $Z(n)/n$ [or $Z(n) - Z(n-1)$] converges only very slowly as a function of n towards the large- n limit and, moreover, the convergence for γ is slower than that for α [39]. On the other hand, since the larger systems tend to have larger values of $Z(n)/n$ than the smaller ones, it is highly relevant to consider the large systems. Thus, considering infinite, periodic systems is a useful alternative.

For finite oligomers of polyacetylene it has been found [41] that the vibrational contribution to the total polarizability amounts to roughly 10% of the total polarizability, and, although it is known that this percentage will increase for the hyperpolarizabilities, we shall here concentrate on the electronic part of the responses.

Most often, (hyper)polarizabilities of polymers are calculated using a perturbation-theoretical approach based on the formalism of Genkin and Mednis [43]. Thereby, both occupied and unoccupied orbitals have to be included in the calculation and the fact that different electronic-structure methods (most notably, Hartree-Fock- and density-functional-based methods) often yield fairly inaccurate results for the unoccupied orbitals may be the reason for the fact that the calculated (hyper)polarizabilities often depend strongly on the method (see, e.g., [42, 44]). Thus, in order to access the accuracy of the different methods or, alternatively, to avoid the problems related to the accuracy of the unoccupied orbitals, one may include a DC field directly in the calculations whereby at least the static (hyper)polarizabilities can be calculated.

However, the inclusion of a static field is a non-trivial endeavor. First, even for the smallest possible system (e.g., an isolated hydrogen atom) and for the smallest possible external field, the eigenvalue spectrum changes dramatically: there is no bound states, and states that in the field-free case were bound change into resonances. And for an infinite system parts of the system will be exposed to a divergent field. On the other hand, for crystalline systems it has been found [45] that the polarization is a bulk property, i.e., is accessible by considering a single unit cell. This can, e.g., be done through the Berry-phase formulation of polarization (see, e.g., [46]). Moreover, finite-chain calculations have indicated [47, 48] that the electron distribution for a chain exposed to a DC field is roughly periodic far away from the boundaries, suggesting that a periodic-chain treatment should be possible.

We finally mention that one further reason for studying infinite, periodic polymers in external DC fields is the findings [48, 49, 50] that currently applied approximate density-functionals (like the one we are using) may be inadequate when calculating responses to external DC fields. Thus, studies like the ones of this contribution may provide further insight into the failures of the functionals. On the other hand, we stress that our basic method is, in principle,

not dependent on these problems and can be modified easily according to new proposals for approximate density functionals.

6.1 A simple Hückel-like model

In order to analyse the problems of treating an infinite, periodic system in an external field, it turned out to be useful to first consider a simpler model system for which many and detailed calculations could be carried through. Ultimately, the results of this analysis gave information on problems related with our initial approach.

The models that we consider are all related to a simple Hückel-like model. As a prototype we consider the Hamiltonian

$$\hat{H} = \hat{H}_{\text{tb}} + \hat{H}_{\text{ext}} \quad (6.4)$$

where the last term is caused by the external field, described within the electric-dipole approximation.

The tight-binding part is given by

$$\hat{H}_{\text{tb}} = \sum_i \alpha_i \hat{c}_i^\dagger \hat{c}_i + \sum_i \beta_i (\hat{c}_{i+1}^\dagger \hat{c}_i + \hat{c}_i^\dagger \hat{c}_{i+1}). \quad (6.5)$$

Here, we have assumed that we have one orbital per site (labeled χ_i with i being the site) and that \hat{c}_i and \hat{c}_i^\dagger are the corresponding annihilation and creation operators. Moreover,

$$\langle \chi_j | \hat{H}_{\text{tb}} | \chi_k \rangle = \begin{cases} \alpha_j & \text{for } j = k \\ \beta_j & \text{for } k = j + 1 \\ \beta_k & \text{for } k = j - 1 \\ 0 & \text{otherwise.} \end{cases} \quad (6.6)$$

We will assume that the external field only affects the diagonal elements,

$$\hat{H}_{\text{ext}} = \sum_i E_i \hat{c}_i^\dagger \hat{c}_i. \quad (6.7)$$

We will assume that the system has one electron per site, that the on-site energies α_i are site-independent (and accordingly can be set equal to 0), and that β_i alternates between $t_- = 0.5$

and $t_+ = 1.5$. For an infinite periodic chain without the external field we will accordingly have an occupied band between -2 and -1 , a gap between -1 and $+1$, and an unoccupied band between $+1$ and $+2$. These numbers can be used in estimating the strength of a field above which the calculations become meaningless. Considering a finite system with N sites and letting $E_i = Eia/2$, the N th atom experiences a potential of roughly $NEa/2$ higher than the 1st atom does. If this value is larger than the gap, electrons will start flowing from one end of the system to the other. In order to avoid this run-away solution, we must require $E < 4|t_+ - t_-|/(aN)$. Therefore, we have chosen the fairly large value of the hopping-integral alternation. Another reason is that calculations for a similar model [47] have shown that the polarizability per site converges the faster as a function of chain length the larger the hopping-integral alternation is.

We shall now use this model in studying different approximations. We set

$$E_i = (i - M)Ea/2 \quad (6.8)$$

($a/2$ is the average interatomic distance) and consider a chain of $2M$ sites with periodic boundary conditions, i.e., in effect we assume that atom 1 and atom $2M$ are bonded, too. A very special case is that of $2M = 2$, where we accordingly assume that the external potential has the periodicity of the lattice. For larger values of $2M$ the approximation is that of assuming that the potential has the shape of a sawtooth curve with the periodicity being that of the Born von Kármán zone. I.e., the approximation is equivalent to considering an infinite, periodic system for which an electronic-structure calculation is been performed using M equidistant k points in the first Brillouin zone. Proposing that the external potential due to the field should have this periodicity is not new [51, 52], and in fact Resta [53] has shown that one **has** to use an operator with the periodicity of the Born von Kármán zone.

These approximations are schematically illustrated in Fig. 6.1.

[width=12cm]fig01.ps

Figure 6.1: Schematic representation of the external field for (a) a finite system with the true field, (b) the approximation that the field has the periodicity of the lattice, and (c) that it has the periodicity of the Born von Kármán zone.

Otto [54] and later Kudin and Scusseria [55] realized that the major problem for directly

including the field in an electronic-structure calculation is related to the fact that the field destroys the periodicity. On the other hand, as mentioned above, both mathematical arguments and actual calculations have found that the charge distribution inside an extended system remains periodic also in the presence of an external field. Therefore, Otto sought a separation of the form

$$\hat{H}_{\text{ext}} = \hat{H}'_{\text{ext}} + \hat{H}''_{\text{ext}}, \quad (6.9)$$

where the first term has the periodicity of the lattice and the second is a remainder. Then, only the first term is kept. We stress that this separation may be rather arbitrary (one may add any lattice-periodic term to \hat{H}'_{ext} when simultaneously subtracting it from \hat{H}''_{ext}).

According to Bloch, in the absence of the external field any orbital is a Bloch wave of the form

$$\psi_n^{\vec{k}}(\vec{r}) = e^{i\vec{k}\cdot\vec{r}} u_n^{\vec{k}}(\vec{r}) \quad (6.10)$$

where n is a band index, and $u_n^{\vec{k}}$ is lattice-periodic. Then

$$\vec{r}\psi_n^{\vec{k}}(\vec{r}) = ie^{i\vec{k}\cdot\vec{r}} \vec{\nabla}_{\vec{k}} e^{-i\vec{k}\cdot\vec{r}} \psi_n^{\vec{k}}(\vec{r}) - i\vec{\nabla}_{\vec{k}} \psi_n^{\vec{k}}(\vec{r}). \quad (6.11)$$

By neglecting the second term, only a lattice-periodic term is kept. Maybe the most important problem of this approach is that it is closely tied to the precise definition of the orbitals, Eq. (6.10), so that different definitions of the Bloch waves may ultimately lead to different definitions of \hat{H}'_{ext} .

6.2 LMTOs

Instead of using the approach based on neglecting the second term in Eq. (6.11), we used the approximation of Fig. 6.1(c). In this case, one may systematically improve the quality of the calculation by increasing the number of k points, whereby the discontinuities become more and more separated, so that their effect should become increasingly reduced. This idea was combined with a parameter-free density-functional method.

We apply our own density-functional method that has been described in detail elsewhere [56, 57] and, therefore, shall be only briefly discussed here.

The method is based on expanding the eigenfunctions to the Kohn-Sham equations in a basis set of LMTOs (Linearized Muffin-Tin Orbitals), which are represented numerically inside non-overlapping, atom-centered, so-called muffin-tin spheres and analytically in the interstitial region outside all spheres. The numerical functions are obtained by considering the spherically symmetric part of the potential inside the muffin-tin spheres and for this solving the Kohn-Sham equations numerically for an orbital energy (denoted ϵ_ν) that is in the energy range where the orbital has its largest support, leading to the atom- and angle-dependent basis function $\phi_{\vec{R},L}$ [L being a short-hand notation for (l, m)]. In addition we define the energy-derivative $\dot{\phi}_{\vec{R},L} = \frac{\partial}{\partial \epsilon_\nu} \phi_{\vec{R},L}$. The analytical functions are decaying, spherical waves [i.e., spherical Hankel functions times harmonic functions, $h_l^{(1)}(|\vec{r} - \vec{R}| \kappa) Y_L(\widehat{r - R}) \equiv h_{\vec{R},L,\kappa}(\vec{r})$]. The functions are matched continuously and differentiably on the sphere boundaries. The basis functions $\chi_{\vec{R},L,\kappa}$ are accordingly eigenfunctions to a muffin-tin potential and, as such, good approximations to the true solutions to the Kohn-Sham equations. It shall, however, be stressed that the full potential is included in the calculations. In our implementation of the method we consider infinite, periodic, isolated polymer chains. The periodicity is utilized in constructing Bloch functions from the basis functions of different unit cells,

$$\chi_{p,L,\kappa}^k = \lim_{N \rightarrow \infty} \frac{1}{\sqrt{2N+1}} \sum_{n=-N}^N \chi_{\vec{R}_{np},L,\kappa} e^{ik\pi n}, \quad (6.12)$$

where \vec{R}_{np} is the position of the p th atom in the n th unit cell. We let the z axis be the polymer axis.

Of computational reasons it is then most convenient to use not Bloch but Wannier functions as the basis functions when calculating the matrix elements for the operator of Fig. 6.1(c). These are defined as

$$w_{jp}(\vec{r}) = \frac{1}{\sqrt{N_k}} \sum_k e^{i\phi_j(k)} \psi_j^k(\vec{r}) e^{-ikp} \quad (6.13)$$

where j is a band index and p labels the unit cell of the Wannier function. The phases $\phi_j(k)$ are determined so that the integral $\int_{0 \leq z \leq h} |w_{j0}(\vec{r})|^2 z^2 d\vec{r}$ is minimized.

6.3 The Breakdown of the Approach

The density-functional method mentioned above was developed and tested for small model systems, including a chain of hardly interacting H_2 molecules. In this case, by performing calculations on the system with the molecules being parallel to the chain axis one can calculate the response of the molecules to a field that is parallel to the chain axis. The same results (within the accuracy of the approach) should be obtained when placing the molecules perpendicular to the chain and, simultaneously, placing the field perpendicular to the chain axis. In this case, the field does not destroy the lattice periodicity and can be included much simpler.

The test calculations gave confidence that the approach was working. Subsequently, it was applied to a conjugated polymer, trans polyacetylene.

However, a further analysis of the Hückel model showed ultimately that the approach is incorrect. In a collaboration with Bernie Kirtman (University of California, Santa Barbara) we were able to prove mathematically that the correct approach is based on using the full Eq. (6.11). It turns out that one then obtains two different contributions to the dipole moment, i.e., a charge term that corresponds to Fig. 6.1(b) and a current term that cannot be represented in figures like those of Fig. 6.1. The second term is the larger, the more the units of the system are interacting, and, therefore, its effects are close to vanishing for the test system of hardly interacting H_2 units. Its existence is closely related to the approximations made in treating the system: for any finite system, no matter how large, it does not exist, but approximating the system as being infinite and periodic, it shows up.

Bibliography

- [1] F. Baletto and R. Ferrando, *Rev. Mod. Phys.* **77**, 371 (2005).
- [2] S. Goedecker, *J. Chem. Phys.* **120**, (2004) 911.
- [3] S. Goedecker and W. Hellmann, *Phys. Rev. Lett.* **95**, (2005) 055501.
- [4] B. A. Berg and T. Neuhaus, *Phys. Lett. B* **267**, (1991) 249-253.
- [5] J. Lee, In-H. Lee and J. Lee, *Phys. Rev. Lett.* **91**, (2003) 080201.
- [6] D. J. Wales and H. A. Scheraga, *Science*. **285**, (1999) 1368.
- [7] R. A. Donnelly, *Chem. Phys. Lett.* **136**, (1994) 274.
- [8] U. Röthlisberger, W. Andreoni, M. Parrinello, *Phys. Rev. Lett.* **72**, (1994) 665.
- [9] G. Rossi, R. Ferrando, A. Rapallo, A. Fortunelli, B. C. Curley, L. D. Lloyd and R. L. Johnston, *J. Chem. Phys.* **122**, (2005) 194309.
- [10] G. Rossi and R. Ferrando, *Chem. Phys. Lett.* **423**, (2006) 17-22.
- [11] P. Liu and B. J. Berne, *J. Chem. Phys.* **118**, (2003) 2999.
- [12] D. J. Wales and J. P. K. Doye, *J. Phys. Chem.* **101**, (1997) 5111-5116.
- [13] S. Yoo, J. Zhao, J. Wang and X. Ch. Zeng, *J. Am. Chem. Soc.* **126**, (2004) 13845-13849.
- [14] D. M. Deaven, K. M. Ho, *Phys. Rev. Lett.* **75**, (1995) 288.

- [15] J.R. Morris, D. M. Deaven, K. M. Ho, Phys. Rev. B. **53**, (1996) R1740.
- [16] D. M. Deaven, N. Tit, J.R. Morris, K. M. Ho, Chem. Phys. Lett. **256**, (1996) 195.
- [17] M. D. Wolf, U. Landman, J. Phys. Chem. **A102**, (1998) 6129.
- [18] Y.-B. Ge, J. D. Head, Chem. Phys. Lett. **398**, (2004) 107-112.
- [19] Y.-B. Ge, J. D. Head, J. Phys. Chem. **B108**, (2004) 6025-6034.
- [20] J.-O. Joswig, M. Springborg, Phys. Rev. **B68**, (2003) 085408.
- [21] D. Cvijović and J. Klinowski, Science. **267**, (1995) 664.
- [22] S. D. Hong and M. S. Jhon, Chem. Phys. Lett. **267**, (1997) 422-426.
- [23] J. Cheng and R. Fournier, Theor. Chem. Acc. **112**, (2004) 7-15.
- [24] A. Votor, J. Chem. Phys. **106**, (1997) 4665.
- [25] F. F. Guimarães, J. C. Belchior, R. L. Johnston and C. Roberts, J. Chem. Phys. **116**, (2002) 8327.
- [26] S. Kirkpatrick, C. D. Gelatt Jr., M. P. Vecchi, Science **220**, (1983) 671.
- [27] D. Porezag, Th. Frauenheim, Th. Köhler, G. Seifert, and R. Kaschner, Phys. Rev. B **51**, (1995) 12947.
- [28] G. Seifert, R. Schmidt, New J. Chem. **16**, (1992) 1145.
- [29] G. Seifert, D. Porezag and Th. Frauenheim, Int. J. Quantum Chem. **58**, (1996) 185.
- [30] I. D. W. Samuel *et al.*, Science. **265**, (1994) 1070.
- [31] Y. Zhang, Z.-H. Lu, J. Mol. Struct. **467**, (1999) 233.
- [32] M. Springborg, O. K. Andersen, J. Chem. Phys. **87**, (1987) 7125.
- [33] H. Shirakawa, Angew. Chem. **113**, 2642 (2001).
- [34] A. G. MacDiarmid, Angew. Chem. **113**, 2649 (2001).

- [35] A. J. Heeger, *Angew. Chem.* **113**, 2660 (2001).
- [36] T. A. Skotheim, R. L. Elsenbaumer, and J. R. Reynolds (eds), *Handbook of Conducting Polymers* (Marcel-Dekker, New York, 1998).
- [37] I. D. W. Samuel, I. Ledoux, C. Dhenaut, J. Zyss, H. H. Fox, R. R. Schrock, and R. J. Silbey, *Science* **265**, 1070 (1994).
- [38] B. Champagne, D. H. Mosley, J. G. Fripiat, and J.-M. André, *Int. J. Quant. Chem.* **46**, 1 (1993).
- [39] D. Lu, B. Marten, M. Ringnalda, R. A. Friesner, and W. A. Goddard III, *Chem. Phys. Lett.* **257**, 224 (1996).
- [40] B. Champagne, D. Jacquemin, J.-M. André, and B. Kirtman, *J. Phys. Chem. A* **101**, 3158 (1997).
- [41] B. Champagne, E. A. Perpète, and J.-M. André, *J. Chem. Phys.* **101**, 10796 (1994).
- [42] D. H. Mosley, B. Champagne, and J.-M. André, *Int. J. Quant. Chem. Symp.* **29**, 117 (1995).
- [43] V. N. Genkin and P. M. Mednis, *Sov. Phys. JETP* **27**, 609 (1968) [*Zh. Eksp. Teor. Fiz.* **54**, 1137 (1968)].
- [44] Z. Shuai and J. L. Brédas, *Phys. Rev. B* **46**, 4395 (1992).
- [45] R. D. King-Smith and D. Vanderbilt, *Phys. Rev. B* **47**, 1651 (1993).
- [46] R. Resta, *Rev. Mod. Phys.* **66**, 899 (1994).
- [47] J.-M. André, J. Delhalle, and J.-L. Brédas, *Quantum Chemistry Aided Design of Organic Polymers* (World Scientific, Singapore, 1991).
- [48] B. Champagne, E. A. Perpète, S. J. A. van Gisbergen, E.-J. Baerends, J. G. Snijders, C. Soubra-Ghaoui, K. A. Robins, and B. Kirtman, *J. Chem. Phys.* **109**, 10489 (1998).
- [49] M. van Faassen, P. L. de Boeij, R. van Leeuwen, J. A. Berger, and J. G. Snijders, *Phys. Rev. Lett.* **88**, 186401 (2002).

- [50] M. van Faassen, P. L. de Boeij, R. van Leeuwen, J. A. Berger, and J. G. Snijders, *J. Chem. Phys.* **118**, 1044 (2003).
- [51] K. Kunc and R. Resta, *Phys. Rev. Lett.* **51**, 686 (1983).
- [52] K. Schmidt and M. Springborg, *Phys. Chem. Chem. Phys.* **1**, 1743 (1999).
- [53] R. Resta, *Phys. Rev. Lett.* **80**, 1800 (1998).
- [54] P. Otto, *Phys. Rev. B* **45**, 10876 (1992).
- [55] K. N. Kudin and G. E. Scuseria, *J. Chem. Phys.* **113**, 7779 (2000).
- [56] M. Springborg and O. K. Andersen, *J. Chem. Phys.* **87**, 7125 (1987).
- [57] M. Springborg, J.-L. Calais, O. Goscinski, and L. A. Eriksson, *Phys. Rev. B* **44**, 12713 (1991).
- [58] J. H. Holland, *Adaption in Natural Algorithms and Artificial systems* (University of Michigan Press, Ann Arbor, USA, 1975).
- [59] D. E. Goldberg, *Genetic Algorithms in Search, Optimization and Machine Learning* (Addison-Wesley, Reading, USA, 1989).

Chapter 7

List of Talks

- 9 Y. Dong, M. Springborg. *Theoretical study on $(\text{HAIO})_n$ clusters*. International conference of computational methods in science and engineering 2005. Oct. 2005, Loutraki, Greece.
- 8 Y. Dong, M. Springborg. *Theoretical study on $(\text{HAIO})_n$ clusters*. 9th national quantum chemistry conference. Oct. 2005, Guiling, PR China.
- 7 Y. Dong, M. Springborg. *Structural and electronic properties of nanostructured $(\text{HAIO})_n$ and AlO* . Seminar in Tsinghua University. Sept. 2005, Beijing, PR China.
- 6 Y. Dong, M. Springborg. *Structural and electronic properties of nanostructured $(\text{HAIO})_n$ and AlO* . 41th Symposium on Theoretical Chemistry. Sept., 2005, Innsbruck, Austria.
- 5 Y. Dong, M. Springborg. *Structural and electronic properties of finite $(\text{HAIO})_n$ clusters*. Seminar in Univeristy of Missouri-Columbia. Apr., 2005, Columbia, USA.
- 4 Y. Dong, M. Springborg. *Structural and electronic properties of finite $(\text{HAIO})_n$ clusters*. Seminar in University of California, Santa Barbara. Apr., 2005, Santa Barbara, California,

USA.

- 3 Y. Dong, M. Springborg. *Structural and electronic properties of finite $(\text{HAIO})_n$ clusters*. APS March Meeting 2005, March, 2005, Los Angeles, California, USA.
- 2 Y. Dong, M. Springborg. *Electronic and structural properties of finite $(\text{HAIO})_n$ clusters*. Seminar in South-East University. Sept., 2004, Nanjing, PR China.
- 1 Y. Dong, M. Springborg. *Electronic and structural properties of finite $(\text{HAIO})_n$ clusters*. First International Conference on Theoretical Chemistry, Molecular Modeling, and Life Science s. Aug., 2003, Beijing, PR China.

Chapter 8

List of Publications

- 24 Y. Dong and M. Springborg. *Unbiased determination of structural and electronic properties of gold clusters with up to 58 atoms*, submitted for publication.
- 23 Y. Dong and M. Springborg. *Properties of Au_N clusters*, submitted for publication.
- 22 M. Springborg, B. Kirtman, Y. Dong and V. Tevekeliyska. *Infinite, periodic system in external fields*, submitted for publication.
- 21 Y. Dong and M. Springborg. *Global structure optimization study on Au_{2-20} Clusters*, submitted for publication.
- 20 V. Tevekeliyska, Y. Dong, M. Springborg and VG. Grigoryan. *Structural and energetic properties of sodium clusters*, submitted for publication.
- 19 D. Alamanova, Y. Dong, H. ur Rehman, M. Springborg and V. G. Grigoryan. *Structure and electronic properties of gold clusters*, Computing Letters.1 (2005) 319-330.
- 18 Y. Dong, M. Burkhardt, M. Veith and M. Springborg. *Structural and Electronic Properties*

- of Nanostructured HAlO*, J. Phys. Chem. **B** (2005) 22820-22829.
- 17 M. Springborg, VG. Grigoryan, Y. Dong, D. Alamanova, H. ur Rehman and V. Teveke-
liyska. *Structural and Electronic Properties of Metal Clusters*, Advances in Computational
Methods in Science and Engineering 2005. **4A** (2005) 1026-1031.
- 16 Y. Dong, M. Springborg, M. Burkhart and M. Veith. *Structural and Electronic Properties
of Nanostructured HAlO and AlO*, Advances in Computational Methods in Science and
Engineering 2005 **4A** (2005) 1010-1013.
- 15 A. Md. Asaduzzaman, K. Schmidt-D'Aloisio, Y. Dong and M. Springborg. *Properties of
polythiophene and related conjugated polymers: a density-functional study*, Phys. Chem.
Chem. Phys. **7** (2005) 2714-2722.
- 14 Y. Dong, M. Springborg. *Theoretical Study of Nanostructured HAlO*, in Proceedings of
3rd International Conference "Computational Modeling and simulation of Materials". Ed.
P. Vincenzini et al., Techna Group Publishers, (2004) 167-174.
- 13 M. Springborg, Y. Dong. *Conjugated Polymer in External DC Fields* Advances in Quan-
tum Chemistry. **47** (2004) 369-292.
- 12 M.Springborg, B.Kirtman and Y. Dong. *Electronic Polarization in Quasilinear Chains*.
Chem. Phys. Lett. **396**(2004) 404-409.
- 11 Y. Dong, M. Springborg. *Infinite Polymers and electrostatic Fields*. Synth. Met., 135-
136(2003) 349-350.
- 10 PS. Ma, MM. Chen and Y. Dong. *Solid-Liquid Equilibria of Several binary and Ternary
systems containing Maleic Anhydride*. Chinese J. Chem. Eng., **10**(3)(2002) 323-327.
- 9 YL. Lu, Y. Dong, MM. Chen and W Xu. *The Synthesis of Maleic Anhydride and the
Exploitation of its backward product*. Chemical Industry and Engineering, 1(**18**)(2001)
52-56.

- 8 H. Xu, Y. Dong, and PS. Ma. *Solubility of MA in Phthalic Diester* . Petrochemical Technology. **29**(7)(2000) 501-503.
- 7 PS. Ma, Y. Dong, and W. Xu. *Studies on the Solid-Liquid Equilibria of Maleic Anhydride in diester sebacate*. Petrochemical Technology. **29**(8)(2000) 586-588.
- 6 PS. Ma, Y. Dong, and W. Xu. *Studies on the Solid-Liquid Equilibria of Maleic Anhydride in Chain dicarboxylic Acid Diester*. Chemical Engineering(China). **28**(4)(2000) 48-51.
- 5 Y. Dong, and PS. Ma and W. Xu. *Study on the Solubility of Maleic Anhydride in 1,2-cyclohexanedicarboxylic Acid Diisobutyl Ester and Diethyl Ester*. **14**(2)(2000) 160-163.
- 4 Y. Dong, XQ. Ruan and JM. Zheng. *Studies on the Triarylmethyl Stable Free-Radical Polymer* Polymer Materials Science and Engineering. **15**(4)(1999) 72-74.
- 3 XQ. Ruan, Y. Dong, JM. Zheng CT. Guo. *Studies on Synthesis of Pyrenebenzaldehyde COPNA RESIN and its Magnetic* , **25**(5)(1997) 469-473.
- 2 XQ. Ruan, Y. Dong and JM. Zheng. *Synthesis and Characterization of Triarylmethane Resin* Apply Chemistry, **14**(3)(1997) 74-77.
- 1 XQ. Ruan, JM. Zheng and Y. Dong. *Magnetic Behavior of Triarylmethane Resin Coal* Chemical Industry, **3**(1997) 53-56.

Infinite Polymers and Electrostatic Fields

Yi Dong, Michael Springborg^{a *}

^aPhysical Chemistry, University of Saarland, 66123 Saarbrücken, Germany

Abstract

Different theoretical methods for treating external DC fields for infinite polymers are compared. Both results of model calculations and those of ab initio, density-functional calculations are reported.

Keywords: Ab initio and semiempirical methods and calculations, polyacetylene

1. Introduction

Conjugated molecules and polymers possess large linear and nonlinear responses to external electromagnetic fields. Studies have shown that the nonlinear responses per monomer converge slowly as a function of chain lengths [1,2], making studies of infinite polymers attractive. Their calculation requires matrix elements for the dipole-moment operator. For infinite systems this operator suffers from two problems: it diverges and it destroys the periodicity. Different solutions have been proposed and here we compare some of those.

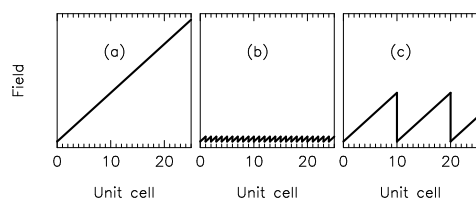


Figure 1. Schematic representation of the z operator (a) as it in reality is and (b,c) when a periodicity with (b) the lattice or (c) the Born-von-Kármán zone is assumed.

For an infinite, periodic chain the wavefunctions are Bloch waves, $\psi_j(\vec{r}) = e^{ikz} u_{k,n}(\vec{r})$, where $u_{k,n}$ is a periodic function. In a calculation one uses a discrete set of N_k equidistant k values, which corresponds to a periodicity of N_k unit cells [the Born-von-Kármán (BvK)

*Tel: +49 681 302 3856; fax: +49 681 302 3857; e-mail: m.springborg@mx.uni-saarland.de

zone]. For the z operator (cf. Fig. 1) one may assume that it has the periodicity of either the BvK zone or of the lattice. Alternatively, z operating on a Bloch wave equals $-i\frac{\partial}{\partial k} + ie^{ikz}\frac{\partial}{\partial k}e^{-ikz}$ operating on it [3]. Only the first term destroys the periodicity and may, as an approximation, be ignored.

In the present contribution we shall show — through theoretical studies with two different approaches — that many of the commonly used approaches may suffer from inaccuracies due to approximations in the treatment of the external field. In a future work we will compare ab initio results obtained with our approach with results of other experimental and theoretical studies.

2. Model calculations

We studied a chain of N sites with periodic boundary conditions and a Hückel-like Hamiltonian with one orbital and electron per atom. Only nearest-neighbour hopping integrals were set non-zero and they alternated between -0.5 and -1.5 (arbitrary units). The field operator is $\vec{E} \cdot \vec{r} = Ez$. Only on-site matrix elements for the z operator were set non-zero. We considered three cases: *i*) the z operator has the symmetry of the BvK zone, *ii*) it has the symmetry of the lattice (i.e., of two atoms), and *iii*) that the first term above is ignored.

The results of Fig. 2 show that the response depends on the approach. Also for the potential of Fig. 1(c) there is an almost regular electron distribution, except for the boundaries, until for large field strengths the electrons

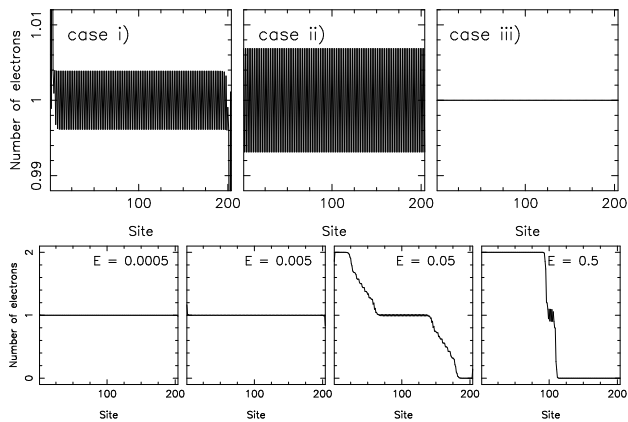


Figure 2. The number of electrons as a function of site for (upper part) $E = 0.02$ and $N = 204$ for different cases and (lower part) for case *i* for different E .

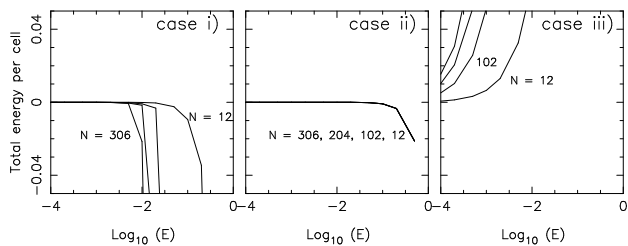


Figure 3. Variation in total energy per two atoms as a function of E . Results for $N = 12, 102, 204,$ and 306 are shown.

start flowing from one end to the other, cf. Fig. 2. Finally, Fig. 3 shows that case *iii*) leads to a fundamentally wrong description of the response, whereas the two other approaches are comparable. Differences suggest, however, that the approach *i*) is the one to be used.

3. Ab initio calculations

Our density-functional method, described in [4], uses LMTOs in expanding the wavefunctions. An LMTO is an analytical function augmented inside the atom-centered, non-overlapping spheres with numerical functions. Our programs can treat infinite, periodic, and isolated chains. The calculations give the Bloch waves in terms of LMTOs. Subsequently, we define Wannier functions, $w_{np}(\vec{r}) = \frac{1}{\sqrt{N_k}} \sum_k e^{i\phi_n(k)} \psi_n^k(\vec{r}) e^{-ikp}$. $\phi_n(k)$ are chosen so that w_{np} is localized. w_{np} has the periodicity of the BvK zone. We studied trans polyacetylene with a realistic structure and $N_k = 20$. The chain was placed in the (x, z) plane with the z axis being parallel to the chain axis. The Wannier functions were calculated for the field-free system. Subsequently, a field along the $x, y,$ or z axis was added. For the last case we considered both approximations of Fig. 1(b) and (c).

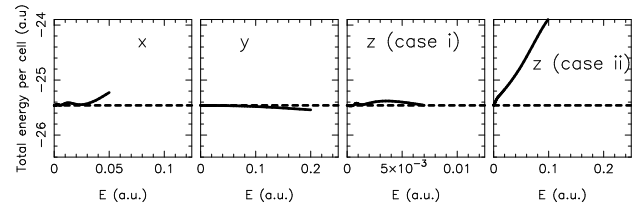


Figure 4. Total energy per C_2H_2 unit as a function of E for a field along different axis. Atomic units are used: fields in $2.571 \cdot 10^{10}$ V/m and energies in 13.606 eV.

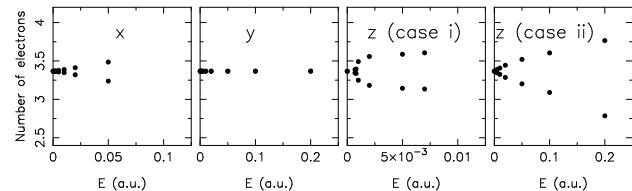


Figure 5. The number of electrons inside the carbon spheres for a field along different axis.

Fig. 4 shows that the total energy changes the least (most) when the field is parallel to the y (z) axis and that the response for fields along the z axis depends strongly on whether an approach like the one of Fig. 1(b) or like the one of Fig. 1(c) is used. The number of electrons inside the spheres is a descriptor of electron redistributions. Fig. 5 shows that a field along the x axis makes the two C atoms per unit different, whereas one along the y axis does not. A similar asymmetry is observed for fields along the z axis with both approaches, but this polarization is much stronger for case *i*) than for case *ii*). For case *i*) we notice that the electron distribution gives only two different ‘types’ of C atoms, although the 40 C atoms per BvK zone experience different fields. When E becomes so large that electrons flow from one end of the BvK zone to the other, our approach can no longer be used. The band structures (not shown) give, finally, that for the largest fields along the z axis significant shifts (some eV) are observed (making the calculations unreliable), whereas more realistic fields give shifts that are hardly observable.

REFERENCES

1. I. D. W. Samuel *et al.*, Science **265** (1994) 1070.
2. Y. Zhang, Z.-H. Lu, J. Mol. Struct. **467** (1999) 233.
3. P. Otto, Phys. Rev. B **45** (1992) 10876.
4. M. Springborg, O. K. Andersen, J. Chem. Phys. **87** (1987) 7125.

Electronic polarization in quasilinear chains

Michael Springborg^{a,*}, Bernard Kirtman^b, Yi Dong^a

^a *Department of Physical Chemistry, University of Saarland, Im Stadtwald, Gebaude 5, 66123 Saarbrücken, Germany*

^b *Department of Chemistry and Biochemistry, University of California, Santa Barbara, CA 93106, USA*

Received 30 July 2004; in final form 13 August 2004

Abstract

Starting with a finite k -mesh version of a well-known equation by Blount, we show how various definitions proposed for the polarization of long chains are related. Expressions used for infinite periodic chains in the ‘modern theory of polarization’ are thereby obtained along with a new single particle formulation. Separate intracellular and intercellular contributions to the polarization are identified and in application to infinite chains, the traditional sawtooth definition is found to be missing the latter. For a finite open chain the dipole moment depends upon how the chain is terminated, but the intracellular and intercellular polarization do not. All of these results are illustrated through calculations with a simple Hückel-like model.

© 2004 Elsevier B.V. All rights reserved.

The purpose of this Letter is to answer some questions that arise in connection with the theoretical treatment of macroscopic polarization in quasi-one dimensional chains. In order to specify the issues let us consider a macroscopic, open-ended, polymeric chain consisting of identical unit cells. For sake of argument this chain is assumed to be polarized due to an asymmetric unit cell and/or an external electric field. There are two contributions to the polarization P , i.e. to the dipole moment per unit cell. One is due to the asymmetric charge distribution within a unit cell in the central region of the chain and the other is due to the charge of opposite sign that accumulates at the chain ends.

Hückel-type calculations (see below) show that the contribution due to the finite chain ends does not vanish even in the infinite chain limit. This is simply due to the fact that, for a charge of fixed magnitude at either end, the dipole moment is directly proportional to the distance between the charges.

Next, imagine that the chain ends are connected to form a ring. In that event there are no ends and all the unit cells are identical. What is the relationship between the unit cell charge distribution of the closed chain and the unit cell charge distribution at the center of the open chain? In fact, they are the same as our Hückel-type calculations confirm. Then, what has happened to the contribution to the polarization associated with the charge build-up at the ends of the open chain? As it turns out this contribution is associated with a charge flow term that arises from Blount’s theoretical expression [1] for the polarization when periodic boundary conditions are applied. This raises the question of whether or not such a term can be accounted for by the conventional sawtooth approach [2,3]. The latter is based on using a finite mesh in k -space, along with periodic boundary conditions [4,5], but it does not correspond to a finite-mesh analogue of Blount’s formula which will be presented here. From a general formulation of this analogue several approximations will be developed including the fundamental equation(s) of the so-called modern theory of polarization [6–10].

Using a Hückel model, discussed below, we demonstrate quantitatively that the sawtooth approach omits

* Corresponding author. Fax: +49 681 302 3857.

E-mail addresses: m.springborg@mx.uni-saarland.de (M. Springborg), kirtman@chem.ucsb.edu (B. Kirtman), y.dong@mx.uni-saarland.de (Y. Dong).

the current term and that Blount's formula gives an accurate approximation for the polarization when applied with a finite set of k points. Finally, it will be seen that the polarization of long finite chains with arbitrary terminal substituents does not depend on the nature of these substituents even though the same cannot be said of the dipole moment D itself.

For a finite chain of alternating A and B atoms the Hückel Hamiltonian may be written in terms of orthonormal atom-centered basis functions $\{\chi_p\}$ as

$$\hat{H} = \sum_{p=-2K+1}^{2K} \epsilon_p \hat{c}_p^\dagger \hat{c}_p - \sum_{p=-2K}^{2K-1} t_{p,p+1} (\hat{c}_{p+1}^\dagger \hat{c}_p + \hat{c}_p^\dagger \hat{c}_{p+1}), \quad (1)$$

where $4K$ is the number of atoms, \hat{c}_p^\dagger and \hat{c}_p are the creation and annihilation operators for the function χ_p , and ϵ_p and $-t_{p,p+1}$ are on-site energies and hopping integrals, respectively. The matrix elements of the position operator are given by $\langle \chi_n | \hat{z} | \chi_m \rangle = \delta_{n,m} z_n$ with z_p being the position of the p th atom. For convenience, the atoms are taken to be equally spaced, $z_p = \frac{a}{2}[p-12]$, with $p = -2K+1, \dots, 2K$ being odd (even) for the A (B) atoms, and $a/2$ being the nearest-neighbor distance. Assuming one electron per atom it is straightforward to evaluate the atomic charges and the electronic polarization, P (dipole moment per A–B unit) as a function of the number of A–B units, $2K$. As an example (using arbitrary units for length and energy and setting the electronic charge equal to +1) for $a = 2.0$, alternating on-site energies $\epsilon_p = \pm 0.5 \equiv \pm \epsilon_0$, and hopping integrals $t_+ = -2.2$, $t_- = -1.8$, we find that the polarization is converged to a value $P = 0.58125$ for $K > 13$ while the charges on the central atoms are $Q(A) = 0.74413$, $Q(B) = 1.25587$. The latter result in a contribution $P_c = P - (a/4)[Q(B) - Q(A)] = 0.32538$ to the polarization due to accumulation of charge at the chain ends. We may think of P_c as an intercellular charge flow term. The existence of a substantial intercellular charge flow term is remarkably robust to variations in the model. Thus, including next-nearest-neighbor interactions, modifying the matrix elements at the chain ends or altering $\langle \chi_n | \hat{z} | \chi_m \rangle$ in realistic ways often changes the total dipole moment, but not the polarization, of sufficiently long chains. The effect of varying terminal (on-site and/or hopping) matrix elements is illustrated in Fig. 1. The figure shows that altering the chain ends changes the charges on the ends (upper part) and the dipole moment (lower part) but neither the polarization (slope of dipole-moment curve) nor the charges in the central region are affected. The right-hand panel of the lower part shows that the polarization can vary for small chains (see, particularly, curve f).

The fact that one may calculate the polarization by studying only the central cells has been shown previously by Vanderbilt and King-Smith [9]. However, this does not imply that different terminating groups, which

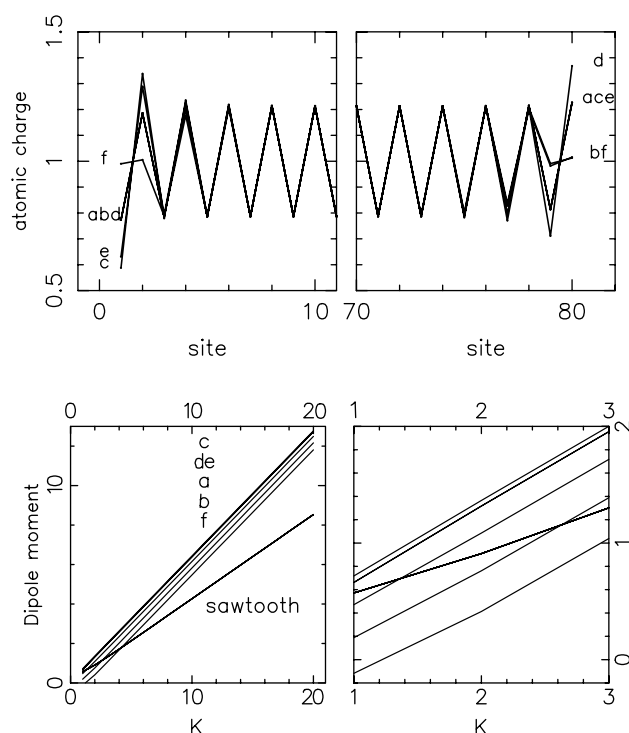


Fig. 1. *Upper part*: Distribution of the atomic charges as a function of atom index for a finite chain with 80 atoms for different cases of the matrix elements for the terminating atoms, i.e. the on-site energies for the first (last) atom have been modified as $\epsilon_0 \rightarrow \epsilon_0 + \Delta\epsilon_l$ ($-\epsilon_0 \rightarrow -\epsilon_0 + \Delta\epsilon_r$), and the hopping integrals between the first (last) two atoms according to $-t_+ \rightarrow -t_+ + \Delta t_l$ ($-t_- \rightarrow -t_- + \Delta t_r$). *Lower part*: The dipole moment for the same cases but as a function of chain length. Here, 'sawtooth' corresponds to the dipole moment for a ring system when using the sawtooth approximation, and the right panel shows a blow-up of the low- K part. The curves marked a, b, c, d, e, and f (in the lower panels these labels are listed in the same order as the curves appear) correspond to the following modifications: $(\Delta\epsilon_l, \Delta\epsilon_r, \Delta t_l, \Delta t_r) = (0,0,0,0)$, $(1,0,0,0)$, $(0,1,0,0)$, $(0,0,-1,0,0)$, $(0,0,0,-1,0)$, and $(1,0,-1,0,-1,0,1,0)$, respectively.

lead to different charge accumulation at the chain ends, give the same polarization because there is a contribution due to intercellular charge flow that could change. Thus, this is a generalization of the Vanderbilt and King-Smith result, which is consistent with the known near-sightedness [11] of the single-particle density matrix. It has obvious implications for the design of donor–acceptor, or push–pull, systems and is valid provided the chain is sufficiently long.

Even for an unsubstituted chain where the ends are connected so that no charge can accumulate there is an important contribution to the polarization that arises from the intercellular charge flow. We now turn to that case and consider a ring of $2K$ identical AB unit cells. Application of periodic boundary conditions leads to the general expression for the eigenfunctions

$$\psi_n^k(\vec{r}) = u_n^k(\vec{r}) e^{ikz} = \frac{1}{\sqrt{2K}} \sum_{m=-K+1}^K e^{ikam} \sum_{p=1}^{N_b} c_{pm}^k \chi_{pm}(\vec{r}) \quad (2)$$

with n being a band index, χ_{pm} the p th basis function of the m th unit cell, and N_b the number of basis functions per cell. In our Hückel model, $n = 1$ ($n = 2$) for the occupied (empty) band, and $p = 1$ ($p = 2$) indicates the function on the A (B) atom. For any given set of parameters and sufficiently long chains the electronic charges, $Q(A)$ and $Q(B)$, turn out to be identical to those at the center of the open-ended chain of the same length. Thus, for either chain, the same intracellular polarization $\frac{a}{4}[Q(B) - Q(A)]$ is obtained. This means that the P_c contribution must be accounted for in some other way. For the ring we can readily identify that contribution by considering Blount's expression for the polarization in the limit $K \rightarrow \infty$

$$P = \frac{ia}{\pi} \sum_n \int \left\langle u_n^k \left| \frac{\partial}{\partial k} u_n^k \right. \right\rangle dk, \quad (3)$$

where the n summation is over the (doubly) occupied bands. Using Eq. (2) it is easy to show (cf. [12]) that

$$P = \frac{1}{\pi} \sum_n \sum_{m=-N}^N \int e^{ikma} \times \sum_{pq} c_{qn}^{k*} \left(\langle \chi_{q0} | z - ma | \chi_{pm} \rangle + i \langle \chi_{q0} | \chi_{pm} \rangle \frac{d}{dk} \right) c_{pm}^k dk. \quad (4)$$

With a finite $2K$ -point-mesh approximation for the integral one can verify that the first term on the right-hand side of Eq. (4) yields the intracellular polarization. This leaves the second term as the periodic cyclic chain analogue of the intercellular charge flow contribution described above in connection with the open chain.

If one is interested in long open-ended chains it is usually advantageous computationally to assume that the chain is infinite and periodic. A number of different proposals have been advanced for calculating the polarization of infinite periodic chains using finite k mesh methods. In order to compare these approaches we follow the treatment of Blount [1], based on the relation

$$z\psi_n^k(\vec{r}) = ie^{ikz} \frac{\partial}{\partial k} e^{-ikz} \psi_n^k(\vec{r}) - i \frac{\partial}{\partial k} \psi_n^k(\vec{r}), \quad (5)$$

to obtain the effect of the coordinate z acting on a single electron whose orbital, $\psi(\vec{r})$, is expanded in terms of Bloch waves

$$\psi(\vec{r}) = \sum_k \sum_n \psi_n^k(\vec{r}) f_n^k = \sum_k \sum_n e^{ikz} u_n^k(\vec{r}) f_n^k. \quad (6)$$

In fact, Blount [1] obtained Eq. (4) by using Eq. (5) on ψ of Eq. (6). Here instead of a continuous k we will use a finite k -mesh, which corresponds to assuming that the system possesses the periodicity of the Born von Kármán (BvK) zone containing $2K$ unit cells. Consequently, the analytical derivatives in Blount's formulation will be replaced by numerical derivatives. In lowest order the numerical derivatives corresponding to the terms in Eq. (5) are:

$$\begin{aligned} \hat{\Delta}'_- \psi(\vec{r}) &= \frac{1}{\Delta k} \sum_k \sum_n [\psi_n^k(\vec{r}) f_n^k - \psi_n^{k-1}(\vec{r}) f_n^{k-1}], \\ \hat{\Delta}''_- \psi(\vec{r}) &= \frac{1}{\Delta k} \sum_k \sum_n e^{ikz} [u_n^k(\vec{r}) f_n^k - u_n^{k-1}(\vec{r}) f_n^{k-1}], \\ \hat{\Delta}'_+ \psi(\vec{r}) &= \frac{1}{\Delta k} \sum_k \sum_n [\psi_n^{k+1}(\vec{r}) f_n^{k+1} - \psi_n^k(\vec{r}) f_n^k], \\ \hat{\Delta}''_+ \psi(\vec{r}) &= \frac{1}{\Delta k} \sum_k \sum_n e^{ikz} [u_n^{k+1}(\vec{r}) f_n^{k+1} - u_n^k(\vec{r}) f_n^k], \\ \hat{\Delta}'_0 &= \frac{1}{2} (\hat{\Delta}'_- + \hat{\Delta}'_+), \\ \hat{\Delta}''_0 &= \frac{1}{2} (\hat{\Delta}''_- + \hat{\Delta}''_+), \end{aligned} \quad (7)$$

with $\Delta k = \pi/aK$. By construction these expressions have the BvK periodicity and it follows that the lowest order finite- k -mesh analogues of $\langle \psi | z | \psi \rangle$ are $(\psi_n^{k+2\pi/a} = \psi_n^k)$:

$$\begin{aligned} \langle \psi | (-i\hat{\Delta}'_- + i\hat{\Delta}''_-) | \psi \rangle &= \left\langle \psi \left| \frac{i}{\Delta k} (1 - e^{i\Delta kz}) \right| \psi \right\rangle = \frac{i}{\Delta k} (1 - S^+), \\ \langle \psi | (-i\hat{\Delta}'_+ + i\hat{\Delta}''_+) | \psi \rangle &= \left\langle \psi \left| \frac{i}{\Delta k} (e^{-i\Delta kz} - 1) \right| \psi \right\rangle = \frac{i}{\Delta k} (S^- - 1), \\ \langle \psi | (-i\hat{\Delta}'_0 + i\hat{\Delta}''_0) | \psi \rangle &= \left\langle \psi \left| \frac{\sin(\Delta kz)}{\Delta k} \right| \psi \right\rangle = \frac{1}{2i\Delta k} (S^+ - S^-), \end{aligned} \quad (8)$$

where $S^\pm = \langle \psi | e^{\pm i\Delta kz} | \psi \rangle$. If the spatial extent of ψ is much smaller than $1/\Delta k$ (this can, e.g., be obtained by increasing the number of k points in an actual calculation), and assuming that $\int_{\text{BvK}} |\hat{z}\psi(\vec{r})|^2 d\vec{r}$ exists (e.g. when ψ is a well-localized Wannier function), then we may make the approximation

$$\left\langle \psi \left| \frac{i}{\Delta k} e^{\pm i\Delta kz} \right| \psi \right\rangle \simeq \frac{i}{\Delta k} e^{\pm i\Delta k \langle \psi | z | \psi \rangle} \quad (9)$$

or

$$\begin{aligned} \langle \psi | z | \psi \rangle &\simeq \frac{-i}{\Delta k} \ln S^+ \simeq \frac{-1}{\Delta k} \text{Im} \ln S^+, \\ \langle \psi | z | \psi \rangle &\simeq \frac{i}{\Delta k} \ln S^- \simeq \frac{1}{\Delta k} \text{Im} \ln S^- \\ \langle \psi | z | \psi \rangle &\simeq \frac{1}{\Delta k} \arcsin \left[\frac{1}{2i} (S^+ - S^-) \right]. \end{aligned} \quad (10)$$

Here, the second equalities in the first two expressions have been obtained by removing the imaginary parts and, accordingly, requiring that $\langle \psi | z | \psi \rangle$ is real. This result comes about automatically in the expressions based on the $\hat{\Delta}_0$ operators.

The treatment for N electrons is similar. In that case the one-electron Bloch waves are replaced by Slater determinants $\Psi_i^k = \hat{\mathcal{A}}[\psi_{i_1}^{k_1}(\vec{r}_1) \psi_{i_2}^{k_2}(\vec{r}_2), \dots, \psi_{i_N}^{k_N}(\vec{r}_N)]$, where $\hat{\mathcal{A}}$ is the antisymmetrizer, and Eq. (5) becomes

$$\begin{aligned} \left(\sum_{n=1}^N z_n \right) \Psi_{\vec{i}}^{\vec{k}} &= i \exp \left(i \sum_{n=1}^N k_n z_n \right) \left(\sum_{n=1}^N \frac{\partial}{\partial k_n} \right) \\ &\times \left(\exp \left(-i \sum_{n=1}^N k_n z_n \right) \Psi_{\vec{i}}^{\vec{k}} \right) - i \left(\sum_{n=1}^N \frac{\partial}{\partial k_n} \right) \Psi_{\vec{i}}^{\vec{k}}. \end{aligned} \quad (11)$$

Then an arbitrary N -electron function can be written as the linear combination $\Psi(\vec{r}_1, \vec{r}_2, \dots, \vec{r}_N) = \sum_{\vec{k}} \Psi_{\vec{i}}^{\vec{k}}(\vec{r}_1, \vec{r}_2, \dots, \vec{r}_N) f_{\vec{i}}^{\vec{k}}$ with the single-particle situation being a special case. The generalization of the quantities in Eq. (7) becomes

$$\begin{aligned} \hat{\Delta}'_- \Psi(\vec{r}_1, \vec{r}_2, \dots, \vec{r}_N) &= \frac{1}{\Delta k} \sum_{\vec{i}} \sum_{\vec{k}} \left[\Psi_{\vec{i}}^{\vec{k}}(\vec{r}_1, \vec{r}_2, \dots, \vec{r}_N) f_{\vec{i}}^{\vec{k}} \right. \\ &\quad \left. - \Psi_{\vec{i}}^{\vec{k}-\Delta\vec{k}}(\vec{r}_1, \vec{r}_2, \dots, \vec{r}_N) f_{\vec{i}}^{\vec{k}-\Delta\vec{k}} \right] \\ \hat{\Delta}''_- \Psi(\vec{r}_1, \vec{r}_2, \dots, \vec{r}_N) &= \frac{1}{\Delta k} \mathcal{A} \left\{ \sum_{\vec{i}} \sum_{\vec{k}} e^{i(k_1 z_1 + k_2 z_2 + \dots + k_N z_N)} \right. \\ &\quad \times \left[u_{i_1}^{k_1}(\vec{r}_1) u_{i_2}^{k_2}(\vec{r}_2) \dots u_{i_N}^{k_N}(\vec{r}_N) f_{\vec{i}}^{\vec{k}} \right. \\ &\quad \left. \left. - u_{i_1}^{k_1-1}(\vec{r}_1) u_{i_2}^{k_2-1}(\vec{r}_2) \dots u_{i_N}^{k_N-1}(\vec{r}_N) f_{\vec{i}}^{\vec{k}-\Delta\vec{k}} \right] \right\} \end{aligned} \quad (12)$$

with analogous expressions for $\hat{\Delta}'_+$ and $\hat{\Delta}''_+$, $\hat{\Delta}'_0$ and $\hat{\Delta}''_0$. Hence, the generalization of Eq. (8) is

$$\begin{aligned} \hat{\Delta}'_- &= -i\hat{\Delta}'_- + i\hat{\Delta}''_- = \frac{i}{\Delta k} [1 - e^{i\Delta k(z_1 + z_2 + \dots + z_N)}], \\ \hat{\Delta}'_+ &= -i\hat{\Delta}'_+ + i\hat{\Delta}''_+ = \frac{i}{\Delta k} [e^{-i\Delta k(z_1 + z_2 + \dots + z_N)} - 1], \\ \hat{\Delta}'_0 &= -i\hat{\Delta}'_0 + i\hat{\Delta}''_0 = \frac{1}{\Delta k} \sin[\Delta k(z_1 + z_2 + \dots + z_N)]. \end{aligned} \quad (13)$$

We will restrict ourselves to the case where there is a finite gap between occupied and unoccupied bands, assume no spin polarization (N is even), and use a single determinant wavefunction (Hartree–Fock or Kohn–Sham theory). Then

$$\begin{aligned} \langle \Psi | \hat{\Delta}'_- | \Psi \rangle &= \frac{i}{\Delta k} [1 - (\det \underline{\underline{\Delta}}^+)^2], \\ \langle \Psi | \hat{\Delta}'_+ | \Psi \rangle &= \frac{i}{\Delta k} [(\det \underline{\underline{\Delta}}^-)^2 - 1], \\ \langle \Psi | \hat{\Delta}'_0 | \Psi \rangle &= \frac{1}{2i\Delta k} [(\det \underline{\underline{\Delta}}^+)^2 - (\det \underline{\underline{\Delta}}^-)^2], \end{aligned} \quad (14)$$

where $\underline{\underline{\Delta}}^{\pm}$ is the $N/2 \times N/2$ matrix containing the single-particle matrix elements $S_{(i,k),(j,l)}^{\pm} = \langle \psi_i^k | e^{\pm i\Delta k z} | \psi_j^l \rangle$. Assuming localized orbitals we may apply the analogue of Eq. (9), i.e.

$$\left\langle \Psi \left| \frac{i}{\Delta k} e^{\pm i\Delta k(z_1 + z_2 + \dots + z_N)} \right| \Psi \right\rangle \simeq \frac{i}{\Delta k} e^{\pm i\Delta k \langle \Psi | z_1 + z_2 + \dots + z_N | \Psi \rangle}, \quad (15)$$

and either of the first two equations in Eq. (14), in combination with Eq. (13), to arrive at the expression

$$P_R = -\frac{a}{\pi} \text{Im} \ln \det \underline{\underline{\Delta}}^+ = \frac{a}{\pi} \text{Im} \ln \det \underline{\underline{\Delta}}^-, \quad (16)$$

for the polarization. Note that $(\underline{\underline{\Delta}}^+)^{\dagger} = \underline{\underline{\Delta}}^-$. An essentially identical formula in terms of Bloch orbitals has been given by Resta [4]. We observe that Eq. (16) is based on a not too accurate finite-difference approximation to the derivative. A more accurate approximation is

$$P_0 = \frac{a}{2\pi} \arcsin \left[\frac{1}{2i} \left((\det \underline{\underline{\Delta}}^+)^2 - (\det \underline{\underline{\Delta}}^-)^2 \right) \right]. \quad (17)$$

Despite this P_R turns out to be more useful computationally. To see why we write

$$\det \underline{\underline{\Delta}}^{\pm} = s \pm it, \quad (18)$$

whereby

$$\begin{aligned} P_R &= -\frac{a}{\pi} \arctan \left(\frac{t}{s} \right), \\ P_0 &= \frac{a}{2\pi} \arcsin(2st). \end{aligned} \quad (19)$$

As $K \rightarrow \infty$, $s^2 + t^2 \rightarrow 1$, while $|s|, |t| < 1$ are increasing functions of K . Accordingly, as our numerical results below confirm, P_R converges faster than P_0 as a function of K . On the other hand, P_0 can be valuable analytically; indeed, it motivated our choice for the operator defined in Eq. (23) below.

The value of $\det \underline{\underline{\Delta}}^{\pm}$ will not be altered by an arbitrary unitary transformation of the single determinant orbitals. So, instead of localized orbitals we may use the occupied Bloch waves from which these orbitals are obtained. Then, the matrix elements of $\underline{\underline{\Delta}}^{\pm}$ are non-zero only for pairs of Bloch waves whose k values differ by Δk (modulus $2\pi/a$). As a result $\underline{\underline{\Delta}}^{\pm}$ can be written as consisting of $2K \times 2K$ square blocks, each of dimension $B = N/(4K)$ (the number of doubly-occupied bands) with non-zero elements only in the set of blocks lying one stripe above and one stripe below the main diagonal.

Given that the Bloch functions are differentiable with respect to k as discussed by Blount we obtain for small Δk

$$\ln(\det \underline{\underline{\Delta}}^{\pm})^2 \simeq \mp 2\Delta k \sum_{k=1}^{2K} \sum_{n=1}^B \left\langle u_n^k \left| \frac{\partial}{\partial k} u_n^k \right. \right\rangle. \quad (20)$$

Inserting this into the right-hand side of Eq. (16) yields another formula for the polarization

$$P_{\text{KSV}} = \frac{i}{K} \sum_{k=1}^{2K} \sum_{n=1}^B \left\langle u_n^k \left| \frac{\partial}{\partial k} u_n^k \right. \right\rangle, \quad (21)$$

which is the 1D discretized Berry phase expression [9] used in the modern theory of polarization.

For the treatment of core orbitals (or those of non-interacting periodically repeated molecules) we suppose that the orbitals are strongly localized so that $\langle \psi_{p_1}(\vec{r} - \vec{R}_{n_1}) | e^{\pm i\Delta k z} | \psi_{p_2}(\vec{r} - \vec{R}_{n_2}) \rangle$ vanishes unless the units n_1 and n_2 , where the functions are centered, are identical. In that case we may write for orbitals of the same unit

$$\begin{aligned} \langle \psi_{p_1} | e^{\pm i\Delta k z} | \psi_{p_2} \rangle &\simeq \delta_{p_1, p_2} e^{\pm i\Delta k z_{p_1, p_2}} \pm i\Delta k \langle \psi_{p_1} | z - z_{p_1, p_2} | \psi_{p_2} \rangle \\ &+ \frac{(i\Delta k)^2}{2} \langle \psi_{p_1} | (z - z_{p_1, p_2})^2 | \psi_{p_2} \rangle + \dots, \end{aligned} \quad (22)$$

with z_{p_1, p_2} being the ‘center’ of the p_1 th and p_2 th orbital. Therefore, the ‘traditional’ contribution to the polarization from these orbitals, i.e., $\sum_p \langle \psi_p | z | \psi_p \rangle$, is obtained only in the case where all terms but the first one on the right-hand side of Eq. (22) are negligible (e.g. in the limit $\Delta k \rightarrow 0$).

So far we have presented an internally consistent approach for how to calculate the polarization in an infinite, periodic chain when basing the discussion on a generalization of Blount’s work to the case of a finite BvK zone. We have arrived at an expression involving the expectation values for N -body operators, i.e., the \underline{S}^{\pm} matrices. This has been taken as a proof that the polarization is a many-body phenomenon [6,7]. However, the polarization can also be written in terms of the single-particle operator

$$\begin{aligned} \hat{P} = \frac{1}{2i\Delta k} \sum_{m=1}^N \sum_{k'} \sum_{n'} &\left[e^{i\Delta k z_m} | \psi_{n'}^{k'-1}(\vec{r}_m) \rangle \langle \psi_{n'}^{k'}(\vec{r}_m) | \right. \\ &\left. - e^{-i\Delta k z_m} | \psi_{n'}^{k'+1}(\vec{r}_m) \rangle \langle \psi_{n'}^{k'}(\vec{r}_m) | \right]. \end{aligned} \quad (23)$$

It is straightforward to show that the expectation value of this operator gives P_0 in the limit $\Delta k \rightarrow 0$.

In order to explore our ideas further, the Hückel-like model described above was used to evaluate the various polarization expressions we have presented. For our purposes it is necessary to have matrix elements of z and $e^{\pm i\Delta k z}$ that are defined consistently. Hence, we calculated the matrix elements in both cases analytically assuming piecewise constant basis functions of adjustable width, w . For simplicity we also assumed that $w < a/2$, whereby the results become independent of w . Other more realistic functions are possible, of course, but the above choice is sufficient to make the desired comparisons.

In Table 1 we show some typical results for the various choices of P obtained using BvK periodic boundary conditions. The finite chain value determined from the increment $\Delta D = 1/2[D(2K+2) - D(2K)]$, where D is the dipole moment, is also presented for comparison. In order to interpret polarization values the reader should recall that P is determined only up to an arbitrary multiple of the unit cell length [cf. Eqs. (16) and (17)], which in this case is 2.0. Bearing this in mind, the table shows that ΔD agrees very well with the polarization of the infinite system given by P_R . Indeed, the finite chain result converges more rapidly to the infinite K limit. The sawtooth approximation (denoted P_{st} in the table) is calculated using periodic boundary conditions with z replaced by

Table 1
Results of model calculations with the Hückel model

ϵ_0	t_+	t_-	K	P_{st}	P_R	P_{KSV}	P_0	ΔD
0.5	2.2	1.8	20	0.25587	-1.41859	-1.41745	0.29410	0.58125
			200	0.25587	-1.41875	-1.41875	0.39798	0.58125
			2000	0.25587	-1.41875	-1.41875	0.41643	0.58125
			20 000	0.25587	-1.41875	-1.41875	0.41852	0.58125
0.5	2.5	1.5	20	0.21337	-1.68291	-1.68305	0.26857	0.31695
			200	0.21337	-1.68305	-1.68305	0.31134	0.31695
			2000	0.21337	-1.68305	-1.68305	0.31638	0.31695
			20 000	0.21337	-1.68305	-1.68305	0.31690	0.31695
0.5	1.5	1.5	20	0.33562	-1.00000	-3.00000	0.00000	1.00000
			200	0.33562	-1.00000	-3.00000	0.00000	1.00000
			2000	0.33562	-1.00000	-3.00000	0.00000	1.00000
			20 000	0.33562	-1.00000	-3.00000	0.00000	1.00000
0.0	2.5	1.5	20	0.00000	-2.00000	-3.00000	0.00000	0.00000
			200	0.00000	-2.00000	-2.00000	0.00000	0.00000
			2000	0.00000	-2.00000	-2.00000	0.00000	0.00000
			20 000	0.00000	-2.00000	-2.00000	0.00000	0.00000
0.5	2.0	0.0	20	0.24254	-1.75735	-1.75746	0.22586	0.24254
			200	0.24254	-1.75746	-1.75746	0.24078	0.24254
			2000	0.24254	-1.75746	-1.75746	0.24236	0.24254
			20 000	0.24254	-1.75746	-1.75746	0.24252	0.24254

The lattice constant equals $a = 2$. All other parameter values are given in the table.

a piecewise linear function having the BvK periodicity. Note that P_{st} gives the correct value only when the system consists of purely non-interacting units (last case in table). Since $\sin(\alpha) = \sin(\pi - \alpha)$ it is not possible to discriminate between P_0 and $(a/2) - P_0$ (cf. the first case in the table). If that is taken into account, we see that P_{KSV} , P_R , and P_0 all give similar results, although the latter converges much slower, and the former much faster, than the others.

In conclusion we have provided a unified picture of electronic polarization in extended quasilinear chains based primarily on the finite k -mesh analogue of Blount's treatment for infinite periodic systems. Separate intracellular and intercellular contributions are identified and compared between closed and open chains. It is shown that neither component is affected by substitution at the end of an open chain, as occurs in a push-pull compound. On the other hand, the traditional sawtooth formulation for infinite closed chains fails to account for the intercellular charge flow term. Several different expressions for the electronic polarization are systematically generated from the same starting point, including those related to the so-called modern theory of polarization.

From the same perspective we obtain an alternative single particle operator, which yields the polarization as its expectation value. Hückel-type calculations are

carried out to illustrate all of these points and to assess the convergence properties of the various polarization formulas as the k -mesh spacing decreases to zero.

Acknowledgements

This work was supported by the German Research Council (DFG) through project Sp 439/11. One of the authors (M.S.) is grateful to Fonds der Chemischen Industrie for generous support.

References

- [1] E.I. Blount, *Solid State Phys.* 13 (1962) 305.
- [2] K. Kunc, R. Resta, *Phys. Rev. Lett.* 51 (1983) 686.
- [3] P. Otto, *Phys. Rev. B* 45 (1992) 10876.
- [4] R. Resta, *Phys. Rev. Lett.* 80 (1998) 1800.
- [5] K. Schmidt, M. Springborg, *Phys. Chem. Chem. Phys.* 1 (1999) 1743.
- [6] R. Resta, *Rev. Mod. Phys.* 66 (1994) 899.
- [7] R. Resta, *Int. J. Quantum. Chem.* 75 (1999) 599.
- [8] R.D. King-Smith, D. Vanderbilt, *Phys. Rev. B* 47 (1993) 1651.
- [9] D. Vanderbilt, R.D. King-Smith, *Phys. Rev. B* 48 (1993) 4442.
- [10] R.W. Nunes, X. Gonze, *Phys. Rev. B* 63 (2001) 155107.
- [11] W. Kohn, *Phys. Rev. Lett.* 76 (1996) 3168.
- [12] B. Kirtman, F.L. Gu, D.M. Bishop, *J. Chem. Phys.* 113 (2000) 1294.

Conjugated polymers in external DC fields

Michael Springborg* and Yi Dong†
Physical Chemistry, University of Saarland,
66123 Saarbrücken, Germany

November 10, 2003

Abstract

Different aspects related to the theoretical treatment of the electronic properties of infinite, periodic, conjugated polymers exposed to external DC fields are discussed. Various proposed methods are studied within a simple Hückel-like model that includes alternating hopping integrals. It is found that when rewriting the extra term due to the DC field as one that involves the k derivatives of the Bloch functions, one has to be very careful. First, only under certain circumstances one may ignore those parts that are non-diagonal in k , whereas under other circumstances results that depend on the (unphysical) phase factors of the Bloch waves are obtained. On the other hand, an approach based on Wannier functions is found to be mathematically well-founded. Based on these results, we subsequently present a density-functional method that uses Wannier functions and that can be used in treating infinite, periodic systems exposed to DC fields. Some first results for an infinite linear chain of carbon atoms are presented and discussed.

*e-mail: m.springborg@mx.uni-saarland.de

†e-mail: y.dong@mx.uni-saarland.de

Contents

1	Introduction	3
2	General considerations and a simple Hückel-like model	6
3	A first-principles method for polymers	16
4	Conclusions	26

1 Introduction

Theoretical chemistry and physics are partly concerned with the development of new theoretical and computational methods for studying special properties and/or materials and partly concerned with the application of these methods to questions of current interest. Thereby, a central issue is that of exploring new materials or properties that so far has been out of reach with theoretical methods.

Slightly more than 10 years ago one of the present authors together with colleagues in Uppsala, including Osvaldo Gosinski, used one of the simplest possible conjugated polymers, trans polyacetylene, $(\text{CH})_x$, as a model compound for exploring new computational tools for calculating electronic properties of infinite, periodic, polymeric systems [1, 2]. In order to celebrate the 65th birthday of Osvaldo Gosinski it therefore seems natural to return to a simple conjugated polymer and use it as a model system for studying specific properties of polymeric systems that are of current interest and, simultaneously, pose challenges to theoretical treatments. Thus, we shall here study the response of conjugated polymers to external electrostatic fields. We stress that although this has been the subject of many theoretical studies over the last 1–2 decades (see, e.g., [3]), there remains still a number of only partly solved problems that warrant more detailed investigations. In this spirit we shall here present results of some simple model calculations together with present and apply a formalism for treating such fields directly in a parameter-free electronic-structure method for infinite, periodic polymers.

Conjugated polymers have been at the focus of a large research activity over more than a quarter of century (see, e.g., [4, 5, 6, 7]). Compared with more traditional plastics, the conjugated polymers contain a backbone with sp^2 - and sp -bonded (and not sp^3 -bonded) carbon atoms. The last valence electron per carbon atom occupies a p orbital and participates in π bonds between the carbon atoms. This has two consequences: the polymers are essentially planar, and the energy gap between occupied and unoccupied orbitals is small (i.e., corresponds to that of conventional semiconductors) with π orbitals appearing closest to the Fermi level.

There is a strong coupling between electrons and phonons (structure) which leads to a lowest-energy structure with alternating C–C bond lengths and to the occurrence of structural defects (i.e., solitons and polarons) when the chains are charged. Both finite oligomers and essentially infinite poly-

mers can be synthesized, and a special class of oligomers is the finite, so-called push-pull systems where the two end-groups are different, so that an excitation involves an internal charge transfer from one end to the other.

Due to the combination of mechanical properties as plastics and electronic properties as crystalline semiconductors, these materials are been considered interesting for many special-purpose applications, including light-emitting diodes, transistors, and sensors. For the present purpose it is, however, most important to observe that the π electrons that are somewhat loosely bound to the backbone, but not so loosely bound that they are free-electron-like, give rise to very large linear and, in particular, non-linear responses to external electric fields. The responses can be quantified through the polarizabilities (α) and hyperpolarizabilities (β, γ, \dots) by expanding either the dipole moment

$$\mu_i = \mu_i^{(0)} + \sum_{j=x,y,z} \alpha_{ij} E_j + \sum_{j,k=x,y,z} \beta_{ijk} E_j E_k + \sum_{j,k,l=x,y,z} \gamma_{ijkl} E_j E_k E_l + \dots \quad (1)$$

or the total energy

$$\begin{aligned} E_{\text{tot}} = E_{\text{tot}}^{(0)} - \sum_{i=x,y,z} \mu_i^{(0)} E_i & - \frac{1}{2} \sum_{i,j=x,y,z} \alpha_{ij} E_i E_j - \frac{1}{3} \sum_{i,j,k=x,y,z} \beta_{ijk} E_i E_j E_k \\ & - \frac{1}{4} \sum_{i,j,k,l=x,y,z} \gamma_{ijkl} E_i E_j E_k E_l + \dots \end{aligned} \quad (2)$$

in the electric-field components. When AC fields are applied, the (hyper)polarizabilities become frequency dependent,

$$p_{i,j,k,\dots,m}(\omega_i, \omega_j, \omega_k, \dots, \omega_m) \quad \text{with } \omega_i = |\omega_j \pm \omega_k \pm \dots \pm \omega_m| \quad (3)$$

with p being $\alpha, \beta, \gamma, \dots$. Non-zero values of β and γ lead to effects like second- and third-harmonic generation, four-wave mixing, electric-field-induced second harmonic, the Kerr effects, and the Pockels effect, which are interesting both for basic and for applied science. Accordingly, much effort is put into obtaining maximally large values of these parameters.

In the thermodynamic limit any property Z for a finite system $A-(X)_n-D$ will be either independent of or proportional to n . Experimental [8] and theoretical [9, 10, 11, 12, 13] studies have, however, shown that when Z is the polarizability α or the hyperpolarizability γ , $Z(n)/n$ [or $Z(n) - Z(n-1)$] converges only very slowly as a function of n towards the large- n limit and,

moreover, the convergence for γ is slower than that for α [10]. On the other hand, since the larger systems tend to have larger values of $Z(n)/n$ than the smaller ones, it is highly relevant to consider the large systems. Thus, considering infinite, periodic systems is a useful alternative.

For finite oligomers of polyacetylene it has been found [12] that the vibrational contribution to the total polarizability amounts to roughly 10% of the total polarizability, and, although it is known that this percentage will increase for the hyperpolarizabilities, we shall here concentrate on the electronic part of the responses.

Most often, (hyper)polarizabilities of polymers are calculated using a perturbation-theoretical approach based on the formalism of Genkin and Mednis [14]. Thereby, both occupied and unoccupied orbitals have to be included in the calculation and the fact that different electronic-structure methods (most notably, Hartree-Fock- and density-functional-based methods) often yield fairly inaccurate results for the unoccupied orbitals may be the reason for the fact that the calculated (hyper)polarizabilities often depend strongly on the method (see, e.g., [13, 15]). Thus, in order to access the accuracy of the different methods or, alternatively, to avoid the problems related to the accuracy of the unoccupied orbitals, one may include a DC field directly in the calculations whereby at least the static (hyper)polarizabilities can be calculated.

However, the inclusion of a static field is a non-trivial endeavour. First, even for the smallest possible system (e.g., an isolated hydrogen atom) and for the smallest possible external field, the eigenvalue spectrum changes dramatically: there is no bound states, and states that in the field-free case were bound change into resonances. And for an infinite system parts of the system will be exposed to a divergent field. On the other hand, for crystalline systems it has been found [16] that the polarization is a bulk property, i.e., is accessible by considering a single unit cell. This can, e.g., be done through the Berry-phase formulation of polarization (see, e.g., [17]). Moreover, finite-chain calculations have indicated [18, 20] that the electron distribution for a chain exposed to a DC field is roughly periodic far away from the boundaries, suggesting that a periodic-chain treatment should be possible. This is what we shall address in this contribution. We shall discuss in detail a simple Hückel-like model that allows for detailed studies of also larger systems and that can give information on the consequences of the different approximations that have been proposed for including an external DC field for an infinite, periodic polymer. Subsequently, we shall present a method for including a

DC field in a parameter-free electronic-structure method, and finally we shall present some results using this approach. For the sake of completeness we mention that some preliminary results have presented previously [19].

We finally mention that one further reason for studying infinite, periodic polymers in external DC fields is the findings [20, 21, 22] that currently applied approximate density-functionals (like the one we are using) may be inadequate when calculating responses to external DC fields. Thus, studies like the ones of this contribution may provide further insight into the failures of the functionals. On the other hand, we stress that our basic method is, in principle, not dependent on these problems and can be modified easily according to new proposals for approximate density functionals.

2 General considerations and a simple Hückel-like model

For a single particle of mass m and charge q , moving in the potential $V(\vec{r})$ (e.g., from nuclei), that is being exposed to an external electro-magnetic field, the Hamilton operator becomes

$$\hat{H} = \frac{1}{2m} \left(\hat{\vec{P}} - \frac{q}{c} \vec{A} \right)^2 + V(\vec{r}) + qU(\vec{r}). \quad (4)$$

Here, c is the speed of light, and \vec{P} is the momentum conjugate to \vec{r} . The electric and magnetic fields are given by

$$\begin{aligned} \vec{E} &= \frac{\partial \vec{A}}{\partial t} - \vec{\nabla} U \\ \vec{B} &= \vec{\nabla} \times \vec{A}. \end{aligned} \quad (5)$$

Whereas \vec{E} and \vec{B} are physical and measurable quantities that are unique, this is not the case for \vec{A} and U and there is some arbitrariness in how these two are chosen, i.e., how the gauge is chosen.

In the electric-dipole approximation, valid for wavelengths of the field much larger than typical distances of the particle, \vec{A} is set equal to 0, giving

$$\hat{H} = \frac{\hat{p}^2}{2m} + V(\vec{r}) + qU(\vec{r}), \quad (6)$$

whereas in the Coulomb gauge, valid for the wavelength of the field being comparable with the typical distances for the particle, U is set to 0, giving

$$\hat{H} = \frac{1}{2m} \left(\hat{\vec{P}} - \frac{q}{c} \vec{A} \right)^2 + V(\vec{r}). \quad (7)$$

We shall here choose the electric-dipole approximation, but comment on the use of the Coulomb gauge below.

In order to explore the effects of further approximations, we shall study in some details the Hückel-like Hamiltonian

$$\hat{H} = \hat{H}_{\text{tb}} + \hat{H}_{\text{ext}} \quad (8)$$

where the last term is caused by the external field, described within the electric-dipole approximation.

The tight-binding part is given by

$$\hat{H}_{\text{tb}} = \sum_i \alpha_i \hat{c}_i^\dagger \hat{c}_i + \sum_i \beta_i (\hat{c}_{i+1}^\dagger \hat{c}_i + \hat{c}_i^\dagger \hat{c}_{i+1}). \quad (9)$$

Here, we have assumed that we have one orbital per site (labeled χ_i with i being the site) and that \hat{c}_i and \hat{c}_i^\dagger are the corresponding annihilation and creation operators. Moreover,

$$\langle \chi_j | \hat{H}_{\text{tb}} | \chi_k \rangle = \begin{cases} \alpha_j & \text{for } j = k \\ \beta_j & \text{for } k = j + 1 \\ \beta_k & \text{for } k = j - 1 \\ 0 & \text{otherwise.} \end{cases} \quad (10)$$

We will assume that the external field only affects the diagonal elements,

$$\hat{H}_{\text{ext}} = \sum_i E_i \hat{c}_i^\dagger \hat{c}_i. \quad (11)$$

We will assume that the system has one electron per site, that the on-site energies α_i are site-independent (and accordingly can be set equal to 0), and that β_i alternates between $t_- = 0.5$ and $t_+ = 1.5$. For an infinite periodic chain without the external field we will accordingly have an occupied band between -2 and -1 , a gap between -1 and $+1$, and an unoccupied band between $+1$ and $+2$. These numbers can be used in estimating the strength of a field above which the calculations become meaningless. Considering a finite system with N sites and letting $E_i = Eia/2$, the N th atom experiences

a potential of roughly $NEa/2$ higher than the 1st atom does. If this value is larger than the gap, electrons will start flowing from one end of the system to the other. In order to avoid this run-away solution, we must require $E < 4|t_+ - t_-|/(aN)$. Therefore, we have chosen the fairly large value of the hopping-integral alternation. Another reason is that calculations for a similar model [18] have shown that the polarizability per site converges the faster as a function of chain length the larger the hopping-integral alternation is.

We shall now use this model in studying different approximations. We set

$$E_i = (i - M)Ea/2 \quad (12)$$

($a/2$ is the average interatomic distance) and consider a chain of $2M$ sites with periodic boundary conditions, i.e., in effect we assume that atom 1 and atom $2M$ are bonded, too. A very special case is that of $2M = 2$, where we accordingly assume that the external potential has the periodicity of the lattice. For larger values of $2M$ the approximation is that of assuming that the potential has the shape of a sawtooth curve with the periodicity being that of the Born von Kármán zone. I.e., the approximation is equivalent to considering an infinite, periodic system for which an electronic-structure calculation is been performed using M equidistant k points in the first Brillouin zone. Proposing that the external potential due to the field should have this periodicity is not new [23, 24], and in fact Resta [25] has shown that one **has** to use an operator with the periodicity of the Born von Kármán zone.

These approximations are schematically illustrated in Fig. 1.

Otto [26] and later Kudin and Scusseria [27] realized that the major problem for directly including the field in an electronic-structure calculation is related to the fact that the field destroys the periodicity. On the other hand, as mentioned above, both mathematical arguments and actual calculations have found that the charge distribution inside an extended system remains periodic also in the presence of an external field. Therefore, Otto sought a separation of the form

$$\hat{H}_{\text{ext}} = \hat{H}'_{\text{ext}} + \hat{H}''_{\text{ext}}, \quad (13)$$

where the first term has the periodicity of the lattice and the second is a remainder. Then, only the first term is kept. We stress that this separation may be rather arbitrary (one may add any lattice-periodic term to \hat{H}'_{ext} when simultaneously subtracting it from \hat{H}''_{ext}).

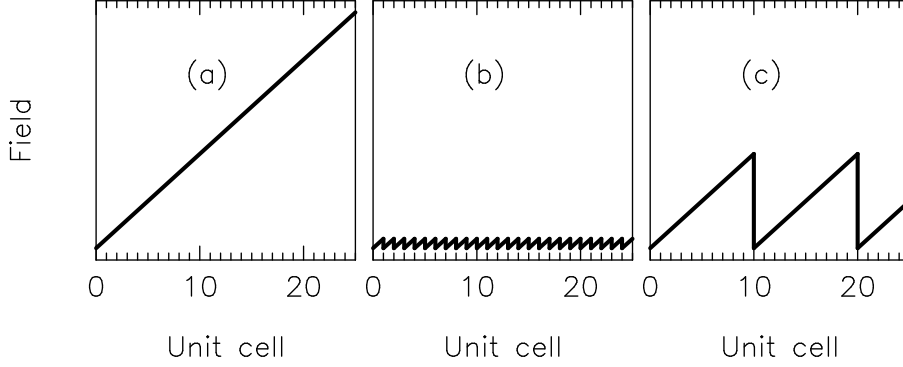


Figure 1: Schematic representation of the external field for (a) a finite system with the true field, (b) the approximation that the field has the periodicity of the lattice, and (c) that it has the periodicity of the Born von Kármán zone.

According to Bloch, in the absence of the external field any orbital is a Bloch wave of the form

$$\psi_n^{\vec{k}}(\vec{r}) = e^{i\vec{k}\cdot\vec{r}} u_n^{\vec{k}}(\vec{r}) \quad (14)$$

where n is a band index, and $u_n^{\vec{k}}$ is lattice-periodic. Then

$$\vec{r}\psi_n^{\vec{k}}(\vec{r}) = ie^{i\vec{k}\cdot\vec{r}} \vec{\nabla}_{\vec{k}} e^{-i\vec{k}\cdot\vec{r}} \psi_n^{\vec{k}}(\vec{r}) - i\vec{\nabla}_{\vec{k}} \psi_n^{\vec{k}}(\vec{r}). \quad (15)$$

By neglecting the second term, only a lattice-periodic term is kept. Maybe the most important problem of this approach is that it is closely tied to the precise definition of the orbitals, Eq. (14), so that different definitions of the Bloch waves lead ultimately to different definitions of \hat{H}'_{ext} . In order to demonstrate this in detail we shall study our simple Hückel model.

For this model and for a ring of $2M$ sites the Bloch functions for the two bands are given by

$$\psi_n^k = \frac{1}{\sqrt{2M}} \sum_{m=1}^M (\chi_{2m-1} \pm e^{i\phi(k)} \chi_{2m}) e^{ikam} e^{i\theta_n(k)}, \quad (16)$$

where a is the length of one unit cell, $e^{i\theta_n(k)}$ is an, in principle, arbitrary k - and band-dependent phase factor, and

$$e^{i\phi(k)} = \sqrt{\frac{t_+ + t_- e^{ika}}{t_+ + t_- e^{-ika}}}. \quad (17)$$

By using that we have assumed that only on-site overlap matrix elements are non-zero, and that the electrostatic field gives non-zero matrix elements only for orbitals on the same atom, we obtain after some manipulations

$$\begin{aligned}
i\langle\psi_{n_1}^{k_1}|e^{ik_2z}\frac{\partial}{\partial k_2}|e^{-ik_2z}\psi_{n_2}^{k_2}\rangle &= -\frac{1}{2M}\sum_m\langle(\chi_{2m-1}\pm e^{i\phi(k_1)}\chi_{2m})|(am-z) \\
&\quad\times(\chi_{2m-1}\pm e^{i\phi(k_2)}\chi_{2m})\pm e^{i\phi(k_2)}\phi'(k_2)\chi_{2m} \\
&\quad+\theta'_{n_2}(k_2)(\chi_{2m-1}\pm e^{i\phi(k_2)}\chi_{2m})\rangle \\
&\quad\times e^{ia(k_2-k_1)m}e^{i(\theta_{n_2}(k_2)-\theta_{n_1}(k_1))} \\
&= \delta_{k_1,k}\delta_{k_2,k}\left[\frac{1}{2}\langle\chi_1|z-a|\chi_1\rangle\pm\frac{1}{2}\langle\chi_2|z-a|\chi_2\rangle\right. \\
&\quad\left.\mp\frac{1}{2}\phi'(k)\langle\chi_2|\chi_2\rangle-\frac{1}{2}\theta'_{n_2}(k)(\langle\chi_1|\chi_1\rangle\pm\langle\chi_2|\chi_2\rangle)\right] \\
&\quad\times e^{i(\theta_{n_2}(k_2)-\theta_{n_1}(k_1))} \\
&= \delta_{k_1,k}\delta_{k_2,k}e^{i(\theta_{n_2}(k)-\theta_{n_1}(k))}\left[-\frac{a}{4}-\frac{Ma}{4}(1\pm 1)\right. \\
&\quad\left.\mp\frac{1}{2}\phi'(k)-\frac{1}{2}\theta'_{n_2}(k)(1\pm 1)\right] \tag{18}
\end{aligned}$$

when using that $\langle\chi_p|z|\chi_p\rangle=(p-M)a/2$. Moreover, in the first right-hand side, we choose the same (different) sign in the expressions for the bra and the ket if $n_1=n_2$ ($n_1\neq n_2$), whereas the upper (lower) sign is used when $n_1=n_2$ ($n_1\neq n_2$) in the subsequent expressions.

This is the term that is kept in the approach by Otto. The one that is neglected is

$$\begin{aligned}
-i\langle\psi_{n_1}^{k_1}|\frac{\partial}{\partial k_2}|\psi_{n_2}^{k_2}\rangle &= \frac{1}{2M}\sum_m\langle(\chi_{2m-1}\pm e^{i\phi(k_1)}\chi_{2m})|am(\chi_{2m-1}\pm e^{i\phi(k_2)}\chi_{2m}) \\
&\quad\pm e^{i\phi(k_2)}\phi'(k_2)\chi_{2m}+\theta'_{n_2}(k_2)(\chi_{2m-1}\pm e^{i\phi(k_2)}\chi_{2m})\rangle \\
&\quad\times e^{ia(k_2-k_1)m}e^{i(\theta_{n_2}(k_2)-\theta_{n_1}(k_1))} \\
&= e^{i(\theta_{n_2}(k_2)-\theta_{n_1}(k_1))}\left[\delta_{k_1,k}\delta_{k_2,k}\frac{1}{2}((1\pm 1)\theta'_{n_2}(k)\pm\phi'(k))\right. \\
&\quad\left.+(1\pm e^{i(\phi(k_2)-\phi(k_1))})\frac{a}{2M}\sum_m me^{iam(k_2-k_1)}\right]. \tag{19}
\end{aligned}$$

It is clear that the term neglected by Otto has contributions also from $k_1=k_2$. Moreover, what is considerably more problematic, the separation into what

is kept and what is ignored depends on the phase factors, which often in a practical calculation are out of control. It is also clear that the largest term that is being ignored is comparable to the largest term that is being kept.

When adding the expressions from Eqs. (18) and (19), one obtains

$$\langle \psi_{n_1}^k | \vec{r} | \psi_{n_2}^k \rangle = e^{i(\theta_{n_2}(k) - \theta_{n_1}(k))} \left[-\frac{a}{4} + \delta_{n_1, n_2} \frac{a}{2} \right], \quad (20)$$

i.e., the unsatisfactory dependence on the phase factors is canceled, except as understandable general pre-factors. One may invert Eq. (16), thereby writing the atom-centered basis functions in terms of the Bloch functions. Subsequently, Eqs. (18) and (19) can be used in identifying $\langle \chi_{m_1} | \hat{H}' | \chi_{m_2} \rangle$. Not surprising, it turns out that also this depends on the phase factors.

Alternatively, one may base the discussion on the Bloch waves constructed from the atom-centered basis functions,

$$\begin{aligned} \chi_1^k &= \frac{1}{\sqrt{M}} \sum_{m=1}^M \chi_{2m-1} e^{ikam} \\ \chi_2^k &= \frac{1}{\sqrt{M}} \sum_{m=1}^M \chi_{2m} e^{ikam}, \end{aligned} \quad (21)$$

whereby

$$i \langle \chi_{n_1}^{k_1} | e^{ik_2 z} \frac{\partial}{\partial k_2} | e^{-ik_2 z} \chi_{n_2}^{k_2} \rangle = \begin{cases} -\frac{(M+1)a}{4} \delta_{k_1, k_2} & \text{for } n_1 = n_2 = 1 \\ -\frac{Ma}{4} \delta_{k_1, k_2} & \text{for } n_1 = n_2 = 2 \\ 0 & \text{otherwise} \end{cases} \quad (22)$$

and

$$-i \langle \chi_{n_1}^{k_1} | \frac{\partial}{\partial k_2} | \chi_{n_2}^{k_2} \rangle = \begin{cases} \frac{a}{M} \sum_{m=1}^M m e^{ia(k_2 - k_1)m} & \text{for } n_1 = n_2 \\ 0 & \text{otherwise.} \end{cases} \quad (23)$$

This case corresponds actually to the separation of Fig. 5, to be discussed below, and when only keeping the term \hat{z}_1 that then replaces \hat{H}'_{ext} .

Returning to Eqs. (4) and (5), an electrostatic term may be described in the electric-dipole approximation through

$$\begin{aligned} U &= -\vec{E}_0 \cdot \vec{r} \\ \vec{A} &= \vec{0} \end{aligned} \quad (24)$$

or, alternatively, in the Coulomb gauge through

$$\begin{aligned} U &= 0 \\ \vec{A} &= t \cdot \vec{E}_0. \end{aligned} \quad (25)$$

The latter case involves a potential that is spatially invariant and, accordingly, attractive from a computational point of view. This was the original idea of Genkin and Mednis [14] that recently was taken up by Kirtman *et al.* [28, 29]. Since the Coulomb gauge is based on a time-dependent external (vector) potential, the solutions become time-dependent, but as argued by Genkin and Mednis they can be written as (time-dependent) Bloch waves characterized by

$$\vec{\kappa} = \vec{k} + \frac{e}{c}\vec{A}(t) \quad (26)$$

with $-e$ being the electronic charge. [Notice that for a polymer, $\vec{k} = (0, 0, k)$, when assuming that the polymer axis is the z axis]. Thus, the Bloch functions (either in form of Bloch waves constructed from a set of atom-centered basis functions, which is the case in the approach of Kirtman *et al.*, or in form of the exact solutions for the field-free case, which is used by Genkin and Mednis) can be used in studying the case of an external field. Then, one has to study matrix elements between different Bloch waves and the perturbing operator, which, it turns out, is \vec{r} . For this, they arrive ultimately at an expression like Eq. (13), and also they obtain

$$\hat{H}'_{\text{ext}} = ie^{i\vec{k}\cdot\vec{r}}\vec{\nabla}_{\vec{k}}e^{-i\vec{k}\cdot\vec{r}}. \quad (27)$$

This result was based partly on earlier arguments by Blount [30] who discussed how to represent \vec{r} for infinite, periodic crystals. Since this discussion is of fundamental importance to the present study we shall reproduce it here with some modifications that take into account the procedures of performing band-structure calculations for a polymer.

Usually, a band-structure calculation for a polymer that is considered periodic in the z direction is performed by considering a discrete, equidistant set of k points,

$$\frac{ka}{\pi} = 0, \pm\frac{1}{K}, \pm\frac{2}{K}, \dots, \pm\frac{K-1}{K}, 1 \quad (28)$$

($M = 2K$). Then, all Bloch functions have the periodicity of the Born von Kármán zone, i.e., of the length $2K \cdot a$, with a being the length of one unit cell. With n being the band index, any function with this periodicity can be expanded in the Bloch functions,

$$f(\vec{r}) = \sum_k \sum_n \psi_n^k(\vec{r}) \cdot f_n^k = \sum_k \sum_n e^{ikz} u_n^k(\vec{r}) \cdot f_n^k. \quad (29)$$

With \hat{z} being the sawtooth representation of z , shown in Fig. 1(c), we consider functions that are in its domain, i.e., functions for which $\int_{\text{BvK}} |\hat{z}f(\vec{r})|^2 d\vec{r}$ exists (BvK denotes one Born von Kármán zone). Also $\hat{z}f(\vec{r})$ has the periodicity of the BvK zone and, accordingly,

$$\hat{z}f(\vec{r}) = \sum_k \sum_n \hat{z}u_n^k(\vec{r})e^{ikz}f_n^k. \quad (30)$$

In contrast to the discussion above, we shall now approach the situation of a real electronic-structure calculation where one does not use an infinite, continuous set of k points, but in most cases a finite set of equidistant points.

We define an operator $\hat{\Delta}$ that is acting on the function $f(\vec{r})$ but whose action is closely linked to the expansion of Eq. (29), i.e., to the definition of the Bloch functions ψ_n^k . Thus, we define $\hat{\Delta}$ through

$$\begin{aligned} \hat{\Delta}f(\vec{r}) &= \hat{\Delta} \left[\sum_k \sum_n \psi_n^k(\vec{r}) \cdot f_n^k \right] \\ &= \hat{\Delta} \sum_k f_k(\vec{r}) \\ &= \sum_k \hat{\Delta} f_k(\vec{r}) \\ &= \sum_k \frac{f_k(\vec{r}) - f_{k-\Delta k}(\vec{r})}{\Delta k}, \end{aligned} \quad (31)$$

with $\Delta k = \frac{\pi}{aK}$. Notice that in the limit of $\Delta k \rightarrow 0$, $\hat{\Delta}$ changes into the differential operator $\frac{\partial}{\partial k}$.

We then have

$$\begin{aligned} -i\hat{\Delta}f(\vec{r}) &+ ie^{ikz}\hat{\Delta}e^{-ikz}f(\vec{r}) \\ &= \frac{i}{\Delta k} \sum_k \sum_n \left\{ e^{ikz} [u_n^k(\vec{r})f_n^k - u_n^{k-\Delta k}(\vec{r})f_n^{k-\Delta k}] \right. \\ &\quad \left. - [\psi_n^k(\vec{r})f_n^k - \psi_n^{k-\Delta k}(\vec{r})f_n^{k-\Delta k}] \right\} \\ &= \frac{i}{\Delta k} [1 - e^{i\Delta kz}] \sum_k \sum_n \psi_n^k(\vec{r})f_n^k, \end{aligned} \quad (32)$$

where the first equality is obtained by using that $\hat{\Delta}$ is a linear operator. Only the second term on the left-hand side gives a non-zero contribution, suggesting to keep only this. Hence, in this case taking the limit $\Delta k \rightarrow 0$ one

obtains the first term on the right-hand side of Eq. (15) for \vec{r} acting on some function, except that the function has to be continuous in k and, accordingly, cannot be a Bloch function.

Some comments of caution are required here. First, as discussed also by Blount [30] and by Kirtman *et al.* [29], one has to be careful with the phases of the Bloch functions. Whereas these functions are continuous in \vec{r} space, this may not be the case in k space. Thus, when considering the limit $K \rightarrow \infty$ (i.e., $\Delta k \rightarrow 0$), it is important that the limit exists, i.e., that $\psi_n^k f_n^k$ is continuous and differentiable in k space. In that case, one may neglect the first term on the left-hand side and, accordingly, arrive at the approximation of Eq. (27). On the other hand, only in that limit the expression on the right-hand side corresponds to a Hermitean operator.

A special case occurs when inserting one of the Bloch functions as $f(\vec{r})$, i.e., choosing

$$f_n^k = \delta_{n,n_0} \delta_{k,k_0}. \quad (33)$$

Then

$$\begin{aligned} -i\hat{\Delta}f(\vec{r}) &= 0 \\ ie^{ikz}\hat{\Delta}e^{-ikz}f(\vec{r}) &= \frac{i}{\Delta k} \left[1 - e^{i\Delta kz} \right] \psi_{n_0}^{k_0}(\vec{r}). \end{aligned} \quad (34)$$

Eqs. (32) and (34) provide an approach for including \vec{r} (or, rather, z) directly in an electronic-structure calculation when using a finite, discrete set of k points. However, only in the limit of an infinite, continuous set, the true z is included, whereas for a discrete set, z is being replaced by

$$\hat{z} = \frac{i}{\Delta k} \left[1 - e^{i\Delta kz} \right] \quad (35)$$

that has the periodicity of the Born von Kármán zone, but is not Hermitean.

It shall be emphasized that the operator $\hat{\Delta}$ acts on a function that is expanded in terms of Bloch functions, and that the action is on the expansion coefficients and Bloch functions, specifically on their dependence on k , i.e., it depends strongly on the precise definition of the Bloch functions.

The situation is different when the function depends explicitly on k and this dependence is included in the action. This is, e.g., the case for the operators defined by Otto [26]. His formalism corresponds to define an operator $\hat{\Delta}'$ through

$$-i\hat{\Delta}'\psi_{n_0}^{k_0}(\vec{r}) = -\frac{i}{\Delta k} \left[\psi_{n_0}^{k_0}(\vec{r}) - \psi_{n_0}^{k_0-\Delta k}(\vec{r}) \right]$$

$$ie^{ikz} \hat{\Delta}' e^{-ikz} \psi_{n_0}^{k_0}(\vec{r}) = \frac{i}{\Delta k} \left[\psi_{n_0}^{k_0}(\vec{r}) - e^{i\Delta k z} \psi_{n_0}^{k_0 - \Delta k}(\vec{r}) \right]. \quad (36)$$

For this, the limits $\Delta k \rightarrow 0$ may exist, provided that the functions ψ_n^k are continuous and differentiable in k space. When only being interested in ‘integrated’ quantities (e.g., the sum of the operator acting on the different Bloch functions), Eqs. (34) and (36) give — when summed over all contributions — identical results. However, when considering the individual terms, for instance when including the term in the calculation of the orbital energies, this is not necessarily the case.

Kirtman *et al.* [28, 29] implemented this approach in an *ab initio* program for infinite, periodic polymers and calculated subsequently both linear and non-linear responses to external fields. The results were compared with similar results for finite oligomers of increasing size. The results of the two independent sets of calculations show a convincing agreement, suggesting that it is justified to ignore the formal problem above, although the mathematical rigor for this is lacking.

The discussion makes it obvious that it is a far from trivial problem how to treat \vec{r} in an actual calculation. Therefore, we decided to first study the Hückel-like model numerically, using two different approximations for \vec{r} . In one case we used the full potential of Fig. 1(c), whereas in the other case we considered only the periodic part of Fig. 1(b). As discussed above, the latter case corresponds to use the separation of Eqs. (13) and (15) applied on the Bloch waves formed by the basis functions (i.e., **not** the eigenfunctions).

Fig. 2 shows some of the results for the calculations. We considered a ring of 204 sites and the two approximations of Figs. 1(b) and (c) for different field strengths. Since the Hückel model assumes a set of atom-centered orthonormal basis functions, the coefficients to the eigenfunctions give directly information on the number of electrons on the different atoms. From the total number of electrons, depicted in the figure, it is immediately seen that, for the largest fields, the approximation of Fig. 1(c) leads to solutions where parts of the electrons flow from one end to the other, but in the middle part of the chain the two curves seem to be very similar. There are, however, also in this case minor differences that may be important. Thus, simply considering the number of electrons around atom number 101, we find this to be $1 \pm n$ with n being 0.00017, 0.00172, 0.01716, and 0.1687 for the sawtooth curve with the lattice periodicity and for the four different field strengths, respectively, whereas the sawtooth curve with the Born von Kármán periodicity gives n of 0.00018, 0.00182, 0.01821, and around 0.17, respectively, i.e.,

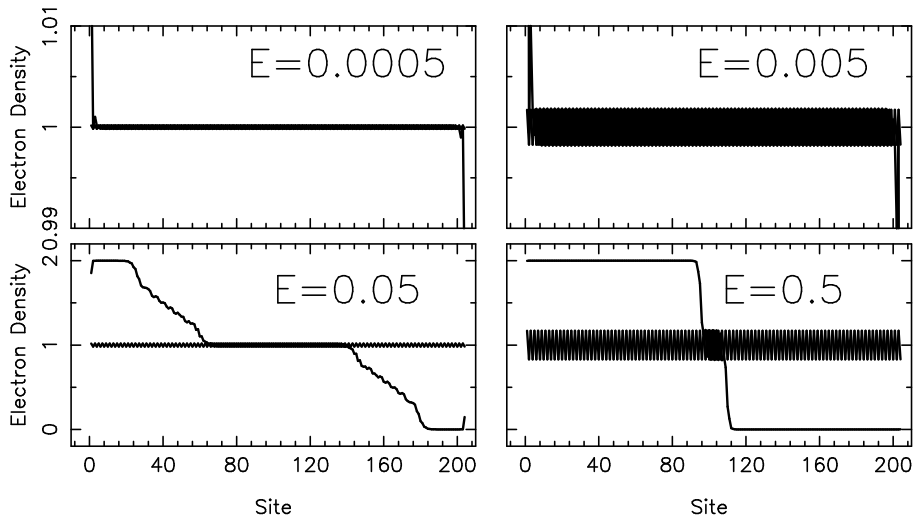


Figure 2: The number of electrons on the different atoms as found for the Hückel model with a ring of 204 sites exposed to an external field. The field strength is given on the figure, and the two curves in each panel corresponds to the two approximation of Figs. 1(b) and (c).

in general slightly larger.

When looking at the variation of the total energy as a function of field strength (Fig. 3), it is clear that also this depends on the approximation. First, as Fig. 3(a) shows, the energy changes dramatically for field strengths exceeding the value where electrons start flowing from one end to the other (which happens earlier for the approximation of Fig. 1(c) than for that of Fig. 1(b)). But also for weaker fields, where the electronic distribution is essentially homogeneous throughout the system [cf. Fig. 3(b)], there are clear differences depending on how the system is treated and in general, the approximation of Fig. 1(c) gives a stronger field dependence of the total energy than the approximation of Fig. 1(b), and for the former the dependence increases as a function of system size, also for fairly large sizes.

3 A first-principles method for polymers

Ultimately, our goal is to include the effects of the external fields in a parameter-free ground-state calculation of the properties of an infinite, peri-

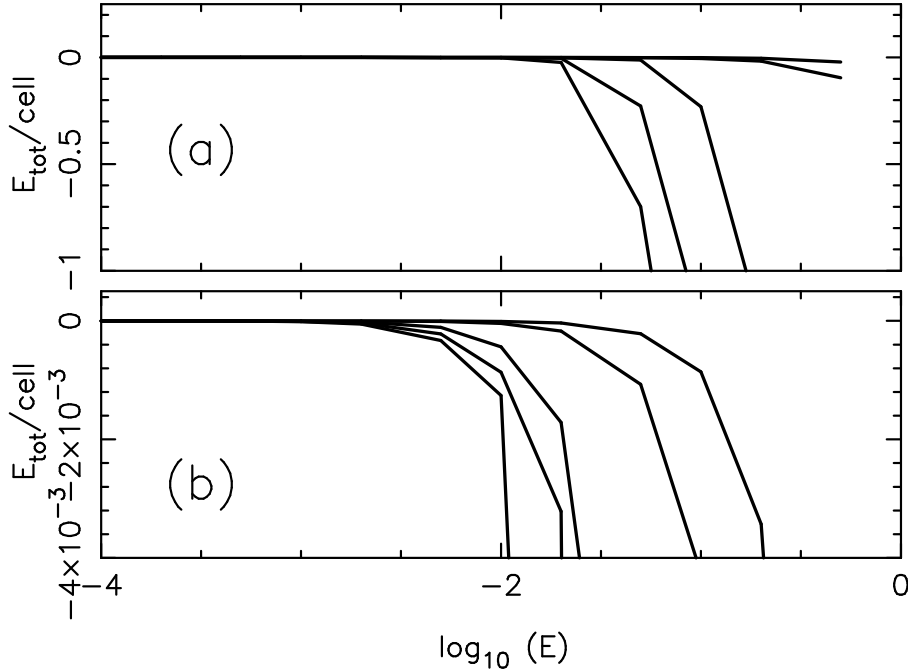


Figure 3: The total energy per two atoms as a function of field strength for the Hückel model with a ring of 12, 102, 204, and 306 sites (from below) with the sawtooth approximation of Fig. 1(c) together with the results for the same chains with the approximation of Fig. 1(b) (uppermost curve). The two panels differ in the scale of the ordinate.

odic polymer. To this end we apply our own density-functional method that has been described in detail elsewhere [31, 2] and, therefore, shall be only briefly discussed here.

The method is based on expanding the eigenfunctions to the Kohn-Sham equations in a basis set of LMTOs (Linearized Muffin-Tin Orbitals), which are represented numerically inside non-overlapping, atom-centered, so-called muffin-tin spheres and analytically in the interstitial region outside all spheres. The numerical functions are obtained by considering the spherically symmetric part of the potential inside the muffin-tin spheres and for this solving the Kohn-Sham equations numerically for an orbital energy (denoted ϵ_ν) that is in the energy range where the orbital has its largest support, leading to the atom- and angle-dependent basis function $\phi_{\vec{R},L}$ [L being a short-hand notation for (l, m)]. In addition we define the energy-derivative $\dot{\phi}_{\vec{R},L} = \frac{\partial}{\partial \epsilon_\nu} \phi_{\vec{R},L}$.

The analytical functions are decaying, spherical waves [i.e., spherical Hankel functions times harmonic functions, $h_l^{(1)}(|\vec{r}-\vec{R}|\kappa)Y_L(\widehat{r-R}) \equiv h_{\vec{R},L,\kappa}(\vec{r})$]. The functions are matched continuously and differentiably on the sphere boundaries. The basis functions $\chi_{\vec{R},L,\kappa}$ are accordingly eigenfunctions to a muffin-tin potential and, as such, good approximations to the true solutions to the Kohn-Sham equations. It shall, however, be stressed that the full potential is included in the calculations.

In our implementation of the method we consider infinite, periodic, isolated polymer chains. The periodicity is utilized in constructing Bloch functions from the basis functions of different unit cells,

$$\chi_{p,L,\kappa}^k = \lim_{N \rightarrow \infty} \frac{1}{\sqrt{2N+1}} \sum_{n=-N}^N \chi_{\vec{R}_{np},L,\kappa} e^{ik\pi n}, \quad (37)$$

where \vec{R}_{np} is the position of the p th atom in the n th unit cell. We let the z axis be the polymer axis.

The method has been applied to a number of conjugated polymers over the last almost two decades (see, e.g., [32]), and as a special application we also studied the case of chains exposed to an external electrostatic field perpendicular to the chain direction. Thereby, the periodicity was not destroyed and, accordingly, the basics of our approach could be kept unchanged.

As one example we show in Fig. 4 results for polycarbonitrile exposed to an external field perpendicular to the chain direction. Polycarbonitrile, $(\text{CHN})_x$, resembles trans polyacetylene but has every second CH group replaced by an N atom. In the figure we show both the band structures and the density of the highest occupied orbital of σ symmetry for different values of the field strength. The largest values, ± 0.05 hartree a.u., are very large compared to typical experimental conditions, so the results of the figure show that the perturbations on the electronic properties due to the field are small. This is an important result because this suggests that the orbitals, etc., calculated for the system without external fields provide good starting points for inclusion of the field. This we shall use.

We shall approximate the scalar potential of the electrostatic field by the sawtooth curve of Fig. 5 that has the periodicity of the Born von Kármán zone, i.e., of the length of one unit cell times the number of k points that is used in a calculation. We have here assumed that the potential takes both positive and negative values. By doing so, the average potential from the field vanishes and we have therefore an optimal starting point for eliminating

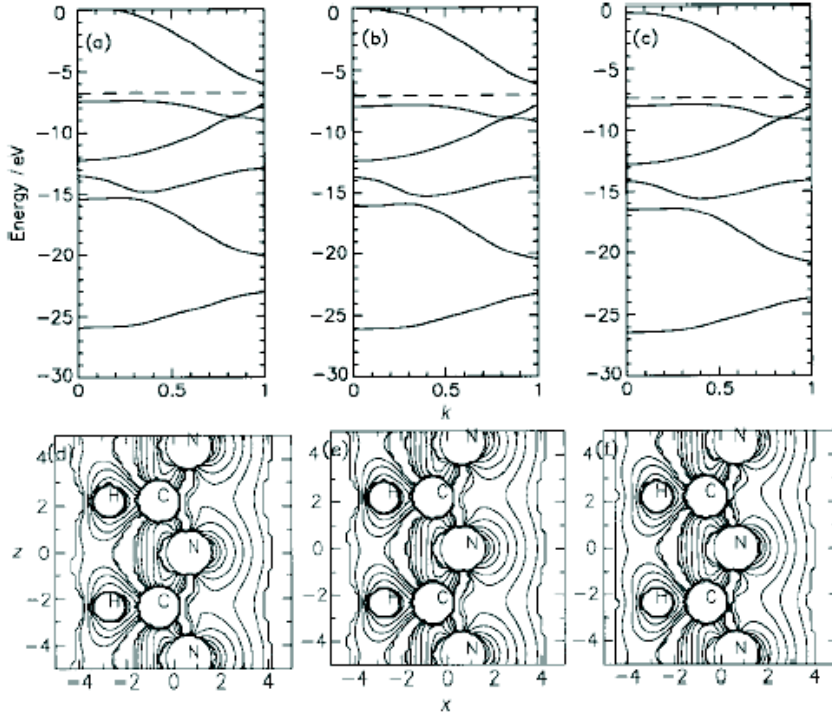


Figure 4: The (top) band structures and (bottom) electron density for the highest occupied orbital at $k = 0$ for polycarbonitrile $(\text{CHN})_x$ been exposed to an external DC field perpendicular to the chain direction but in the plane of the nuclei. The strength of the field is (left) -0.05 , (middle) 0 , and (right) $+0.05$ hartree atomic units.

effects that are linear in the number of k points of the calculation (i.e., in the length of the Born von Kármán zone).

In order to make use of the fact that the orbitals of the unperturbed system provide good approximations to those of the perturbed system, we construct Wannier functions from the Bloch orbitals of the unperturbed state. The Bloch functions are given through

$$\psi_n^k(\vec{r}) = \sum_{p,L,\kappa} c_{n;p,L,\kappa}^k \chi_{p,L,\kappa}^k(\vec{r})$$

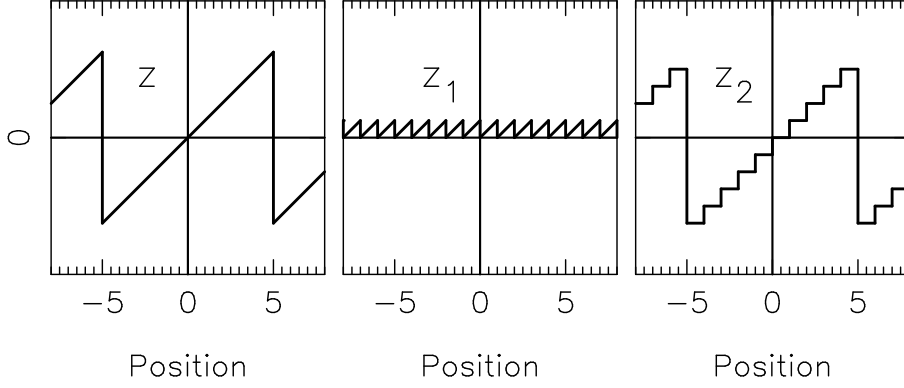


Figure 5: The left part shows the sawtooth curve \hat{z} that is periodic (and linear) with the periodicity of the Born von Kármán zone. It is decomposed into the lattice-periodic part of the middle part, and the piecewise constant part shown in the right part of the figure, $\hat{z} = \hat{z}_1 + \hat{z}_2$.

$$= \begin{cases} \sum_L \left[a_{n;p,L,\kappa}^k \phi_{\vec{R}_{0p},L}(\vec{r}) + b_{n;p,L,\kappa}^k \dot{\phi}_{\vec{R}_{0p},L}(\vec{r}) \right] \\ \sum_{p,L,\kappa} d_{n;p,l,\kappa}^k \lim_{N \rightarrow \infty} \frac{1}{\sqrt{2N+1}} \sum_{m=-N}^N h_{\vec{R}_{mp},L,\kappa}(\vec{r}) \end{cases} \quad (38)$$

where the first expression is valid for \vec{r} in sphere at \vec{R}_{0p} and the second is valid for \vec{r} in interstitial region.

Then, the Wannier functions are defined through

$$\begin{aligned} w_{lp}(\vec{r}) &= \frac{1}{\sqrt{2K}} \sum_k \psi_l^k(\vec{r}) e^{i\phi_l(k)} e^{-ik\pi p} \\ &= \lim_{N \rightarrow \infty} \frac{1}{\sqrt{2N+1}} \sum_{n=-N}^N \sum_{j,n,L,\kappa} w_{lp,jnL\kappa} \chi_{\vec{R}_{nj},L,\kappa}(\vec{r}) \\ &= \begin{cases} \sum_L \left[a_{lp;q,L,\kappa}^w \phi_{\vec{R}_{0q},L}(\vec{r}) + b_{lp;q,L,\kappa}^w \dot{\phi}_{\vec{R}_{0q},L}(\vec{r}) \right] \\ \sum_{p,L,\kappa} d_{lp;q,l,\kappa}^w \lim_{N \rightarrow \infty} \frac{1}{\sqrt{2N+1}} \sum_{m=-N}^N h_{\vec{R}_{mq},L,\kappa}(\vec{r}), \end{cases} \end{aligned} \quad (39)$$

where, once again, the first expression is valid for \vec{r} in sphere at \vec{R}_{0p} and the second is valid for \vec{r} in interstitial region. In addition, $e^{i\phi_l(k)}$ is a phase factor that can be chosen free (see below), and l is a band index. Moreover, the Wannier functions (that have the periodicity of the Born von Kármán zone) obey the important property

$$w_{l,p+1}(\vec{r}) = w_{lp}(\vec{r} - \vec{a}) \quad (40)$$

with \vec{a} being the lattice vector. A further property is that when the phase factors $e^{i\phi_l(k)}$ are chosen properly, the Wannier functions take the form of Eq. (29) with f_l^k being continuous and differentiable, so that the problems discussed at the end of the preceding section vanish.

Using the Wannier functions as basis functions in the electronic-structure calculation means writing any orbital as

$$\psi_i(\vec{r}) = \sum_{lp} c_{i,lp} w_{lp}(\vec{r}). \quad (41)$$

Inserting this expression into the Kohn-Sham equations means, ultimately, that we have to calculate matrix elements $\langle w_{l_1,p_1}(\vec{r}) | \hat{h}_{\text{eff}} | w_{l_2,p_2}(\vec{r}) \rangle$, where \hat{h}_{eff} is the effective Kohn-Sham operator, containing the kinetic-energy operator, the Coulomb potentials from the electrons and from the nuclei, the exchange-correlation potential in some approximation (e.g., a local-density or a generalized-gradient approximation), and, finally, the potential from the external electrostatic field,

$$\hat{h}_{\text{eff}} = -\frac{\hbar^2}{2m_e} \nabla^2 + V_C(\vec{r}) + V_n(\vec{r}) + V_{\text{xc}}(\vec{r}) + V_{\text{DC}}(\vec{r}). \quad (42)$$

Just as for the field-free case where we use the expansion of Eq. (38), the orbitals, and consequently also the electron density, is expressed in terms of the numerically given functions ϕ and $\dot{\phi}$ inside the muffin-tin spheres and in terms of the analytically given Hankel functions in the interstitial region. Accordingly, the calculation of the matrix elements for all parts of the Kohn-Sham operator except for V_{DC} proceeds just as in for the periodic, field-free case (see [31, 2]). Actually, it is useful to split \hat{h}_{eff} into

$$\hat{h}_{\text{eff}} = \hat{h}_{\text{eff}}^{(0)} + \Delta V_C(\vec{r}) + \Delta V_{\text{xc}}(\vec{r}) + V_{\text{DC}}(\vec{r}), \quad (43)$$

where $\hat{h}_{\text{eff}}^{(0)}$ is the self-consistent Kohn-Sham operator in the field-free case. When expressing the wavefunctions in terms of the Bloch waves of Eq. (38),

$$\langle w_{l_1,p_1} | \hat{h}_{\text{eff}}^{(0)} | w_{l_2,p_2} \rangle = \delta_{l_1,l_2} \frac{1}{2K} \sum_k \epsilon_{l_1}^k \cdot e^{i\pi k(p_2-p_1)} \quad (44)$$

with ϵ_l^k being the orbital energy of the Bloch wave ψ_l^k in the field-free case. Moreover,

$$\langle w_{l_1,p_1} | w_{l_2,p_2} \rangle = \delta_{l_1,l_2} \delta_{p_1,p_2}. \quad (45)$$

Thus, here we only need to discuss the treatment of V_{DC} . We may write

$$V_{\text{DC}}(\vec{r}) = E_x \cdot x + E_y \cdot y + E_z \cdot \hat{z}. \quad (46)$$

The first two terms do not break the translational symmetry and can fairly simply be incorporated into the calculations. The matrix elements can be calculated using the expression of the Wannier functions in terms of the Bloch functions, and subsequently performing the required integrals analytically in the interstitial region and numerically inside the spheres with expressions that are very similar to those we need for the other lattice-periodic parts of the potential (see, e.g., [31, 2]).

For \hat{z} we use the sawtooth function of Fig. 5. Then,

$$\begin{aligned} \langle w_{l_1 p_1} | \hat{z} | w_{l_2 p_2} \rangle &= \lim_{N \rightarrow \infty} \frac{1}{2N+1} \sum_{n_1, n_2 = -2NK+1}^{2NK} \sum_{j_1, j_2} \sum_{L_1, L_2} \sum_{\kappa_1, \kappa_2} w_{l_1 p_1, j_1 n_1 L_1 \kappa_1}^* \\ &\times w_{l_2 p_2, j_2 n_2 L_2 \kappa_2} \langle \chi_{\vec{R}_{n_1 j_1, L_1, \kappa_1}}(\vec{r}) | \hat{z} | \chi_{\vec{R}_{n_2 j_2, L_2, \kappa_2}}(\vec{r}) \rangle. \end{aligned} \quad (47)$$

We write

$$\hat{z} = \hat{z}_1 + \hat{z}_2, \quad (48)$$

where \hat{z}_1 has the periodicity of the lattice, and \hat{z}_2 that of the Born von Kármán zone (cf. Fig. 5). Then,

$$\begin{aligned} \langle w_{l_1 p_1} | \hat{z}_1 + \hat{z}_2 | w_{l_2 p_2} \rangle &= \frac{1}{2K} \sum_{k_1, k_2} \sum_{j_1, j_2} \sum_{L_1, L_2} \sum_{\kappa_1, \kappa_2} c_{l_1; j_1, L_1, \kappa_1}^{k_1 *} c_{l_2; j_2, L_2, \kappa_2}^{k_2} \\ &\times e^{i(\phi_{l_2}(k_2) - \phi_{l_1}(k_1))} e^{-i\pi(k_2 p_2 - k_1 p_1)} \langle \chi_{j_1, L_1, \kappa_1}^{k_1} | \hat{z} | \chi_{j_2, L_2, \kappa_2}^{k_2} \rangle. \end{aligned} \quad (49)$$

Here,

$$\begin{aligned} \langle \chi_{j_1, L_1, \kappa_1}^{k_1} | \hat{z} | \chi_{j_2, L_2, \kappa_2}^{k_2} \rangle &= \langle \chi_{j_1, L_1, \kappa_1}^{k_1} | \hat{z}_1 | \chi_{j_2, L_2, \kappa_2}^{k_2} \rangle + \langle \chi_{j_1, L_1, \kappa_1}^{k_1} | \hat{z}_2 | \chi_{j_2, L_2, \kappa_2}^{k_2} \rangle \\ &= \delta_{k_1, k_2} \lim_{N \rightarrow \infty} \sum_{n_1, n_2 = -N}^N e^{ik_1 \pi(n_2 - n_1)} \\ &\times \langle \chi_{\vec{R}_{j_1 n_1, L_1, \kappa_1}} | \hat{z}_1 | \chi_{\vec{R}_{j_2 n_2, L_2, \kappa_2}} \rangle_0 \\ &+ \lim_{N \rightarrow \infty} \frac{1}{2K} \sum_{n_1, n_2 = -N}^N \sum_{n = -K+1}^K e^{i\pi(k_2 n_2 - k_1 n_1)} \\ &\times \langle \chi_{\vec{R}_{j_1 n_1, L_1, \kappa_1}} | (n-1)a | \chi_{\vec{R}_{j_2 n_2, L_2, \kappa_2}} \rangle_0, \end{aligned} \quad (50)$$

where a is the length of the unit cell. Moreover, the subscript ‘0’ on the brackets indicates that the integration is to be taken over the reference unit cell, i.e., whereas x and y are unlimited, the z integration is over the interval of length a .

Since

$$\frac{1}{2K} \sum_{n=-K+1}^K (n-1)a = -\frac{a}{2}, \quad (51)$$

both expressions above can be evaluated by performing an integral over a z interval of length a together with infinite x and y integrations. Except for the basis functions, the integrand is z^m , with $m = 0$ and $m = 1$. We shall also add the integral for $m = 2$ of reasons to be explained below.

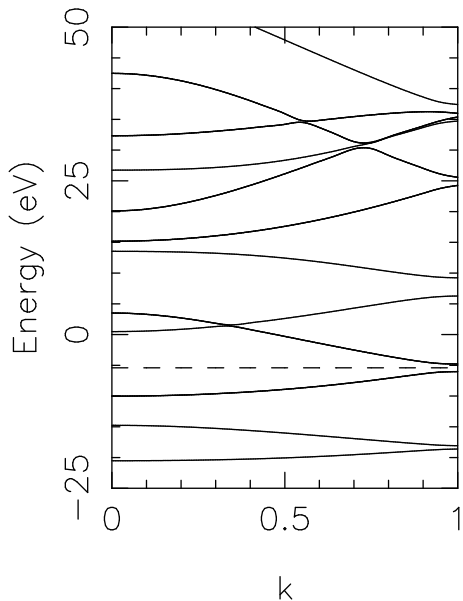


Figure 6: The band structures for a linear chain of carbon atoms with alternating bond lengths. $k = 0$ and $k = 1$ are the center and the edge of the first Brillouin zone, respectively, and the dashed line shows the Fermi level.

Starting with our field-free calculations we have implemented the calculations of these finite- z -interval integrals. It turned out that these were best performed numerically, also in the interstitial region where the basis functions are represented analytically. The reason is that the planar boundary of our integration region is only with great difficulties combined with our representation for the basis functions in spherical coordinates.

The reasons for adding $m = 2$ is that the phases $\phi_l(k)$ of the Wannier functions [cf. Eq. (39)] at best are determined by requiring that $\langle w_{lp}(\vec{r}) | (z - z_p)^2 | w_{lp} \rangle_0$ is maximized [30] (here, z_p is the z coordinate of the center of the p th unit cell).

We have applied this approach on a linear chain of carbon atoms with alternating bond lengths of 2.7 and 2.5 a.u. In Fig. 6 we show the band structures for this system without any external field. The calculations were done using 7 k points in half-part of the Brillouin zone, giving a Born von Kármán zone of 12 unit cells, each with two carbon atoms. Moreover, we included the 20 energetically lowest bands that all are shown in the figure (notice, however, that π and δ bands are pairwise degenerate) and, for the sake of simplicity, we applied a local-density approximation within density-functional theory.

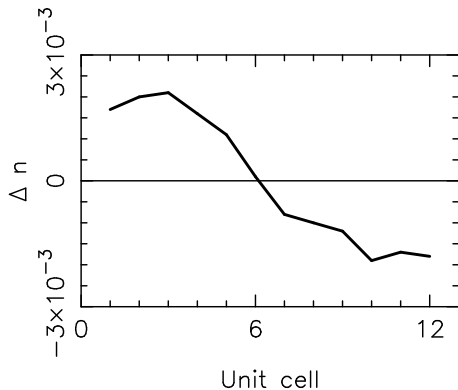


Figure 7: Changes in the number of electrons ascribed to the different unit cells for the field with the symmetry of the Born von Kármán zone and with a strength of $e \cdot E_z = 0.0002$ Hartree.

The occupied valence bands consist of two low-lying σ bands and a double degenerate π band just below the Fermi level. Also the lowest unoccupied band is of π symmetry. Thus, without the DC field the four energetically lowest valence bands are double occupied and all other bands are empty. We shall use this information below in quantifying the effects of the external DC field in different approximations, i.e., we shall analyse the occupation of the different bands as a function of band index. Moreover, in order to quantify the electronic distribution we shall use the number of electrons inside the muffin-tin spheres (with radii of 1.1 a.u.) for the 24 atoms per Born von

Kármán zone.

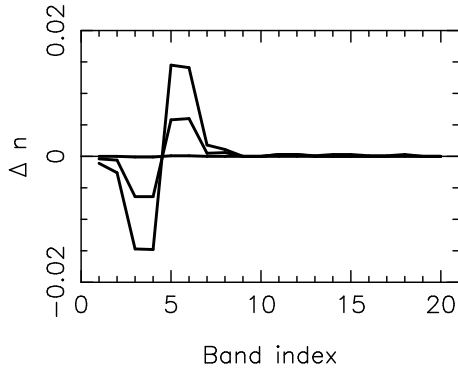


Figure 8: Changes in the number of electrons for the different bands relative to the numbers for the undistorted system (24 for the first 4 bands, and 0 for the remaining). The curves are (in order of decreasing amplitude) for field strengths of $e \cdot E_z = 0.0002$, 0.0005 , and 0.0002 Hartree for (the most oscillating curve) the case of the field with the symmetry of the Born von Kármán zone, and (the other curves) for the case that the field has the lattice periodicity.

We considered two approximate treatments of the DC field, i.e., one where we only included \hat{z}_1 of Fig. 5 and Eqs. (48)–(50), and another where the full sawtooth curve \hat{z} was included. Some representative results are shown in Figs. 7 and 8. Since the Wannier functions can be ascribed to individual unit cells, we show in Fig. 7 the number of electrons (relative to the number, 8, for the undistorted system) of each unit cell in the case that the field operator has the symmetry of \hat{z} of Fig. 5. As may not surprise, the electrons do show an asymmetric distribution, although the flow from one end of the Born von Kármán zone to the other is small. The number of electrons inside the muffin-tin spheres give also information on the electron redistributions. Thus, for $e \cdot E_z = 0.0002$ Hartree these numbers are 3.2403 and 3.2413 for the two carbon atoms per unit cell for the operator \hat{z}_1 of Fig. 5, and 3.2217 and 3.2575 for the operator \hat{z} . Here we also see a larger effect for \hat{z} than for \hat{z}_1 . However, for the \hat{z} all atomic spheres show the same numbers, so that the charge redistribution of Fig. 6 is restricted to the interstitial region.

For the undistorted system, the four lowest bands will contain each 24 electrons, whereas the higher-lying bands will contain 0 electrons. Turning on the field will lead to partial occupation of the higher-lying bands, and in

order to quantify this, we show in Fig. 8 the changes in the band occupancies due to the field both for the field with the operator given by \hat{z} in Fig. 5 and given by \hat{z}_1 of that figure. Two things are immediately clear: the significant changes occur for the bands closest to the Fermi level, giving support for basing the calculation on the Wannier functions, and the operator \hat{z} leads to significantly larger redistributions than the operator \hat{z}_1 does, once the field strength has been fixed.

Finally, also the total energy shows different behaviours depending on how the electric field is being treated. It turned out, however, that the calculations only with great difficulties could be stabilized against oscillations and, therefore, we refrain from presenting results for the total energy.

4 Conclusions

In this contribution we have concentrated on presenting some fundamental considerations concerning the theoretical treatment of an infinite, periodic, polymeric chain being exposed to an external electrostatic field. The analysis of a simple Hückel-like model revealed that only under certain circumstances one can base the discussion on Bloch functions and substituting \vec{r} with a derivative with respect to k . Thus, this was not the case when including the field directly in the calculations, but could, e.g., be used when using Wannier functions as basis functions which are continuous functions not only of \vec{r} but also of k .

Subsequently, we presented the general strategy for including the field in a self-consistent electronic-structure method for density-functional studies of infinite, periodic polymers and applied the method for a linear chain of carbon atoms. Here we found similar results, i.e., the response of the system to the external field was significantly stronger when the field was approximated by a sawtooth curve with the periodicity of the Born von Kármán zone than when it possessed the periodicity of the lattice. However, by analysing the occupancies of the band orbitals for different field strengths, we could see that our approach based on Wannier functions is healthy: the main changes occur for the orbitals closest to the Fermi level.

Finally, we stress that our study does not answer all questions. Thus, the fact that we use an approximate density functional in our parameter-free calculations may be one source of errors in the calculated quantities, although this problem is only marginally related to that of a proper treatment of the

external field in an electronic-structure method. Second, our method is still in its infancy and many tests are required before it can be established whether it is a useful approach. Third, we have presented a method for directly including a DC field in the calculations, whereas other approaches, based on perturbation theory, also allow for the treatment of AC fields. Our approach allows for an alternative control of the results of the latter in the limit of vanishing frequencies, but it still is an open question how the results can be used in improving the perturbation-theoretic approaches.

But, as has been the case with much of the work of Osvaldo Gosinski, science proceeds by proposing and trying new approaches. And in this spirit we close this contribution to the honour of Osvaldo Gosinski!

Acknowledgements

This work was supported by the German Research Council (DFG) through project Sp 439/11. One of the authors (MS) is grateful to Fonds der Chemischen Industrie for generous support. Moreover, the authors have benefitted very much from useful discussions with Bernie Kirtman.

References

- [1] M. Springborg, J.-L. Calais, O. Goscinski, and L. A. Eriksson, *Synth. Metals* **41–43**, 3309 (1991).
- [2] M. Springborg, J.-L. Calais, O. Goscinski, and L. A. Eriksson, *Phys. Rev. B* **44**, 12713 (1991).
- [3] B. Champagne and D. M. Bishop, *Adv. Chem. Phys.* **126**, 41 (2003).
- [4] H. Shirakawa, *Angew. Chem.* **113**, 2642 (2001).
- [5] A. G. MacDiarmid, *Angew. Chem.* **113**, 2649 (2001).
- [6] A. J. Heeger, *Angew. Chem.* **113**, 2660 (2001).
- [7] T. A. Skotheim, R. L. Elsenbaumer, and J. R. Reynolds (eds), *Handbook of Conducting Polymers* (Marcel-Dekker, New York, 1998).
- [8] I. D. W. Samuel, I. Ledoux, C. Dhenaut, J. Zyss, H. H. Fox, R. R. Schrock, and R. J. Silbey, *Science* **265**, 1070 (1994).
- [9] B. Champagne, D. H. Mosley, J. G. Fripiat, and J.-M. André, *Int. J. Quant. Chem.* **46**, 1 (1993).
- [10] D. Lu, B. Marten, M. Ringnalda, R. A. Friesner, and W. A. Goddard III, *Chem. Phys. Lett.* **257**, 224 (1996).
- [11] B. Champagne, D. Jacquemin, J.-M. André, and B. Kirtman, *J. Phys. Chem. A* **101**, 3158 (1997).
- [12] B. Champagne, E. A. Perpète, and J.-M. André, *J. Chem. Phys.* **101**, 10796 (1994).
- [13] D. H. Mosley, B. Champagne, and J.-M. André, *Int. J. Quant. Chem. Symp.* **29**, 117 (1995).
- [14] V. N. Genkin and P. M. Mednis, *Sov. Phys. JETP* **27**, 609 (1968) [*Zh. Eksp. Teor. Fiz.* **54**, 1137 (1968)].
- [15] Z. Shuai and J. L. Brédas, *Phys. Rev. B* **46**, 4395 (1992).
- [16] R. D. King-Smith and D. Vanderbilt, *Phys. Rev. B* **47**, 1651 (1993).

- [17] R. Resta, *Rev. Mod. Phys.* **66**, 899 (1994).
- [18] J.-M. André, J. Delhalle, and J.-L. Brédas, *Quantum Chemistry Aided Design of Organic Polymers* (World Scientific, Singapore, 1991).
- [19] Y. Dong and M. Springborg, *Synth. Met.* **135-136**, 349 (2003).
- [20] B. Champagne, E. A. Perpète, S. J. A. van Gisbergen, E.-J. Baerends, J. G. Snijders, C. Soubra-Ghaoui, K. A. Robins, and B. Kirtman, *J. Chem. Phys.* **109**, 10489 (1998).
- [21] M. van Faassen, P. L. de Boeij, R. van Leeuwen, J. A. Berger, and J. G. Snijders, *Phys. Rev. Lett.* **88**, 186401 (2002).
- [22] M. van Faassen, P. L. de Boeij, R. van Leeuwen, J. A. Berger, and J. G. Snijders, *J. Chem. Phys.* **118**, 1044 (2003).
- [23] K. Kunc and R. Resta, *Phys. Rev. Lett.* **51**, 686 (1983).
- [24] K. Schmidt and M. Springborg, *Phys. Chem. Chem. Phys.* **1**, 1743 (1999).
- [25] R. Resta, *Phys. Rev. Lett.* **80**, 1800 (1998).
- [26] P. Otto, *Phys. Rev. B* **45**, 10876 (1992).
- [27] K. N. Kudin and G. E. Scuseria, *J. Chem. Phys.* **113**, 7779 (2000).
- [28] B. Kirtman, F. L. Gu, and D. M. Bishop, *J. Chem. Phys.* **113**, 1294 (2000).
- [29] D. M. Bishop, F. L. Gu, and B. Kirtman, *J. Chem. Phys.* **114**, 7633 (2001).
- [30] E. I. Blount, *Solid State Phys.* **13**, 305 (1962).
- [31] M. Springborg and O. K. Andersen, *J. Chem. Phys.* **87**, 7125 (1987).
- [32] M. Springborg, *J. Mol. Struct. (Theochem)* **593**, 155 (2002).

THEORETICAL STUDY OF NANOSTRUCTURED HALO

Yi DONG, Michael SPRINGBORG

Physical Chemistry, University of Saarland, 66123 Saarbrücken, Germany

Using two unbiased methods for optimizing the structure together with a parameterized density-functional method we have calculated the structural and electronic properties of isolated $(\text{HAIO})_n$ clusters for n up to 26. The results include relative stability, interatomic distances, and overall shape. A main finding is that the hydrogen atoms form a surface layer on an AlO core where, in turn, only heteroatomic bonds are found. Subsequently, in order to study the properties of the macroscopic, nanoscaled HAIO material we also considered the properties of two interacting clusters that were optimized in the first part.

1. INTRODUCTION

Nanostructured materials have attracted interest of research for many years. An interesting material in this respect is layers of oxoaluminumhydride that can be produced in chemical-vapor-deposition experiment of aluminumhydride complexes on metal surfaces. The resulting nanostructured material contains various aluminum oxides, pure aluminum, as well as HAIO. This material can be used as a substrate for organized structures of organic molecules. However, except for the fact that HAIO is stoichiometric, very little is known about the structural and electronic properties of HAIO. Therefore, we decided to study the electronic and structural properties of HAIO. The very limited information on the material makes it a considerable challenge to study its properties with theoretical methods. Thus, a complete study should consider both isolated $(\text{HAIO})_n$ clusters as well as clusters that interact with each other and with other materials without essentially making any assumptions on the structure.

As a first step in this direction we shall here report results of our theoretical study of structural and electronic properties of isolated $(\text{HAIO})_n$ clusters with n up to 26 as well as of the interactions of two such clusters. In the determination of the structure we have used two largely unbiased approaches, so that we in many cases have had to perform extremely many total-energy calculations for a given value of n . This has only been possible by applying a parameterized electronic-structure method. This as well as our approaches for determining the structure shall be presented briefly in the next section. Subsequently, we present some of our main results both for the isolated clusters and for the interaction of two clusters. Our main findings are summarized in Sec. 4.

2. CALCULATIONAL METHOD

The calculations were performed using the parameterized, tight-binding, density-functional method of Seifert *et al.*¹⁻³ According to this method, the binding energy of a given compound with a given structure is written as a difference in the orbital energies of the compound minus those of the isolated energy, $\sum_i \epsilon_i - \sum_m \sum_i \epsilon_{mi}$ (with m being an atom index and i an orbital index), augmented with pair potentials, $\sum_{m_1 \neq m_2} U_{m_1, m_2}(|\vec{R}_{m_1} - \vec{R}_{m_2}|)$ (with \vec{R}_m being the position of the m th atom). In calculating the orbital energies we need the Hamilton matrix elements $\langle \chi_{m_1 n_1} | \hat{H} | \chi_{m_2 n_2} \rangle$ and the overlap matrix elements $\langle \chi_{m_1 n_1} | \chi_{m_2 n_2} \rangle$. Here, χ_{mn} is the n th atomic orbital of the m th atom. The Hamilton operator contains the kinetic-energy operator as well as the potential. The latter is approximated as a superposition of the potentials of the isolated atoms, $V(\vec{r}) = \sum_m V_m(|\vec{r} - \vec{R}_m|)$, and, subsequently, we assume that the matrix element $\langle \chi_{m_1 n_1} | V_m | \chi_{m_2 n_2} \rangle$ vanishes unless at least one of the atoms m_1 and m_2 equals m . With these approximations all relevant information on the above-mentioned matrix elements can be extracted from parameter-free density-functional calculations on isolated two-atomic systems, in our case on H_2 , HA , HO , Al_2 , AlO , and O_2 . Finally, the pair potentials U_{m_1, m_2} are obtained by requiring that the total-energy curves from parameter-free density-functional calculations on the diatomics are accurately reproduced.

In optimizing the structures of HAIO clusters, we have used two different, unbiased approaches, i.e., our own 'Aufbau' method as well as a method based on genetic algorithms. The only information we use is that HAIO is stoichiometric.⁴ With our 'Aufbau' method, that is closely related to our 'Aufbau/Abbau' method that we have used in optimizing the structure of large metal clusters,⁵ we start out optimizing the structure of a single HAIO molecule by choosing the structure of the lowest total energy from a very large number of calculations on randomly constructed structures that were allowed to relax to their closest total-energy minimum. Subsequently, we only assume that the structure of the cluster with $n + 1$ units can be obtained by adding one Al, one O, and one H atom to the cluster with n units. Thus, out of very many calculations where we randomly add those three atoms to the optimized structure of the cluster with n units (imposing only the constraints that the extra atoms should not be too close to any other atom or too far from all the other ones) we obtain an optimized structure of the system with $n + 1$ units. The resulting cluster of such a calculation is not with absolute certainty that of the global total-energy minimum, but, hopefully, a very good approximation to it.

Our other approach is based on the so-called genetic algorithms, which are based on the principles of natural evolution and are, therefore, also called evolutionary algorithms^{6,7}, and was

found to provide an efficient tool for global geometry optimizations. Our version of the genetic algorithms is as follows. Suppose that we have optimized the structure of the cluster with n units. From this structure we construct a first generation consisting of M independent clusters for the $(n - 1)$ -unit system by randomly adding one Al, one O, and one H atom and letting these structures relax to their nearest total-energy minima. Subsequently, a new set of clusters is constructed by cutting each of the M original ones randomly into two parts that are interchanged (under the constraints mentioned above) and, afterwards, allowed to relax. Out of the total set of $2M$ structures, the M ones of the lowest total energy are kept as the next generation. This procedure is repeated until the lowest total energy is unchanged for a large number of generations.

By comparing the results from the two sets of (independent) calculations, i.e., using the 'Aufbau' method and the genetic algorithms we have a possibility to check the reliability of each approach.

The material HAIO is nanostructured, i.e., is believed to consist of smaller 'clusters' that, however, are very close. This means that the properties of the individual clusters may to only a smaller extent be found for the nanostructured material. In order to obtain some first insights into the latter, we have also considered the consequences of putting two clusters together. I.e., we studied the system consisting of the cluster with n_1 and n_2 units that are placed at positions so close that they interact. Subsequently, they are allowed to relax. We select the structure of the lowest total energy from a large set of calculations where we have varied the relative orientations of the two clusters.

3. RESULTS AND DISCUSSION

We shall here present results of $(\text{HAIO})_n$ clusters that were optimized for n up to 26 using the 'Aufbau' method and up to 10 using the genetic-algorithms approach. In order to analyse the results we shall define radial distances r_i for the $3n$ atoms by first constructing the center of the cluster $\vec{R}_0 = \frac{1}{3n} \sum_{i=1}^{3n} \vec{R}_i$ from the positions \vec{R}_i of the atoms. Then, $r_i = |\vec{R}_i - \vec{R}_0|$.

In order to compare the results of the two types of structure optimizations we list in Table I a set of key quantities, including the total energies and two parameters that compare the structures. Here, $\Delta_r = \left[\frac{1}{3n} \sum_{i=1}^{3n} (r_i^{\text{auf}} - r_i^{\text{ga}})^2 \right]^{1/2}$ and $\Delta_R = \left[\frac{2}{3n(3n-1)} \sum_{i=1}^{3n(3n-1)/2} (R_i^{\text{auf}} - R_i^{\text{ga}})^2 \right]^{1/2}$, where $\{R_i\}$ are the interatomic distances, and where we have assumed that r_i and R_i have been sorted in increasing order. Finally, 'auf' and 'ga' refer to 'aufbau' method and genetic algorithms, respectively. From the table, we see that the energy minima from the two approaches are very close, and the structure difference is also very small. Accordingly, the two unbiased approaches

give almost the same structures of the HAIO clusters, making us believe that we have found the global total-energy minimum of the $(\text{HAIO})_n$ clusters, and that our approaches are reliable.

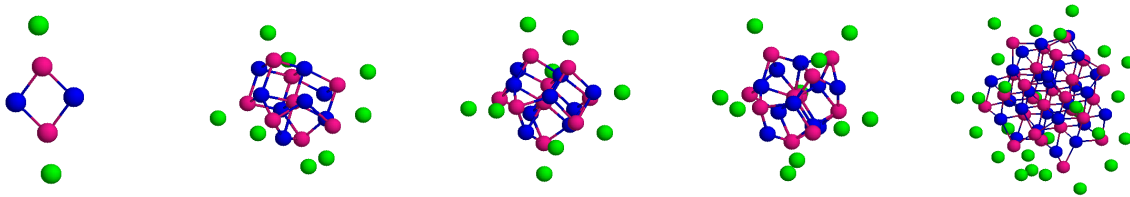


FIGURE 1

The structure of $(\text{HAIO})_n$ for $n= 2, 8, 9, 10,$ and 26 . The outer light spheres represent hydrogen atoms and the light and dark spheres of the inner parts represent aluminum and oxygen atoms, respectively.

The optimized $(\text{HAIO})_n$ clusters for $6, 24, 27, 30,$ and 78 atoms are shown in Fig. 1. The figure shows that the Al and O atoms form the inner part of the clusters, whereas the H atoms are only found on the surface of the clusters. Moreover, in the inner part we only find Al-O bonds and no Al-Al or O-O bonds, and on the surface the H atoms are only bonded to Al atoms.

In Fig. 2 we show the pair correlation functions $g_{AB}(R)$ for the cluster with $n = 2$ and $n = 26$. Here, $g_{AB}(R)$ is the number of A-B pairs with an interatomic distance of R . This figure shows the strong preference for Al-O and Al-H nearest neighbours both for the small and for the large clusters.

The overall shape of the clusters can be analysed as follows. We construct the matrix containing the moments of inertia relative to the center of the cluster and diagonalize this, subsequently. For simplicity we have not bothered about the difference masses of the three types of atoms. For a homogeneous sphere with $N = 3n$ atoms, the eigenvalues will be proportional to $N^{5/3}$, which is

n	2	3	4	5	6	7	8	9	10
$E_{\text{tot}}^{\text{auf}}$	-4.8238	-4.9275	-5.0673	-5.1190	-5.1892	-5.2367	-5.2892	-5.3377	-5.3795
$E_{\text{tot}}^{\text{ga}}$	-4.8238	-4.9275	-5.0673	-5.1190	-5.1914	-5.2376	-5.2908	-5.3396	-5.3762
Δ_r	0.00	0.01	0.00	0.00	0.47	0.44	0.16	0.13	1.38
Δ_d	0.00	0.00	0.00	0.00	0.30	0.20	0.075	0.01	2.00

TABLE I

The total energy in Hartree per unit for $(\text{HAIO})_n$ clusters as found with the ‘Aufbau’ method (second row) and the genetic algorithms (third row) together with the two parameters Δ_r and Δ_b (in a.u.) describing the difference in the structure.

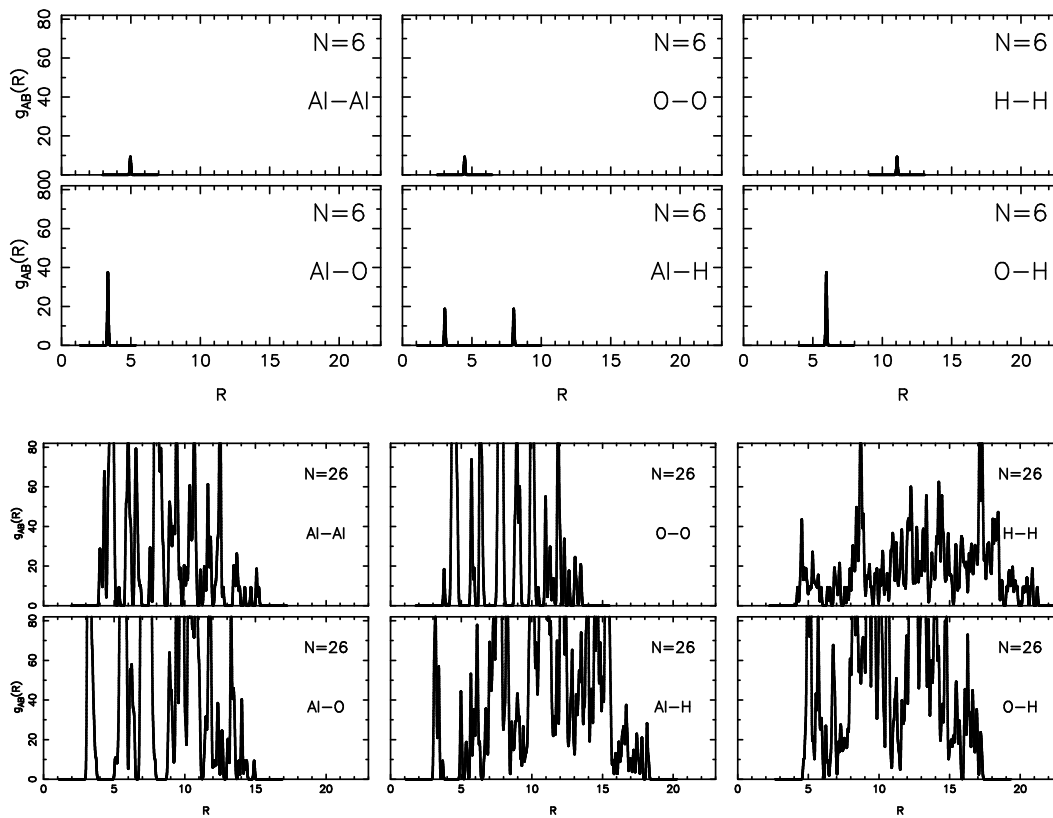


FIGURE 2

The pair-correlation functions (in arbitrary units) for (upper part) $n = 2$ and (lower part) $n = 26$ with R in a.u.

why we divide by this quantity. If all three eigenvalues are identical, the cluster has an overall spherical shape, whereas two large and one small eigenvalue results in an overall lens-like shape, and the third possibility gives an overall cigar-like shape. The results (cf. Fig. 3) shows that only one cluster ($n = 4$) has an overall spherical shape, whereas the two other structures both occur. On the other hand, the eigenvalues do not differ much from being identical so the clusters are close to be roughly spherical.

When we consider the cluster with $n + 1$ units it is highly relevant to study how similar it is to the one with n units, i.e., whether the larger can be considered as a result of a growth process starting with the smaller one. In order to study this question quantitatively, we define a similarity function as follows. We consider all those n -unit fragments of the $(n + 1)$ -unit cluster that can be obtained by removing one H, one Al, and one O atom. Subsequently, we calculate and sort all interatomic distances for this fragment $\{R'_{n+1,i}\}$. These are compared with the sorted interatomic distances $\{R_{n,i}\}$ for the n -unit system, i.e., we construct $\frac{3n(3n-1)}{2}q^2 = \sum_{i=1}^{n(3n-1)/2} (R'_{n+1,i} - R_{n,i})^2$. The smallest value of q , q_{\min} defines the similarity function $S = 1/(1 + q_{\min})$, which approaches 1 when the $(n + 1)$ -unit cluster is the n -unit cluster plus an extra unit. The results of Fig. 3 show that

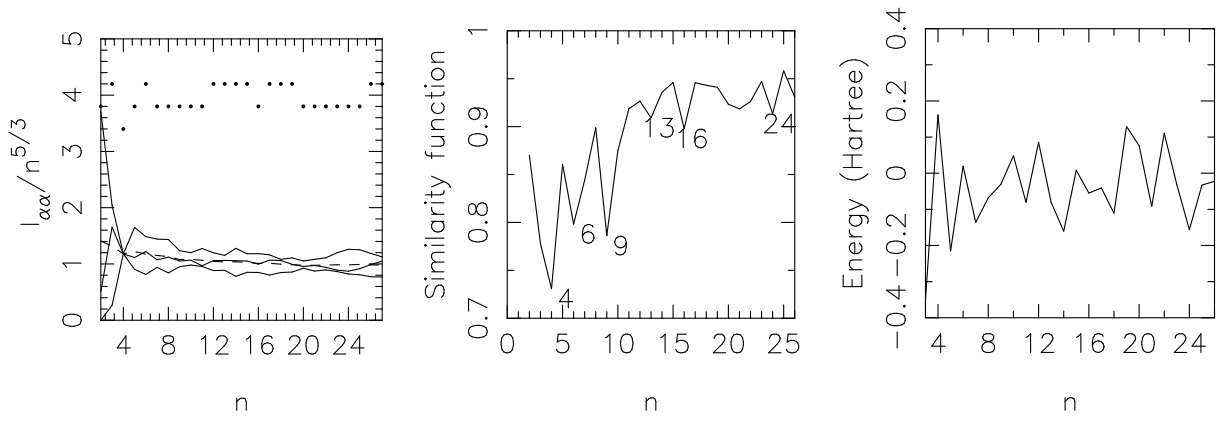


FIGURE 3

The (left part) eigenvalues of the matrix with the moments of inertia, (middle part) the similarity function, and (right part) the stability function. In the left part, the rows on the top indicate whether the cluster has an overall spherical shape (lowest row), a cigar-like shape (middle row), or a lens-line shape (upper row). The dashed line is the average of the three eigenvalues.

in particular for the smallest clusters this is certainly not the case, but also for the larger clusters (marked on the figure) structural changes occur that, actually, partly correlate with the changes in the overall shape as given by the left part of Fig. 3.

Finally, the stability of a given cluster can be analysed through the total energies, i.e., by using the stability function $\Delta_2(n) = E_{\text{tot}}(n+1) + E_{\text{tot}}(n-1) - 2E_{\text{tot}}(n)$. This functions, that has peaks for particularly stable clusters, is also shown in Fig. 3. The peak for $n = 4$ is clearly recognized, i.e., the highly symmetric cluster is also particularly stable.

n	n_1	n_2	$E_{\text{tot}}^{\text{com}}$	$E_{\text{tot}}^{\text{auf}}(n)$	$E_{\text{tot}}^{\text{ga}}(n)$	$E_{\text{tot}}^{\text{auf}}(n_1) + E_{\text{tot}}^{\text{auf}}(n_2)$	$E_{\text{tot}}^{\text{ga}}(n_1) + E_{\text{tot}}^{\text{ga}}(n_2)$
5	2	3	-25.5948	-25.5948	-25.5948	-24.4301	-24.4301
6	2	4	-31.0983	-31.1353	-31.1483	-29.9168	-29.9168
12	4	8	-64.9534	-65.2908		-62.5828	-62.5956
17	8	9	-94.0379	-94.6440		-90.3529	-90.3828

TABLE II

The total energy in Hartree for $(\text{HAIO})_n$ systems, where we have considered either interacting $(\text{HAIO})_{n_1}$ and $(\text{HAIO})_{n_2}$ clusters (giving the total energy denoted 'com') or an isolated, optimized $(\text{HAIO})_n$ cluster in comparison with the total energy of the two isolated, non-interaction clusters. 'auf' and 'ga' mark the results from the 'Aufbau' method and the genetic algorithms, respectively.

As mentioned above, the 'Aufbau' method and the genetic algorithms result in structures with all H atoms on the surface. When having a macroscopic, nanostructured materials, some H atoms will necessarily be confined to the inner parts of the complete system, which may result in different structures. In order to study such systems we considered two clusters of n_1 and n_2 units and

brought them so close that they would interact. Table II shows the total energies in comparison with those of the optimized clusters with $n = n_1 + n_2$ units. We see that the combined systems are considerably more stable than the two separate, non-interacting clusters, but, on the other hand, less stable than the optimized larger system.



FIGURE 4

From left to right: The structure of the $n = 6$ system in comparison with that of two interacting $n_1 = 2$ and $n_2 = 4$ systems, as well as the structures of the $n = 17$ system and that of interacting $n_1 = 8$ and $n_2 = 9$ systems.

Finally, Fig. 4 shows the structures of two of those systems (i.e., $n_1 + n_2 = 2 + 4$ and $n_1 + n_2 = 8 + 9$) together with the $n = 6$ and $n = 17$ unit systems. In this case it is clearly seen that the hydrogen atoms are placed between the two cores of AIO and from Table II we see that this structure is, although less stable than the completely optimized system of n unit, considerably stabler than the non-interacting system. Thus, our results lend support to the consensus that nanostructured HAIO consisting of interacting $(\text{HAIO})_n$ clusters is (meta-)stable with hydrogen sitting on the surface of the single clusters but between the different cluster.

4. CONCLUSIONS

In this work we have presented our unbiased approach for optimizing the structure of a complex material, HAIO, that has more types of atoms. By comparing the results of our ‘Aufbau’ method with those of the genetic algorithms we could argue that we have most likely identified the global total-energy minimum structures for $(\text{HAIO})_n$ clusters with n up to 26. Although our approach avoids having to search the complete structure space for each value of n , we had nevertheless to perform very many total-energy calculations for a given n , so that a parameterized density-functional method was considered the best choice for an electronic-structure method.

The most stable structure was found to be formed by a clusters with an AIO core containing only heteroatomic bonds and covered by a layer of H atoms. For the smallest clusters it was not possible to identify some growth pattern, but for the larger ones, the structure became more

regular. Very stable was the cluster for $n = 4$ that had an overall spherical shape.

Bringing two smaller clusters of n_1 and n_2 units together resulted in a united system only slightly less stable than the cluster of $n_1 + n_2$ units, but significantly more stable than the isolated, non-interacting parts. For the united system, the AlO cores were separated by H atoms. Thus, nanostructured HAIO may very likely consists of such $(\text{HAIO})_n$ clusters that are forced together in some (meta-)stable arrangement.

5. ACKNOWLEDGEMENTS

This work was supported by the SFB 277 at the University of Saarland. The authors are very grateful to Michael Veith for many useful discussions and to the Fonds der Chemischen Industrie for generous support.

REFERENCES

- 1) D. POREZAG, TH. FRAUENHEIM, TH. KÖHLER, G. SEIFERT, R. KASCHNER, Phys. Rev. B **51** (1995) 12947.
- 2) G. SEIFERT, R. SCHMIDT, New J. Chem. **16** (1992) 1145.
- 3) G. SEIFERT, D. POREZAG, TH. FRAUENHEIM, Int. J. Quant. Chem. **58** (1996) 185.
- 4) M. VEITH, private communication.
- 5) V. G. GRIGORYAN, M. SPRINGBORG, Phys. Chem. Chem. Phys. **3** (2001) 5125.
- 6) J. H. HOLLAND, Adaption in Natural Algorithms and Artificial Systems (University of Michigan Press, Ann Arbor, USA, 1975).
- 7) D. E. GOLDBERG, Genetic Algorithms in Search, Optimization and Machine Learning (Addison-Wesley, Reading, USA, 1989).

Structural and Electronic Properties of Nanostructured HAIO and AIO

Yi Dong,^{a1} Michael Springborg,^{a2} Markus Burkhardt,^{b3} and Michael Veith^{b4}

^aPhysical and Theoretical Chemistry
and ^bInorganic Chemistry
University of Saarland,
66123 Saarbrücken,
Germany

Received 10 July, 2005; accepted in revised form 10 July, 2005

Abstract: The results of theoretical studies of nanostructured HAIO and AIO are presented. We have considered isolated clusters, the interactions between two clusters, and two-dimensional layers. In most of the calculations we used a parameterized density-functional tight-binding method in the calculation of the electronic properties for a given structure, combined with two different unbiased approaches, i.e., an 'Aufbau' and a genetic-algorithm method, for optimizing the structure for clusters. The results for the isolated clusters are analyzed by means of similarity, stability, and shape parameters. Smaller structures were also studied with parameter-free DFT methods.

Keywords: Clusters, structure, stability, density-functional calculations

PACS: 36.40.-c, 36.90.+f, 61.46.+w, 73.22.-f

1 Introduction

HAIO is an interesting material that can be used as a substrate for organized structures of organic materials, but only little is known about its precise structure. Here, we shall show that theoretical studies can give useful information that ultimately turns out to extend and support the experimental information about it.

HAIO can be prepared either by CVD (chemical vapor deposition) at low temperatures as a thin glassy layer using the precursor bis-(*tert*-butoxyalane) $[\text{AlH}_2(\text{OtBu})_2]$ and various metals as target substrates [1, 2], or as an amorphous powdered nanostructured material by the reaction of different methylsiloxanes with the alane $\text{H}_3\text{Al-NMe}_3$ in either ether or aromatic solvents under mild conditions [3, 4].

The purpose of the present work is to obtain further information on HAIO by considering both finite clusters and infinite, periodic layers and ultimately present a proposal for the structure of the HAIO compounds. In agreement with experimental indications, we find that the HAIO clusters consist of an AIO core with H atoms on the surface. We shall therefore also consider isolated AIO clusters, here.

¹e-mail: y.dong@mx.uni-saarland.de

²Corresponding author. e-mail: m.springborg@mx.uni-saarland.de

³e-mail: m.burkhardt@mx.uni-saarland.de

⁴e-mail: veith@mx.uni-saarland.de

We studied theoretically the structural properties of the (HAIO) $_n$ clusters with n up to 26 using a density-functional-theory tight-binding method. This method can give the electronic properties for a given structure as well as determine a structure of a local total-energy minimum once an initial structure has been chosen. However, the method is not directly able to determine the structure of the global total-energy minimum. In order to search for that for the (HAIO) $_n$ clusters, we have used two unbiased approaches, i.e., a method we have called the ‘Aufbau’ method as well as genetic algorithms.

To verify the results of these methods we also performed parameter-free DFT calculations on smaller (HAIO) $_n$ units with $n = 1, 2, 3, 4, 6$. For each n we considered several different isomers, as well as calculated their vibrational spectra.

Since the experimentally produced nanostructured material is extended, it must contain nanostructures in close contact. Therefore, we also studied the interactions between pairs of optimized (HAIO) $_{n_1}$ and (HAIO) $_{n_2}$ clusters for different values of n_1 and n_2 . Finally, the fact that HAIO can be synthesized as a layer compound made us study infinite, periodic, two-dimensional layers of HAIO, too.

Finally, we also used the parameterized density-functional method together with the genetic algorithms in studying stoichiometric AIO clusters.

2 Theoretical Methods

For most of the calculations, we used the density-functional tight-binding method (DFTB) of Seifert and coworkers [5, 6]. With this method, the binding energy is written as the difference in the orbital energies of the compound minus those of the isolated atoms, i.e., as $\sum_i \epsilon_i - \sum_m \sum_i \epsilon_{mi}$ (with m being an atom index and i an orbital index), augmented with pair potentials, $\sum_{m_1 \neq m_2} U_{m_1, m_2} (|\vec{R}_{m_1} - \vec{R}_{m_2}|)$ (with \vec{R}_m being the position of the m th atom). In calculating the orbital energies we need the Hamilton matrix elements $\langle \chi_{m_1 n_1} | \hat{H} | \chi_{m_2 n_2} \rangle$ and the overlap matrix elements $\langle \chi_{m_1 n_1} | \chi_{m_2 n_2} \rangle$. Here, χ_{mn} is the n th atomic orbital of the m th atom. The Hamilton operator contains the kinetic-energy operator as well as the potential. The latter is approximated as a superposition of the potentials of the isolated atoms, $V(\vec{r}) = \sum_m V_m (|\vec{r} - \vec{R}_m|)$, and subsequently we assume that the matrix element $\langle \chi_{m_1 n_1} | V_m | \chi_{m_2 n_2} \rangle$ vanishes unless at least one of the atoms m_1 and m_2 equals m . Finally, the pair potentials U_{m_1, m_2} are obtained by requiring that the total-energy curves from parameter-free density-functional calculations on the diatomics are accurately reproduced.

Finally, we used the parameter-free, density-functional program package TURBOMOLE [7] for the smallest (HAIO) $_n$ clusters.

We used two different methods in determining the structures of the clusters.

In some of the calculations we used our own *Aufbau* method [8]. The method is based on simulating experimental conditions, where clusters grow by adding atom by atom to a core. By repeating this process **very** many times, we can identify the structures of the lowest total energy. Alternatively, we optimized the structures using the so-called genetic algorithms [8, 9, 10]. Here, from a set of structures we generate new ones through cutting and pasting the original ones. Out of the total set of old and new clusters those with the lowest total energies are kept, and this process is repeated until the lowest total energy is unchanged for a large number of generations.

3 Results for the (HAIO) $_n$ Clusters

First, we optimized the structure of (HAIO) $_n$ clusters with n up to 26 using our ‘Aufbau’ and with n up to 18 using the genetic-algorithms approaches, respectively. We define a radial distance \vec{r}_i for each of the $3n$ atoms as $r_i = |\vec{R}_i - \vec{R}_0|$, where \vec{R}_0 is the center of the cluster, $\vec{R}_0 = \frac{1}{3n} \sum_{i=1}^{3n} \vec{R}_i$. Fig. 1 shows the radial distance for the different clusters and atoms. The figure shows, for each

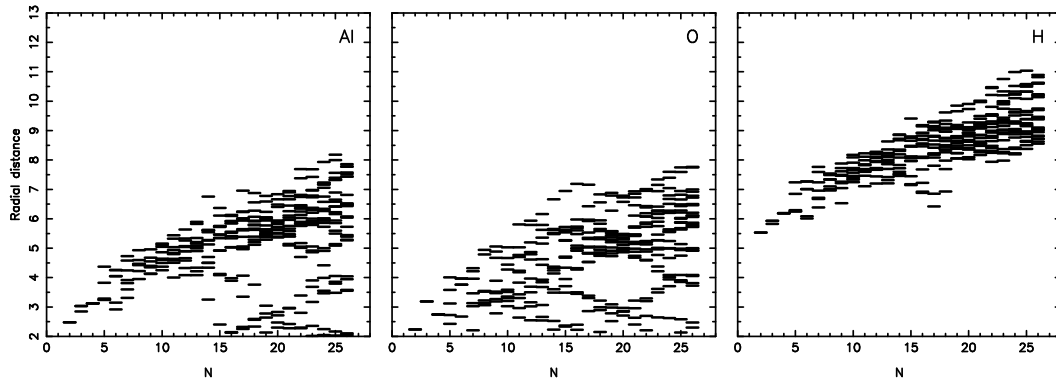


Figure 1: The radial distances (in a.u.) for Al, O, and H atoms, separately, as a function of the size of the cluster n for $(\text{HAIO})_n$ clusters. In each panel, a small horizontal line shows that at least one atom of the corresponding type has that distance to the center of the cluster for a given value of n .

type of atoms separately, the radial distances for the different values of n . It is very clear that the largest radial distances are found for H atoms and, in addition, that essentially all H atoms always have larger radial distances than the Al and O atoms. On the other hand, the central part of the clusters are clearly formed by both Al and O atoms.

Also the parameter-free DFT calculations on various (in total, 28) isomers of $(\text{HAIO})_6$ supports this consensus. For each of the 28 $(\text{HAIO})_6$ clusters we calculated the radial distances of the different atoms. Subsequently we plotted this as a function of the total energy per unit and show in Fig. 2 the results. When comparing the clusters of roughly the lowest total energies we see that Al and O are those atoms with smaller radial distances, whereas those of hydrogen are larger. For the higher total energies, the radial distances of Al and O show a weak tendency to increase and simultaneously those of H are slightly decreasing. In total this analysis confirms the tendency for the $(\text{HAIO})_n$ clusters to possess a Al-O core covered with H atoms.

By analysing the overall shape of the clusters we also found that there are particularly stable clusters (most pronounced for $n = 4$) for which the structure is roughly spherical.

4 Conclusions

The results of this study are unique as they have been obtained by using several different experimental and theoretical approaches independently of each other. By combining the results from all approaches, we have arrived at an unusually detailed picture of the structural properties of nanostructures HAIO despite the complications determining this directly in experimental studies.

All approaches indicate that nanostructured HAIO consists of subsystems with an AlO core covered by H atoms. This structure can, e.g., be obtained by keeping the $(\text{HAIO})_n$ clusters not too large, but, alternatively, also two-dimensional sheets HAIO can also satisfy these constraints. The calculations (not shown here) give indeed that also such sheets are stable with a binding energy comparable with that of the largest clusters considered here.

Finally, we stress that some of the conclusions could only be obtained after a careful analysis of the results of the calculations by means of special descriptors.

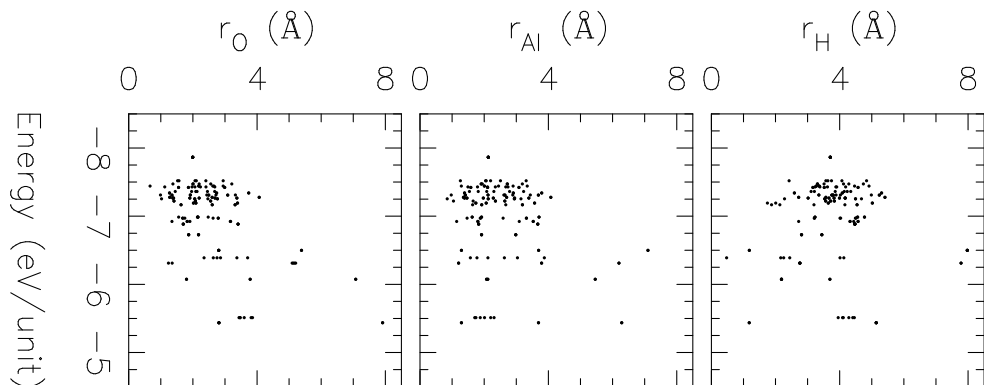


Figure 2: The radial distances for the different smaller clusters as function of the total energy per unit. The different panels show the different types of atoms. The results are from the DFT calculations for the $(\text{HAlO})_n$ clusters with $n = 1, 2, 3, 4, 6$.

Acknowledgment

We gratefully acknowledge *Fonds der Chemischen Industrie* for very generous support. This work was supported by the SFB 277 of the University of Saarland.

References

- [1] M. Veith, K. Andres, S. Faber, J. Blin, M. Zimmer, Y. Wolf, H. Schnöckel, R. Köppe, R. Masi, S. Hüfner, *Eur. J. Inorg. Chem.* **2003**, 4387 (2003).
- [2] M. Veith, K. Andres, *J. Metastable Nanocryst. Mater.* **15-16**, 279 (2003).
- [3] S. W. Liu, R. J. Wehmschulte, C. M. Burba, *J. Mater. Chem.* **13**, 3107 (2003).
- [4] S. W. Liu, J. Fookan, C. M. Burba, M. A. Eastman, R. J. Wehmschulte, *Chem. Mater.* **15**, 2803 (2003).
- [5] G. Seifert and R. Schmidt, *New J. Chem.* **16**, 1145 (1992).
- [6] G. Seifert, D. Porezag, and Th. Frauenheim, *Int. J. Quant. Chem* **58**, 185 (1996).
- [7] R. Ahlrichs, M. Bär, M. Häser, H. Horn, C. Kölmel, *Chem. Phys. Lett.* **162**, 165 (1989).
- [8] Y. Dong and M. Springborg, in *Proceedings of 3rd International Conference "Computational Modeling and Simulation of Materials"*, Ed. P. Vincenzini *et al.*, Techna Group Publishers, p. 167 (2004).
- [9] J.-O. Joswig, M. Springborg, and G. Seifert, *Phys. Chem. Chem. Phys.* **3**, 5130 (2001).
- [10] J.-O. Joswig and M. Springborg, *Phys. Rev. B* **68**, 085408 (2003).

Structural and Electronic Properties of Nanostructured HAIO

Yi Dong,^{‡,§} Markus Burkhardt,^{‡,||} Michael Veith,^{‡,⊥} and Michael Springborg^{*,†}

Departments of Physical and Theoretical Chemistry and of Inorganic Chemistry, University of Saarland, Postfach 15 11 50, D-66041 Saarbrücken, Germany

Received: July 18, 2005; In Final Form: October 3, 2005

The results of a theoretical study of the nanostructured ternary compound HAIO are presented. We have considered isolated (HAIO)_n clusters, the interactions between two such clusters, and two-dimensional layers of HAIO. In many of the calculations we used a parametrized density-functional tight-binding method in the calculation of the electronic properties for a given structure, combined with two different unbiased approaches, i.e., an “Aufbau” and a genetic-algorithm method, for optimizing the structure for clusters with *n* up to 26. The results for the isolated clusters are analyzed by means of similarity, stability, and shape parameters. Isolated structures with *n* up to 6 were also studied intensively with pure DFT methods.

I. Introduction

Theoretical studies on the structural and electronic properties of materials continue to constitute a useful complement to experimental studies, and often the combination of the two approaches gives more information than each of them separately could have contributed. In this work we shall present results of such a study for HAIO with, however, the main emphasis on the theoretical results, although we repeatedly shall make mention of experimental results.

The ternary compound HAIO is an interesting material that can be used as a substrate for organized structures of organic materials, but only little is known about its precise structure. Here, we shall show that theoretical studies can give useful information that ultimately turns out to extend and support the experimental information about it.

HAIO can be prepared either by CVD (chemical vapor deposition) at low temperatures as a thin glassy layer using the precursor bis(*tert*-butoxyalane), [AlH₂(*Ot*Bu)]₂, and various metals as target substrates,^{1,2} or as an amorphous powdered nanostructured material (with considerable content of bymaterial) by the reaction of different methylsiloxanes with the alane H₃Al·NMe₃ in either ether or aromatic solvents under mild conditions.^{3,4} The different preparation routes lead to materials that have similar infrared (IR) spectra, showing a distinctive absorption for the $\nu(\text{Al-H})$ stretching mode at 1925 cm⁻¹ (layer compound) and 1895–1929 cm⁻¹ (powder compound), respectively. Using angle-dependent reflection IR spectroscopy for the layer, a shoulder at 1670 cm⁻¹ becomes more prominent when the angle is decreased. This feature can be ascribed to bridging Al–H···Al entities.^{6,7} Annealing both layer and powder compound causes the hydride band in the IR spectrum to decrease in intensity. Furthermore, ²⁷Al{¹H} MAS NMR spectra show resonances for sixfold, fivefold, and fourfold (at 6, 30 and 58 ppm, respectively) coordinated aluminum species; XPS analysis of an HAIO film is consistent with these results.^{1,2}

The purpose of the present work is to obtain further information on HAIO by considering both finite clusters and infinite, periodic layers and ultimately present a proposal for the structure of the HAIO compounds.

We studied theoretically the structural properties of the (HAIO)_n clusters with *n* up to 26 using a density-functional-theory tight-binding method. This method can give the electronic properties for a given structure as well as determine a structure of a local total-energy minimum once an initial structure has been chosen. However, the method is not directly able to determine the structure of the global total-energy minimum. To search for that for the (HAIO)_n clusters, we have used two unbiased approaches, i.e., a method we have called the “Aufbau” method as well as genetic algorithms.

To verify the results of these methods, we also performed pure DFT calculations on smaller (HAIO)_n units with *n* = 1, 2, 3, 4, and 6. For each *n* we considered several different isomers, as well as the calculation of their vibrational spectra.

Since the experimentally produced nanostructured material is extended, it must contain nanostructures in close contact. Therefore, we also studied the interactions between pairs of optimized (HAIO)_{n₁} and (HAIO)_{n₂} clusters for different values of *n*₁ and *n*₂. Finally, the fact that HAIO can be synthesized as a layer compound made us study infinite, periodic, two-dimensional layers of HAIO, too.

The paper is organized as follows. In section II we describe details of the calculational methods that are used to study the HAIO clusters and layers. Subsequently, the results for isolated clusters are presented in section III, and in that section we also discuss the interaction between two clusters, as well as the properties of two-dimensional layers of HAIO. A brief summary of our conclusions is given in section IV. Finally, for the sake of completeness we mention that a brief account of parts of the present study was published previously.⁵

II. Computation Methods

A. Parametrized Density-Functional Method. Many of the calculations of the electronic properties for a given structure were performed using the parametrized tight-binding density-functional method of Seifert et al.^{8–10} According to this method, the relative total energy of a given compound with a chosen

* To whom correspondence should be addressed. E-mail: m.springborg@mx.uni-saarland.de.

[†] Department of Physical and Theoretical Chemistry.

[‡] Department of Inorganic Chemistry.

[§] E-mail: y.dong@mx.uni-saarland.de.

^{||} E-mail: m.burkhardt@mx.uni-saarland.de.

[⊥] E-mail: veith@mx.uni-saarland.de.

structure is written as the difference in the orbital energies of the compound minus those of the isolated atoms, i.e., as

$$\sum_i \epsilon_i - \sum_m \sum_i \epsilon_{mi} \quad (1)$$

(with m being an atom index and i an orbital index), augmented with pair potentials,

$$\sum_{m_1 \neq m_2} U_{m_1, m_2} (|\vec{R}_{m_1} - \vec{R}_{m_2}|) \quad (2)$$

(with \vec{R}_m being the position of the m th atom).

In calculating the orbital energies, we need the Hamilton matrix elements $\langle \chi_{m_1 n_1} | \hat{H} | \chi_{m_2 n_2} \rangle$ and the overlap matrix elements $\langle \chi_{m_1 n_1} | \chi_{m_2 n_2} \rangle$. Here, χ_{mn} is the n th atomic orbital of the m th atom. The Hamilton operator contains the kinetic-energy operator as well as the potential. The latter is approximated as a superposition of the potentials of the isolated atoms,

$$V(\vec{r}) = \sum_m V_m (|\vec{r} - \vec{R}_m|) \quad (3)$$

and subsequently we assume that the matrix element $\langle \chi_{m_1 n_1} | V_m | \chi_{m_2 n_2} \rangle$ vanishes unless at least one of the atoms m_1 and m_2 equals m . Finally, the pair potentials U_{m_1, m_2} are obtained by requiring that the total-energy curves from parameter-free density-functional calculations on the diatomics are accurately reproduced. With these approximations, all relevant information on the above-mentioned matrix elements can be extracted from calculations on isolated two-atomic systems, in our case on H_2 , HA , HO , Al_2 , AlO , and O_2 .

B. Unbiased Structure Optimizations. With the method above we can calculate the total energy of a given structure, and by calculating also the forces acting on the atoms, i.e., the derivatives of the total energy with respect to nuclear coordinates, also the structure of a local total-energy minimum can be identified. To search for the structure of the global total-energy minimum for the isolated $(\text{HAIO})_n$ clusters, we have used two different, unbiased approaches, i.e., our own Aufbau method as well as a method based on genetic algorithms. The only information we use is that HAIO is stoichiometric.^{1,2} With our Aufbau method, that is closely related to our ‘‘Aufbau/Abbau’’ method that we have used in optimizing the structure of large metal clusters,¹¹ we start out optimizing the structure of a single HAIO molecule (i.e., $n = 1$) by choosing the structure of the lowest total energy from a very large number of calculations on randomly constructed structures that were allowed to relax to their closest total-energy minimum. Subsequently, we only assume that the structure of the cluster with $n + 1$ units can be obtained by adding one Al, one O, and one H atom to the cluster with n units. Thus, out of very many calculations where we randomly add those three atoms to the optimized structure of the cluster with n units (imposing only the constraints that the extra atoms should not be too close to any other atom or too far from all the other ones, and subsequently allowed to relax) we obtain an optimized structure of the system with $n + 1$ units. This is repeated starting from $n = 1$ up to, in our case, $n = 26$.

The resulting cluster of such a calculation is not with absolute certainty that of the global total-energy minimum but, hopefully, a very good approximation to it.

Our other approach is based on the so-called genetic algorithms, which in turn are based on the principles of natural evolution and are, therefore, also called evolutionary algorithms.^{12,13} We found that it provides an efficient tool for global geometry optimizations. Our version of the genetic algorithms

is as follows. Suppose that we have optimized the structure of the cluster with n units. From this structure we construct a first generation consisting of M independent clusters for the $(n + 1)$ -unit system by randomly adding one Al, one O, and one H atom and letting these structures relax to their nearest total-energy minima. Subsequently, a new set of clusters is constructed by cutting each of the original ones randomly into two parts that are interchanged (under the constraints mentioned above) and, afterward, allowed to relax. Out of the total set of $2M$ structures, the M ones of the lowest total energy are kept as the next generation. This procedure is repeated until the lowest total energy is unchanged for a large number of generations.

By comparing the results from the two sets of (independent) calculations, i.e., using the Aufbau method and the genetic algorithms, we have a possibility to check the reliability of each approach.

C. Pure DFT Calculations. In addition to the calculations using the Aufbau method and the genetic algorithms, we performed calculations using Ahlrichs’ program system TURBOMOLE.¹⁴ All calculations used pure DFT with the Becke–Perdew functional,^{15,16,17,18} employing SV(P) basis sets.¹⁹ The Coulomb terms were treated by the RI- J approximation to speed up computation time for the geometry optimizations (*riBP/SV(P)*).^{20,21}

We studied very many structures of $(\text{HAIO})_n$ with $n = 1, 2, 3, 4$, and 6 . Here, starting from ‘‘reasonable’’ starting geometries, relaxed structures were obtained and, subsequently, analyzed. This gave 2, 5, 7, 8, and 28 different structures for $n = 1, 2, 3, 4$, and 6 , respectively.

D. Interacting Clusters and Layers. The material HAIO is nanostructured in the powder form and glasslike in the layer form; that is, is believed to consist of smaller ‘‘clusters’’ that, however, are very close to each other. This means that the properties of the individual clusters may to only a smaller extent be recovered for the nanostructured material. To obtain some first insight into the latter, we have also considered the consequences of putting two clusters together. That is, we studied systems consisting of the clusters with n_1 and n_2 units that are placed at positions so close that they interact. Subsequently, they are allowed to relax. We finally select the structure of the lowest total energy from a large set of calculations where we have varied the relative orientations of the two clusters.

Finally, we also studied infinite, periodic, two-dimensional layers of HAIO. Here, we considered both systems containing only one layer as well as systems containing two, covalently bonded, layers. In all cases we constructed an Al–O square lattice from a periodically repeated unit of $N \times N$ Al and O atoms. In one case we considered just a single layer with $N = 8$ and with H atoms added to the Al atoms on only one side of the layer. In another case we considered a single layer with $N = 6$ but with the H atoms added to the Al atoms alternately on one or the other side of the layer. Furthermore, we considered two layers placed on top of each other and still with H atoms added to the Al atoms. Here, we had $N = 6$ for the case that the two layers were placed so that Al–Al and O–O bonds between the layers could be formed, whereas we had $N = 4$ for the case when we only had Al–O bonds between the layers. In all cases we varied the lattice constants of the repeated units in order to determine the optimized value, and by varying the value of N , we checked that the results were converged as a function of this parameter.

We add that the calculations on the interacting clusters and on the layers all were performed using the parametrized density-functional method that was described in section IIA.

TABLE 1: Various Parameters Describing the Results of the Optimization of the (HAIO)_n Clusters Using Either the Aufbau or the Genetic-Algorithms Approach^a

	<i>n</i> = 2	<i>n</i> = 3	<i>n</i> = 4	<i>n</i> = 5	<i>n</i> = 6	<i>n</i> = 7	<i>n</i> = 8	<i>n</i> = 9
$E_{\text{tot}}^{\text{auf}}$	-4.8238	-4.9275	-5.0673	-5.1190	-5.1892	-5.2367	-5.2892	-5.3377
$E_{\text{tot}}^{\text{ga}}$	-4.8238	-4.9275	-5.0673	-5.1190	-5.1914	-5.2376	-5.2908	-5.3396
Δ_r	0.00	0.01	0.00	0.00	0.47	0.44	0.16	0.13
Δ_d	0.00	0.00	0.00	0.00	0.30	0.20	0.075	0.01

^a *n* describes the size of the cluster, $E_{\text{tot}}^{\text{auf}}$ and $E_{\text{tot}}^{\text{ga}}$ are the calculated total energies (in au per unit) with the two methods, and Δ_r and Δ_d are the two parameters (in au) that are used in quantifying the difference between the structures.

III. Results

First, we optimized the structures of (HAIO)_n clusters with *n* up to 26 using our Aufbau approach and with *n* up to 18 using the genetic-algorithms approach. A set of key quantities are shown in Table 1, of which some are introduced in order to compare the results from the two approaches. We define a radial distance \bar{r}_i for each of the 3*n* atoms as

$$r_i = |\vec{R}_i - \vec{R}_0| \quad (4)$$

where \vec{R}_0 is the center of the cluster,

$$\vec{R}_0 = \frac{1}{3n} \sum_{i=1}^{3n} \vec{R}_i \quad (5)$$

Subsequently, two parameters are defined as follows

$$\Delta_r = \left[\frac{1}{3n} \sum_{i=1}^{3n} (r_i^{\text{auf}} - r_i^{\text{ga}})^2 \right]^{1/2}$$

$$\Delta_d = \left[\frac{2}{3n(3n-1)} \sum_{i=1}^{3n(3n-1)/2} (d_i^{\text{auf}} - d_i^{\text{ga}})^2 \right]^{1/2} \quad (6)$$

where d_i are the interatomic distances and where we have assumed that r_i and d_i have been sorted in increasing order. Finally, the upper indices ‘auf’ and ‘ga’ refer to the Aufbau and genetic-algorithms approaches, respectively. The parameter approaches 0 if the two structures are very similar. In Table 1 we see that the lowest total energies from the two approaches are very close and, moreover, in both cases show the same tendency that the energy per unit decreases with increasing size of the cluster. Furthermore, the two parameters defined above that quantify the structural differences are also very small. The above analysis gives us strong reasons to suggest that the global total-energy minimum of the (HAIO)_n clusters has been found and also that our two unbiased approaches are reliable.

Further support for our conclusion is obtained from the results of the pure DFT calculations, as shall be discussed below. Using this pure DFT technique, we first studied the HAIO monomers in order to compare with previously published data using SCF and MP3 methods.²² Our calculations show that for the HAIO monomer the hydroxyde AIOH is more stable than the hydride HAIO, as also found in the SCF and MP3 calculations. For *n* ≥ 2 the hydric species become more stable than the corresponding hydroxides. Comparing the geometries, our bond lengths are slightly longer than those of the previously published results. Maybe not surprising, the structures of the energetically lowest isomers of (HAIO)_n for *n* > 2 as calculated with the parametrized method and as calculated with the parameter-free method are not identical, which may be ascribed to the occurrence of several (meta-)stable structures with a different

energetic ordering in the two theoretical approaches. However, as we shall see below, the overall picture that emerges from the calculations with the two different methods is mutually consistent.

As examples of the results of the calculations, we show in Figure 1 optimized structures using the different methods. As exemplified in the figure, it turned out that all optimized (HAIO)_n clusters have a structure where the Al and O atoms form an inner part of the cluster, whereas the H atoms are only found on the surface of the cluster. Moreover, in the inner part of the clusters there are mainly Al–O bonds and essentially no Al–Al or O–O bonds, and on the surface the H atoms are bonded only to Al atoms. Parts of this are illustrated in Figure 4, which shows the radial distances for the different clusters and atoms. The figure contains, for each type of atoms separately, the radial distances for the different values of *n*. It is very clear that the largest radial distances are found for H atoms and, in addition, that essentially all H atoms always have larger radial distances than the Al and O atoms. On the other hand, the central parts of the clusters are clearly formed by both Al and O atoms.

Experimental results on (HAIO)_n clusters are not available, but derivatives of the type (RAIO)_n (R = bulky organic ligand) have been prepared and the crystal structures of (RAIO)₄ (R = C₆H₂-2,4,6-*t*-Bu₃) and (RAIO)₆ (R = *t*-Bu) have been determined.^{23,24} While the tetrameric unit forms a twisted Al₄O₄ ring, which is due to the special ligand used, (*t*-BuAlO)₆ has a drum-shaped structure very similar to one of our calculated isomers.^{23,24}

Also, the DFT calculations on the smallest cluster give results in support of this general structure. As mentioned above, we considered in total 50 isomers of (HAIO)_n with *n* = 1, 2, 3, 4, and 6. To extract information from these results, we proceed as follows. First we analyzed the interatomic distances for all 50 structures. It turned out that none possessed O–O or H–H nearest neighbors and that it was relative easy to identify Al–H, Al–O, and O–H bonds as being pairs with an interatomic distance smaller than 2.2, 2.5, and 1.5 Å, respectively. The Al–Al interatomic distances, on the other hand, showed a large spread, and it was not possible to readily identify a cutoff distance below which the Al atoms could be considered as being bonded. In the subsequent analysis we therefore considered two extreme values, 2.5 and 4.1 Å.

Next we studied the total energy per unit as a function of number of A–B bonds per unit, with A and B being H, Al, and O. The results are shown in Figure 2. The results are very scattered, but nevertheless, it is possible to identify certain trends. First, the total energy decreases as the number of Al–O bonds increases. Second, a similar, but much weaker, trend can be identified for the number of Al–Al bonds (here we have used 4.1 Å as our cutoff value, but 2.5 Å gives very similar results). Third, there is a clear preference for structures with one Al–H bond per unit. These observations can be quantified

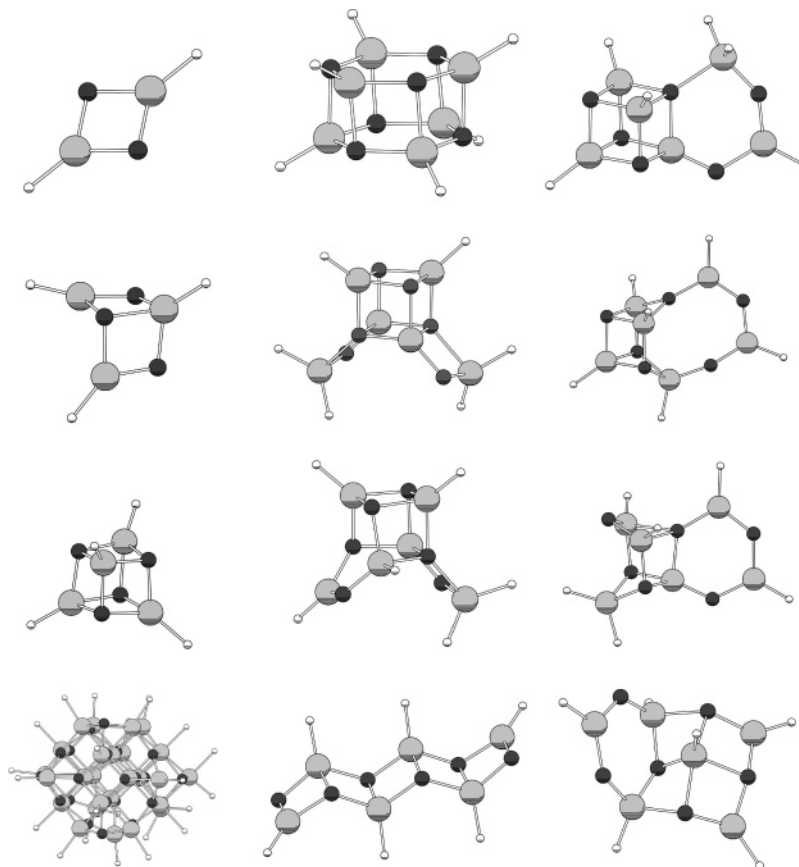


Figure 1. $(\text{HAIO})_n$ structures. The left side shows clusters with $n = 2, 3, 4,$ and 26 from DFT-TB calculations using the Aufbau method in the structure optimization (top to bottom). The other structures show different isomers (DFT calculations) for the $(\text{HAIO})_6$ system. Hydrogen, aluminum, and oxygen are represented with small white spheres, large gray spheres, and black spheres, respectively.

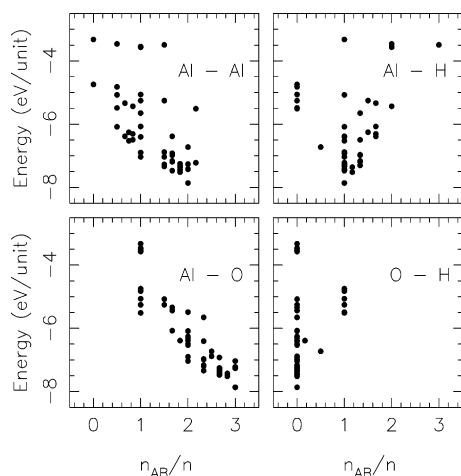


Figure 2. Variation in the total energy per unit as a function of the number of A–B bonds per unit. The results are from the DFT calculations for the $(\text{HAIO})_n$ clusters with $n = 1, 2, 3, 4,$ and 6 , and the meaning of A and B is given in the panels.

by approximating the total energy of the various $(\text{HAIO})_n$ isomers as

$$E_{\text{tot}} \approx nE_0 + n_{\text{AlAl}}E_{\text{AlAl}} + n_{\text{AlO}}E_{\text{AlO}} + n_{\text{AlH}}E_{\text{AlH}} + n_{\text{OH}}E_{\text{OH}} \quad (7)$$

A least-squares fit to our 50 DFT results gave $E_{\text{AlAl}} = -0.175$ eV (-0.122 eV), $E_{\text{AlO}} = -1.000$ eV (-1.170 eV), $E_{\text{AlH}} = 0.750$ eV (0.678 eV), and $E_{\text{OH}} = 1.119$ eV (0.798 eV), when using 4.1 Å (2.5 Å) as the cutoff distance for Al–Al bonds. These numbers show that Al–O bonds are strongly preferred and that

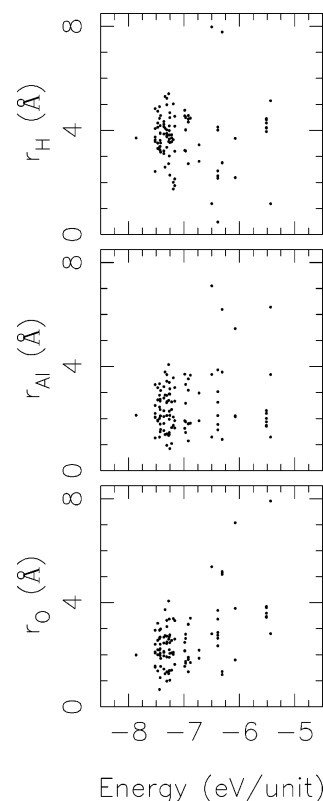


Figure 3. Radial distances for the different smaller clusters as a function of the total energy per unit. The different panels show the different types of atoms. The results are from the DFT calculations for the $(\text{HAIO})_n$ clusters with $n = 6$.

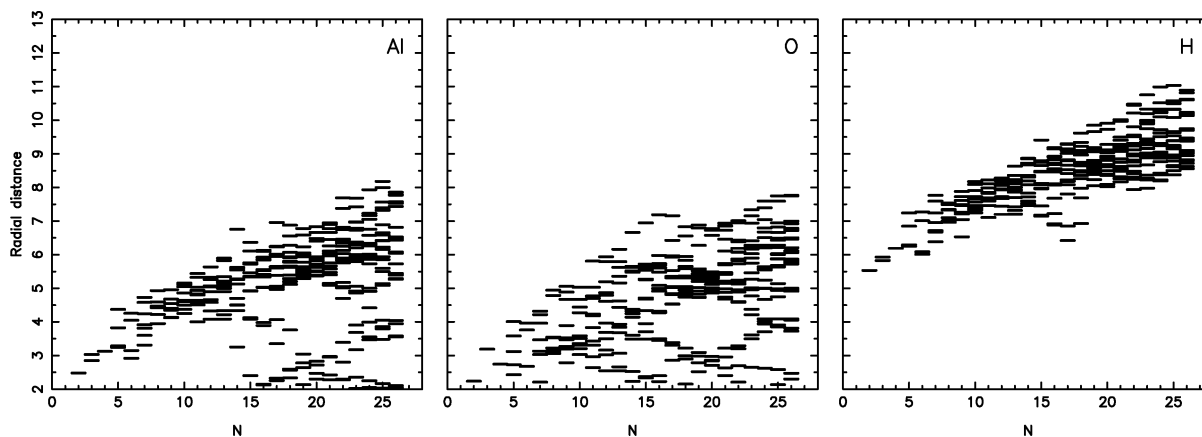


Figure 4. Radial distances (in au) for Al, O, and H atoms, separately, as a function of the size of the cluster n for $(\text{HAIO})_n$ clusters. In each panel, a small horizontal line shows that at least one atom of the corresponding type has that distance to the center of the cluster for a given value of n .

when choosing between adding H to either Al or O, it is energetically preferred to create Al–H bonds. These features are in perfect agreement with the results for the structure optimizations for the larger clusters obtained using the Aufbau or genetic-algorithms method.

For each of the 28 $(\text{HAIO})_6$ clusters, we also calculated the radial distances of the different atoms. Subsequently, we plotted this as a function of the total energy per unit, and we show the results in Figure 3. One should remember that the radial distance for each atom of the smaller clusters is on the average smaller than that of the larger clusters. Therefore, we chose to consider only the clusters of the same size, i.e., $(\text{HAIO})_6$. When comparing the clusters of roughly the lowest total energies, we see that Al and O are those atoms with smaller radial distances, whereas those of hydrogen are larger. For the higher total energies, the radial distances of Al and O show a weak tendency to increase and simultaneously those of H are slightly decreasing. In total, this analysis confirms the tendency for the $(\text{HAIO})_n$ clusters to possess a Al–O core covered with H atoms.

The DFT calculations strongly indicate that the stables hydrides mainly have terminal hydrides. Moreover, it is interesting to observe that when comparing isomers with bridging H atoms with isomers with bridging hydroxy groups, isomers with OH groups usually are more stable than the corresponding isomer with bridging H atoms.

We now return to the larger clusters that were studied with the parametrized density-functional method. Figure 5 shows the smallest interatomic distances for different types of pairs, and in Figure 6 we show the pair correlation functions $g_{AB}(R)$ for the clusters with $n = 2$ and $n = 26$. Here, $g_{AB}(R)$ is the number of A–B pairs with an interatomic distance of R . It is seen that there is a strong preference for Al–O and Al–H nearest-neighbor bonds, both for the small and for the large clusters. For the sake of completeness, we add that the bond lengths for diatomic AlO and AlH are 3.33 au = 1.76 Å and 3.06 au = 1.62 Å, respectively. By analyzing the nearest surroundings of the Al atoms, we find that the coordination number of Al is between 3 and 6 with the value 6 for Al atoms that are in the central part of the clusters. This is in excellent agreement with the NMR data.

The stability of a given cluster can be analyzed through the total energies. Most conveniently, this is done by using the stability function

$$\Delta E_n = E_{\text{tot}}(n+1) + E_{\text{tot}}(n-1) - 2E_{\text{tot}}(n) \quad (8)$$

This function is shown in Figure 7. It has peaks for particularly stable clusters, i.e., for $n = 4, 19,$ and 22 . As we

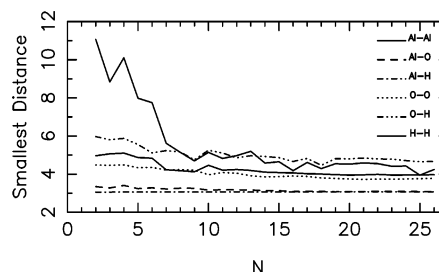


Figure 5. Smallest interatomic A–B distances (in au) for $(\text{HAIO})_n$ clusters for different values of n and different pairs of atoms.

shall see below, the cluster for $n = 4$ is highly symmetric and, as shown in Figure 7, also particularly stable.

The overall shape of the clusters can be quantified by considering the eigenvalues $I_{\alpha\alpha}$ of the matrix containing the moments of inertia relative to the center of the cluster. The shape of the cluster is roughly spherical if all three eigenvalues are identical, whereas the cluster has a lenslike shape if two eigenvalues are larger than the average eigenvalue, and finally, it has an overall cigarlike shape if two eigenvalues are smaller than the average eigenvalue. This analysis is shown in Figure 8. For a homogeneous sphere of constant density, the eigenvalues scale as $n^{5/3}$ and, therefore, the results of Figure 8 have been scaled with $n^{-5/3}$. In Figure 8 it is seen, as mentioned above, that the cluster with $n = 4$ has spherical shape, whereas lenslike and cigarlike shapes occur for all other clusters studied here.

Our two approaches for structure optimization, i.e., the Aufbau and genetic algorithms, are both based on building up the $(n+1)$ cluster from the one with n units, suggesting that the structure of the $(n+1)$ cluster is closely related to that of the n cluster. Also, Figure 8 suggests that the structure is, at least over certain ranges of n , relatively unchanging. We can quantify whether the structure of the cluster with $n+1$ units is similar to the structure of the cluster with n units as follows. We consider all the n -unit fragments of the $(n+1)$ -unit cluster that can be obtained by removing one H, one Al, and one O atom [i.e., in total we consider $(n+1)^3$ different fragments]. Subsequently, we calculate and sort all interatomic distances for this fragment $\{R'_{n+1,i}\}$. These are compared with the sorted interatomic distances $\{R_{n,i}\}$ for the n -unit system; that is, we construct

$$\frac{3n(3n-1)}{2} q^2 = \sum_{i=1}^{3n(3n-1)/2} (R'_{n+1,i} - R_{n,i})^2 \quad (9)$$

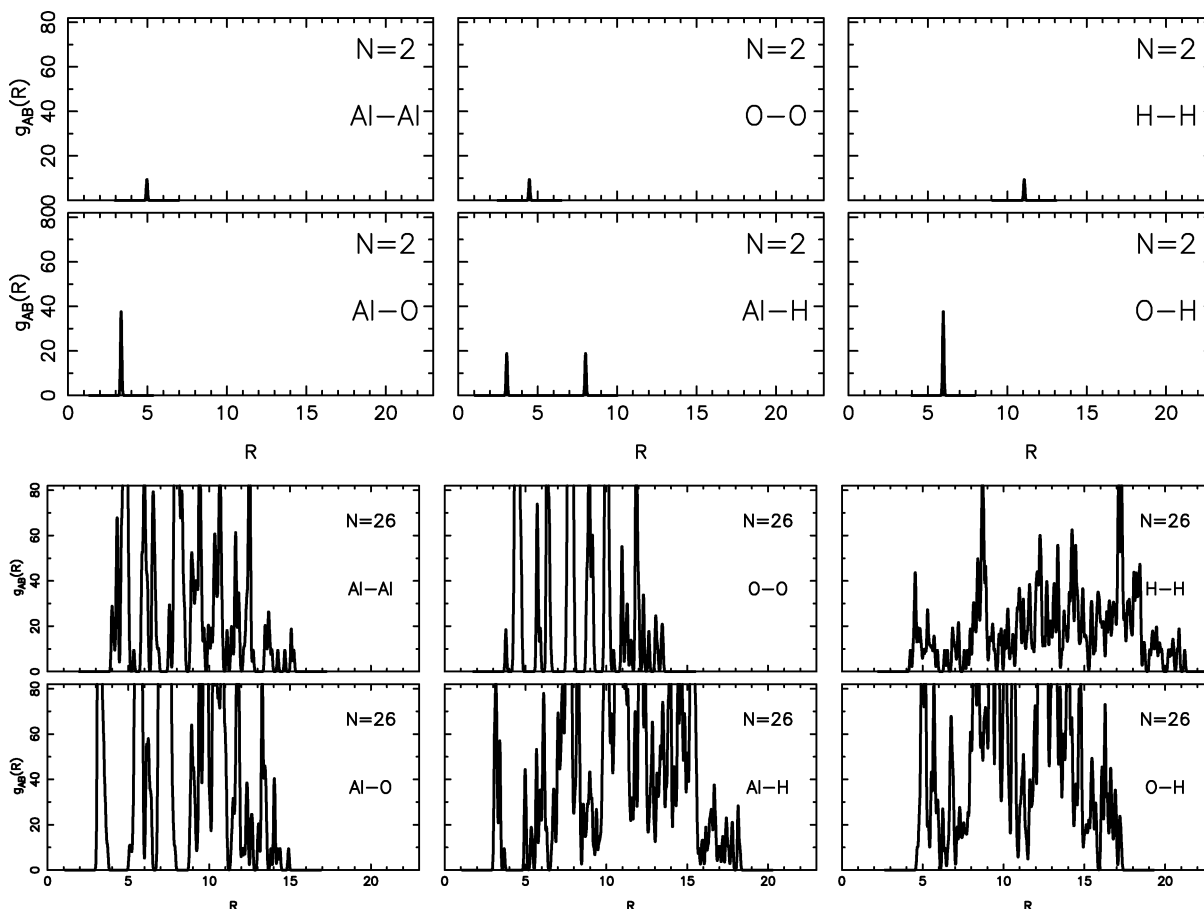


Figure 6. Pair-correlation functions $g_{AB}(R)$ for (upper part) $n = 2$ and (lower part) $n = 26$ with R in au.

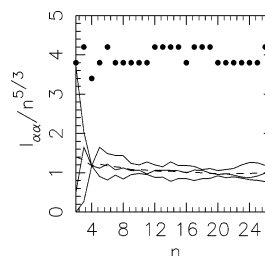
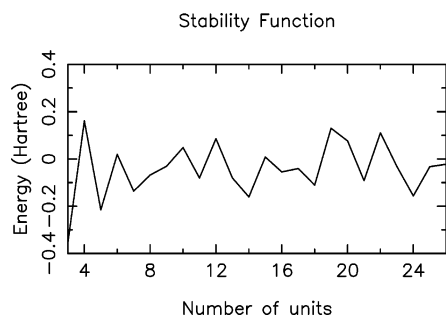


Figure 7. Stability function for $(\text{HAIO})_n$ clusters as a function of n .

Out of the $(n + 1)^3$ values of q , we choose the smallest value of q , i.e., q_{\min} , that subsequently defines the similarity function

$$S = \frac{1}{1 + q_{\min}/a_0} \quad (10)$$

with a_0 chosen equal to 1 au, S approaches 1 if the $(n + 1)$ -unit cluster is very similar to the n -unit cluster plus one unit and 0 for structurally very different systems.

Figure 9 shows this similarity function for the clusters with $n = 2$ to $n = 25$. It is obvious that, for the smaller clusters, the cluster with $n + 1$ units is certainly not similar to the n -unit cluster, and the growth of the clusters is, accordingly, not regular. On the other hand, for the larger clusters, the similarity function approaches 1, although, also for those, significant structural changes occur, as we have also seen through our other structure descriptors.

In discussing the electronic properties of the clusters, we consider solely the largest one of the present study, i.e., the

Figure 8. Eigenvalues, $I_{\alpha\alpha}$, of the matrix with the moments of inertia for $(\text{HAIO})_n$ clusters as a function of n . To obtain values of $I_{\alpha\alpha}$ that are roughly independent of n , they have been scaled by $n^{-5/3}$. The marks on the top indicate whether the cluster has an overall spherical shape (lowest row), a cigarlike shape (middle row), or a lenslike shape (upper row). The dashed curve is the average of the three eigenvalues.

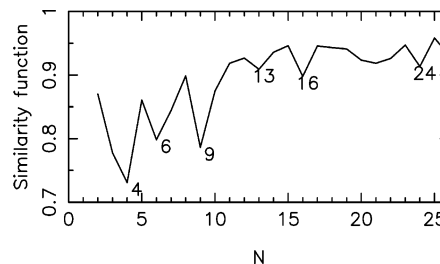


Figure 9. Similarity function for $(\text{HAIO})_n$ clusters as a function of n .

one with $n = 26$. First we show in Figure 10 the radial distributions of the Mulliken *gross* populations; that is, we calculate the *gross* population for each atom separately and depict them subsequently as a function of the radial distance of eq 4. This picture confirms the consensus from above that the H atoms are those with the largest radial distances. Moreover,

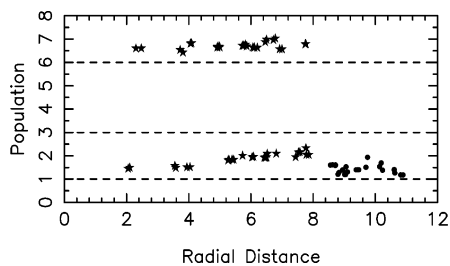


Figure 10. Radial distribution of the Mulliken *gross* populations of the valence electrons for the $(\text{HAIO})_{26}$ cluster. The horizontal dashed lines mark the values for the neutral atoms, i.e., 1, 3, and 6 for H, Al, and O, respectively. Al and O atoms are marked by stars, H atoms are marked by closed circles, and the radial distance is given in au.

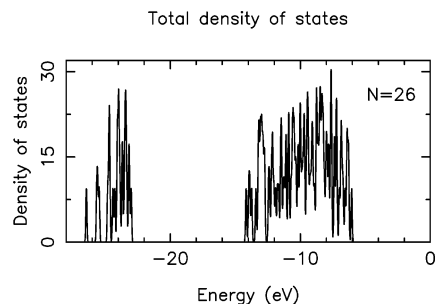


Figure 11. Density of states of the valence orbitals in arbitrary units for the $(\text{HAIO})_{26}$ cluster. It has been obtained from the discrete energy levels upon a broadening with narrow Gaussians. All shown orbitals are occupied, whereas the unoccupied ones appear at positive energies.

it is seen that both O and H atoms receive electrons, whereas the Al atoms donate electrons. For the Al atoms, there seems to be a larger donation of electrons in the innermost parts of the cluster, whereas a similar trend not is observed for the O atoms.

For all geometries that were studied with the DFT method, we also calculated the IR spectrum. Therefore, we can compare the theoretical vibrational bands with those of the layer compound. Figure 15 shows this result. The theoretical spectrum was constructed as the sum of the spectra for the lowest-total-energy structures of $(\text{HAIO})_n$ ($n = 2, 3, 4,$ and 6). Except for the shoulder at 1670 cm^{-1} , there is a very good agreement between theory and experiment. The fact that we do not find the shoulder is reasonable, since all minimal structures of our calculations have terminal hydrides, whereas the shoulder may be due to bridging Al–H–Al units, although a final assignment is lacking at the moment.

In Figure 11 we show the density of states of the valence orbitals for the same cluster. This curve is clearly split into two parts, i.e., a low-energy part around -25 eV due to O 2s functions as well as a high-energy part due to Al 3s, 3p, O 2p,

and H 1s functions. The unoccupied orbitals appear at positive energies, so that the gap between occupied and unoccupied orbitals is large.

The HAIO clusters form parts of a nanostructured material, so that they may very likely interact with each other. In this context it is an interesting issue whether the H atoms will try to remain outside a central part, as we have observed for the individual, isolated clusters. We decided, therefore, to study the interaction between two clusters by putting two of the previously optimized clusters together. This was done as follows. We placed two clusters of n_1 and n_2 units so close to each other that they would interact. The initial structures were those of the isolated $(\text{HAIO})_{n_1}$ and $(\text{HAIO})_{n_2}$ clusters, and we considered very many relative orientations of the two clusters, out of which we chose the one that led to the lowest total energy after structural relaxation. Table 2 shows the total energies in comparison with those of the optimized clusters with $n = n_1 + n_2$ units. From the table we see that the interacting clusters are more stable than the two separate, noninteracting clusters but clearly less stable than the larger cluster of n units. For the case that the two clusters were brought so close that they interact, before the combined cluster was relaxed, it was found that the hydrogen atoms are placed between the two cores of AIO, but after the combined cluster was relaxed, the hydrogen atoms are only sitting on the surface of the combined cluster. This supports our consensus that clusters with hydrogen sitting on the surface of the clusters are most stable.

Figure 12 illustrates this idea even further. This figure has been obtained as follows. We consider the case of $n_1 = 8$ and $n_2 = 9$ units before and after relaxation. In each case (i.e., before and after relaxation) we calculate the center of the two parts according to eq 5. The line joining these two centers defines the z axis in a cylindrical coordinate system with $z = 0$ being the midpoint between the two centers. Subsequently, we superpose the two coordinate systems in one figure and show the initial and final values of z and the distance to the z axis (denoted d) for each atom separately by joining these points with a straight line. Finally, we depict these lines for each type of atom individually. The stars mark the final positions of the $n_1 = 8$ system whereas the closed circles mark the final positions of the $n_2 = 9$ system. In particular, the H atoms tend to increase d upon relaxation, i.e., to move away from the region between the two clusters. On the other hand, the first of all the O atoms but also to a lesser extent the Al atoms are seeking to fill out the space between the two clusters when they are combined.

Our experimentally synthesized material is a glasslike, amorphous film.^{1,2} Moreover, our theoretical findings, i.e., that the H atoms prefer to stay outside an AIO core, which for larger clusters becomes increasingly difficult when requiring that the

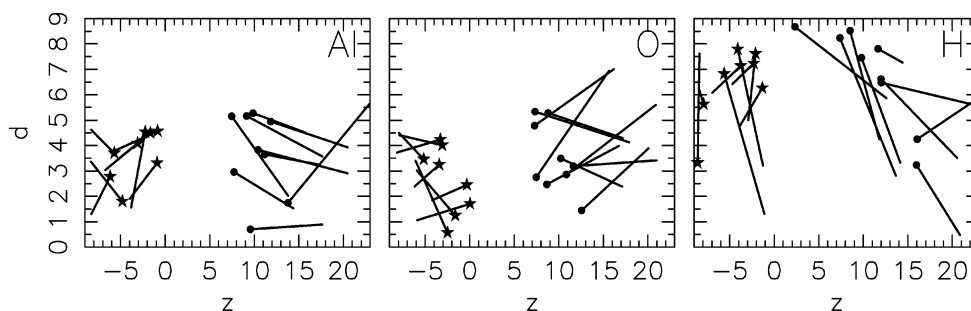


Figure 12. Graphical illustration of the structural relaxations of bringing the $n_1 = 8$ (left part) and $n_2 = 9$ (right part) clusters together. Shown are the relaxations in a cylindrical coordinate system with z and d being the position along the cylindrical axis and the distance from it, respectively, both in au. The three panels show the displacements of the Al, O, and H atoms, individually. For details about the presentation, see the text.

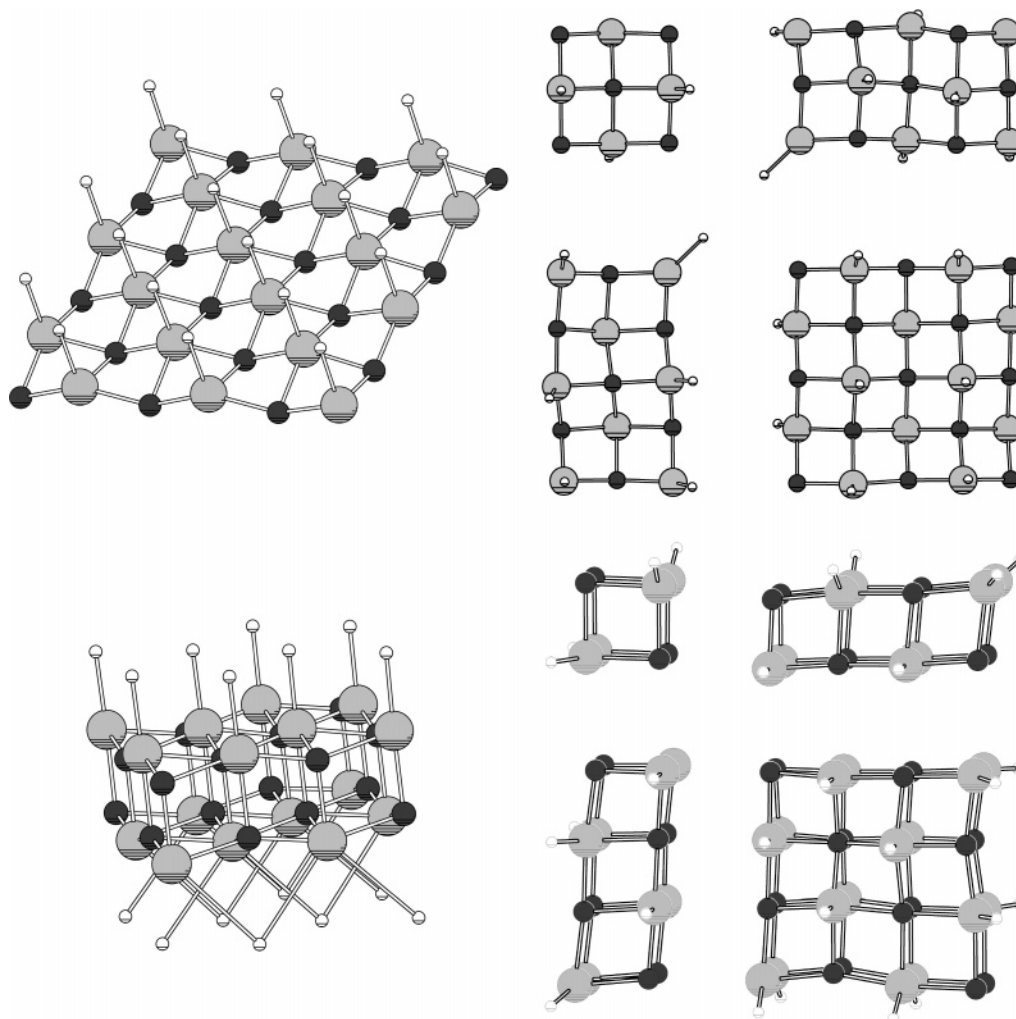


Figure 13. Structure of layers of HAIO for one layer where H atoms are on one side (upper left) or two sides (upper right), as well as for two layers with the Al atoms of one layer above either the O (lower left) or the Al (lower right) atoms of the other layer. We use the same color coding as in Figure 1. Notice that interlayer interactions were not included in the calculations. Moreover, the structures on the right-hand part are seen to split into smaller fragments whose size, however, may be biased by the size of the repeated unit in the calculations.

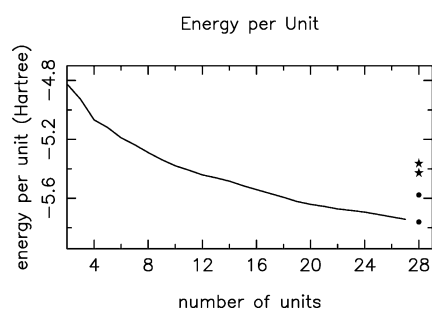


Figure 14. Variation in energy per unit for isolated clusters and for the layers of HAIO. The results for the layers are shown to the right with the one-layer results marked with stars (here, the lowest total energy is for the case when the H atoms are on the same side, whereas they are alternating on the two different sides in the other case) and the two-layer results marked with circles (here, the lowest total energy is for the case when Al–O bonds form the bonds between the layers).

material is stoichiometric, suggest that stable structures of HAIO may occur for layers of HAIO. To study this proposal further, we considered theoretically extended HAIO systems consisting of either one or two layers of HAIO. We add that these calculations ignore interlayer interactions that can be very important and that, therefore, may modify our conclusions significantly, when included.

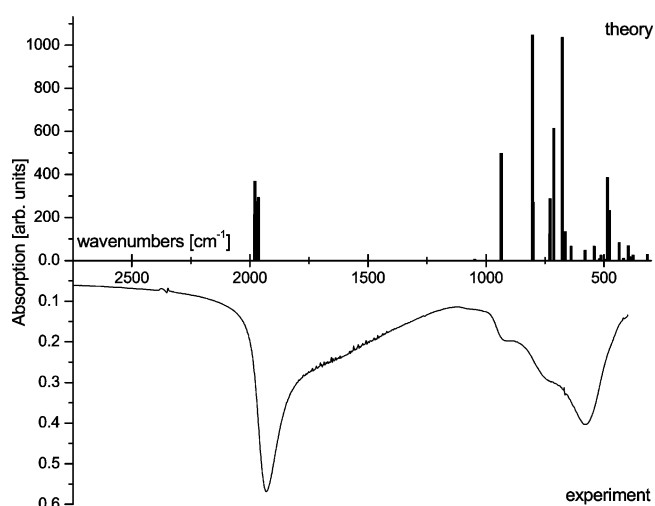


Figure 15. Comparison of calculated and experimental infrared spectra. The upper theoretical spectrum is calculated as the weighted average of the line spectra for the optimized structures of the $(\text{HAIO})_n$ ($n = 2, 3, 4,$ and 6) clusters. The experimental spectrum has been taken from a HAIO layer on a steel target with a reflection technique (angle 30°).

For a single layer of HAIO, one can imagine two highly symmetric cases, i.e., one where all H atoms are on one side of

TABLE 2: Properties of Two Interacting Clusters of n_1 and n_2 Units Giving in Total $n = n_1 + n_2$ Units^a

n	n_1	n_2	$E_{\text{tot}}^{\text{com}}(n)$	$E_{\text{tot}}^{\text{auf}}(n)$	$E_{\text{tot}}^{\text{ga}}(n)$	$E_{\text{tot}}^{\text{auf}}(n_1) + E_{\text{tot}}^{\text{auf}}(n_2)$	$E_{\text{tot}}^{\text{ga}}(n_1) + E_{\text{tot}}^{\text{ga}}(n_2)$
5	2	3	-25.5948	-25.5948	-25.5948	-24.4301	-24.4301
6	2	4	-31.0983	-31.1353	-31.1483	-29.9168	-29.9168
7	3	4	-36.5535	-36.6566	-36.6632	-35.0518	-35.0518
12	4	8	-64.9534	-65.2908	-65.3370	-62.5828	-62.5956
17	8	9	-94.0379	-94.6440	-94.6602	-90.3529	-90.3828

^a $E_{\text{tot}}^{\text{auf}}$ or $E_{\text{tot}}^{\text{ga}}$ gives the calculated total energy (in au) with either the Aufbau or the genetic-algorithms approach, respectively. $E_{\text{tot}}(n_1) + E_{\text{tot}}(n_2)$ gives results for the relaxed, noninteractions clusters, whereas $E_{\text{tot}}(n)$ gives results for the relaxed cluster of n units. Finally, $E_{\text{tot}}^{\text{com}}(n)$ gives results for the relaxed, combined clusters.

the layer, and one where every second H atom is above and every second H atom is below the AIO layer. These are shown in Figure 13. For the case that all H atoms are on the same side of the layer, the Al and O atoms form a layer with bond lengths of 3.33 au = 1.76 Å and 3.34 au = 1.77 Å. Moreover, the hydrogen atoms are sitting on the outside of the layer bonded to the Al atoms with Al–H bond lengths of 3.21 au = 1.70 Å. The Al–O–Al bond angles are 85°–86° and 147°–152°.

Remarkably different things occur when the H atoms are sitting alternately on the two sides of the single AIO layer. Then we found that the layer split into several small parts all with the same kind of structure; that is, the H atoms are binding to the Al atoms with Al–H bond lengths around 3.08 au = 1.63 Å, whereas the Al–O bond lengths are around 3.40 au = 1.80 Å.

For the case of two layers of HAIO, we studied two cases, i.e., either the Al atoms of one layer were placed on top of the O atoms of the other layer, or they were placed on top of the Al atoms of the other layer. It turned out that the first situation was much more stable than the second one, which may not be surprising, and in the second case we find that the system breaks into small parts.

Finally, it is interesting to study the energy per unit for the finite clusters in comparison with that for the layers, shown in Figure 14. It is remarkable that the two-layer structure is not significantly more stable than the finite clusters. We believe that the systems prefer to have H atoms on some surface. However, since the surface area scales as $n^{2/3}$, the available area per H atom scales such as $n^{-1/3}$, meaning that, above a certain critical size, the finite (HAIO)_{*n*} clusters will be less stable simply due to too little space for the H atoms on the surface. This effect is not found for the layers that per construction are infinite, but it suggests that there is a competition between clusters of HAIO and layers of HAIO, which may explain why the two different synthetic routes lead to different materials. It is not possible to determine directly the critical size of the finite (HAIO)_{*n*} clusters above which they become unstable, but our results suggest that this size may be comparable to the largest clusters of the present study.

IV. Conclusions

HAIO, like other amorphous glasses, consists of many different structural entities. Experimental data (Al–NMR, IR) indicate that the aluminum atoms are coordinated by four, five, and six ligands (oxygen and hydrogen). Al–H as well as Al–H···Al entities, but no hydroxides, can be detected using infrared spectroscopy, in accordance with the results of the calculations.

In the present work we have determined the structure of HAIO clusters using two different unbiased approaches, i.e., the Aufbau and the genetic-algorithms approaches, in combination with a

parametrized density-functional method for the calculation of electronic and energetic properties for a given structure. Moreover, for smaller clusters we also performed a large number of parameter-free density-functional calculations. The fact that all methods give very similar results makes us believe that the results are reliable. Also, the infrared spectra could be reproduced by the parameter-free density-functional calculations.

The optimized HAIO clusters were found to contain a core of AIO where, moreover, mainly heteroatomic bonds exist. The H atoms are found only on the surface of the core and are only bonded to Al. From the parameter-free density-functional calculations we could see that there is a strong energetic driving force for creating systems with Al–O bonds and, moreover, the clusters would prefer to have one Al–H bond per unit. The cluster with $n = 4$ has a very high symmetry. Moreover, the stability function shows that with increasing n the total energy per unit decreases monotonically. The combined clusters $n_1 + n_2$ are slightly more stable than the two isolated clusters of n_1 and n_2 units but significantly less stable than the optimized $n_1 + n_2$ cluster. We also found that infinite layered HAIO can be stable, in particular for a system consisting of two AIO layers bonded via Al–O bonds and with additional H atoms attached to the Al atoms. It turned out, however, that this system was only marginally more stable than the most stable cluster of our study.

These findings are in accord with our experimental results: We find that by thermal treatment of HAIO, the system loses hydrogen in the first place. The (AIO)_{*n*} core is not affected in the first instance, but as it is electronically unsaturated, it decomposes by disproportionation to Al and Al₂O₃. Apart from the use of this metastability of the system in our experiments, we are also interested in the transient (AIO)_{*n*} state, about which further theoretical and experimental work is underway.

Acknowledgment. This work was supported by the SFB 277 at the University of Saarland. The authors are very grateful to the Fonds der Chemischen Industrie for generous support.

Supporting Information Available: Results from the parameter-free density-functional calculations on the 50 isomers of (HAIO)_{*n*} with $n = 1, 2, 3, 4,$ and 6 , including structural and energetic information. This material is available free of charge via the Internet at <http://pubs.acs.org>.

References and Notes

- (1) Veith, M.; Andres, K.; Faber, S.; Blin, J.; Zimmer, M.; Wolf, Y.; Schnöckel, H.; Köppe, R.; Masi, R.; Hüfner, S. *Eur. J. Inorg. Chem.* **2003**, 4387.
- (2) Veith, M.; Andres, K. *J. Metastable Nanocryst. Mater.* **2003**, 15–16, 279.
- (3) Liu, S. W.; Wehmschulte, R. J.; Burba, C. M. *J. Mater. Chem.* **2003**, 13, 3107.
- (4) Liu, S. W.; Fooker, J.; Burba, C. M.; Eastman, M. A.; Wehmschulte, R. J. *Chem. Mater.* **2003**, 15, 2803.
- (5) Dong, Y.; Springborg, M. In *Proceedings of 3rd International Conference "Computational Modeling and Simulation of Materials"*; Vincenzini, P., et al., Eds.; Techna Group Publishers: Faenza, Italy, 2004; p 167.
- (6) Roszinski, H.; Dautel, R.; Zeil, W. *Z. Phys. Chem.* **1963**, 36, 26.
- (7) Go, E. P.; Tuermer, K.; Reutt-Robey, J. E. *Surf. Sci.* **1999**, 437, 377.
- (8) Porezag, D.; Frauenheim, Th.; Köhler, Th.; Seifert, G.; Kaschner, R. *Phys. Rev. B* **1995**, 51, 12947.
- (9) Seifert, G.; Schmidt, R. *New J. Chem.* **1992**, 16, 1145.
- (10) Seifert, G.; Porezag, D.; Frauenheim, Th. *Int. J. Quantum Chem.* **1996**, 58, 185.
- (11) Grigoryan, V. G.; Springborg, M. *Phys. Chem. Chem. Phys.* **2001**, 3, 5125.
- (12) Holland, J. H. *Adaption in Natural Algorithms and Artificial systems*; University of Michigan Press: Ann Arbor, MI, 1975.

- (13) Goldberg, D. E. *Genetic Algorithms in search, Optimization and Machine Learning*; Addison-Wesley: Reading, MA, 1989.
- (14) Ahlrichs, R.; Bär, M.; Häser, M.; Horn, H.; Kölmel, C. *Chem. Phys. Lett.* **1989**, *162*, 165.
- (15) Becke, A. D. *Phys. Rev. B* **1988**, *38*, 3098.
- (16) Vosko, S. H.; Wilk, L.; Nusair, M. *Can. J. Phys.* **1980**, *58*, 1200.
- (17) Perdew, J. P. *Phys. Rev. B* **1986**, *33*, 8822.
- (18) Perdew, J. P. *Phys. Rev. B* **1986**, *34*, 7406.
- (19) Schfer, A.; Horn, H.; Ahlrichs, R. *J. Chem. Phys.* **1992**, *97*, 2571.
- (20) Eichkorn, K.; Treutler, O.; Öhm, H.; Häser, M.; Ahlrichs, R. *Chem. Phys. Lett.* **1995**, *240*, 283.
- (21) Eichkorn, K.; Weigend, F.; Treutler, O.; Ahlrichs, R. *Theor. Chim. Acta* **1997**, *97*, 119.
- (22) Hirota, F.; Tanimoto, M.; Tokiwa, H. *Chem. Phys. Lett.* **1993**, *208*, 115.
- (23) Mason, M. R.; Smith, J. M.; Bott, S. G.; Barron, A. R. *J. Am. Chem. Soc.* **1993**, *115*, 4971.
- (24) Wehmschulte, R. J.; Power, P. P. *J. Am. Chem. Soc.* **1997**, *119*, 8387.

Properties of Au_N Clusters

Yi Dong¹ and Michael Springborg²

Physical and Theoretical Chemistry, University of Saarland, 66123 Saarbrücken, Germany

Received 10 July, 2006; accepted in revised form 10 July 2006

Abstract: The geometries and electronic properties of the most stable small Au_n clusters are presented. An intensive search for low-energy minima of Au_n clusters was carried through using a density-functional tight-binding method combined with genetic algorithms for an unbiased global structure optimization. The structural and energetic properties of the small gold clusters are compared with those of planar Au_n clusters with $n = 5$ to 15.

Keywords: Gold clusters, structure, stability

PACS: 36.40.Cg, 61.46.Bc

1 Introduction

In contrast to the case of semiconductors, the electrons of metals are assumed to be delocalized and not to participate in directional bonds. Thereby, the structure of metals becomes dictated by packing arguments. As a consequence, for infinite, periodic solids of only one element, the fcc and hcp lattice structures result. For finite systems, i.e., clusters, symmetry elements that are not allowed for the infinite, periodic system, like five-fold symmetry axes, can occur, whereby closed-packed structures like the icosahedron can show up.

Gold seems to show deviations from this behaviour, while simultaneously being one of the most studied elements in the context of clusters (see, e.g., [1]). For instance, the structure of Au_N clusters with N up to around 15 has been found to be planar [2, 3]. Moreover, for larger clusters indications for the existence of cage-like structures have been observed [4, 5, 6]. And Häkkinen *et al.* [7] found that for $53 \leq N \leq 58$, low-symmetry ‘amorphous’ structures are found, whereas the high-symmetric structures for the 55-atomic clusters are not the most stable structures. It is believed that a subtle interplay between relativistic effects, directional orbital interactions, and delocalized electrons is responsible for these results.

From this brief discussion it is clear that the properties of Au_N clusters only partly are understood. But, for an understanding of any property of clusters it is mandatory to have accurate information on their structures. However, this information is not easily accessible, neither with experimental nor with theoretical methods. From a theoretical point of view, the combination of low symmetry, a large-dimensional structure space, and an exponentially growing number of metastable structures with size makes it very demanding to determine the structure of a whole set of clusters without making severe approximations either in the description of the interatomic interactions or concerning the structure of the systems. As a consequence, most theoretical studies on Au_N clusters are based on either applying accurate methods on the smallest possible systems or on larger ones with selected high-symmetry structures or, alternatively, using approximate methods

¹Corresponding author; *e-mail:* y.dong@mx.uni-saarland.de

²*e-mail:* m.springborg@mx.uni-saarland.de

that do not explicitly include electronic degrees of freedom on a larger set of clusters for which the structures of the global total-energy minima are sought in an unbiased way.

In this work, we apply a parameterized density-functional tight-binding method combined with an unbiased approach to determine the lowest energy structures of gold clusters. In contrast to previous unbiased structure optimizations, our total-energy method includes electronic degrees of freedom, making it, we believe, more accurate. Because of the recent interest in planar gold clusters, we also included such ones, together with the icosahedral Au_{13} and tetragonal Au_{20} clusters, and in this presentation we shall concentrate on our results for the Au_N clusters with $1 \leq N \leq 20$. Our results for clusters with N up to around 60 will be published elsewhere.

2 Computational Method

We have used a parameterized tight-binding density-functional method combined with genetic algorithms to determine the global total-energy-minimum structures for gold clusters containing up to 20 atoms. The planar gold clusters with $N = 5 - 15$ and the icosahedral Au_{13} and tetragonal Au_{20} clusters were relaxed locally.

The density-functional tight-binding method [8, 9, 10] is based on the density functional theory of Hohenberg and Kohn in the formulation of Kohn and Sham. The Kohn-Sham orbitals of the system of interest are expanded in terms of atom-centered basis functions. The Kohn-Sham operator is $\hat{h} = \hat{t} + V_{\text{eff}}(\vec{r})$ with \hat{t} being the kinetic-energy operator and $V_{\text{eff}}(\vec{r})$ being the effective Kohn-Sham potential which in our approach is approximated as a simple superposition of the potentials of the neutral atoms $V_{\text{eff}}(\vec{r}) = \sum_j V_j^0(|\vec{r} - \vec{R}_j|)$. In the present method, only two-center terms in the Hamiltonian matrix are considered, but all those are calculated exactly.

From the Kohn-Sham eigenvalues $\{\epsilon_i\}$ of the system of interest and those of the isolated atoms, $\{\epsilon_{jm}\}$ (with m being an atom index and j an orbital index), we obtain an approximate total energy of the system of interest relative to that of the non-interacting atoms, $E_r \simeq \sum_i \epsilon_i - \sum_j \sum_m \epsilon_{jm} + \frac{1}{2} \sum_{j \neq j'} U_{jj'}(|\vec{R}_j - \vec{R}_{j'}|)$. The last term is a set of short-ranged, repulsive pair potentials. These are obtained by requiring that the total energy of two-atomic systems (in our case, on Au_2) as a function of interatomic distance is accurately reproduced. Finally in the present study only the $5d$ and $6s$ electrons of the Au atom are explicitly included in the calculations, whereas the rest are treated within a frozen-core approximation. Ultimately, we checked the accuracy of our approach by calculating the lattice constant of crystalline Au. The result is within 0.3% of the experimental value.

In optimizing the structures of gold clusters, we have used genetic algorithms [11, 12]. Our version is as follows. Suppose that we have optimized the structure of the cluster with $N - 1$ atoms. From this we construct a first generation consisting of M independent clusters for the N -atom system by randomly adding one Au atom and letting each of these structures relax to its nearest total-energy minimum. Subsequently, a new set of clusters is constructed by cutting each of the original ones randomly into two parts that are interchanged (under the constraints that no atom should be too close to any other atom or too far from all the other ones) and, afterwards, let relax. Out of the total set of $2M$ structures, the M ones of the lowest total energy are kept for the next generation. This procedure is repeated until the lowest total energy is unchanged for a large number of generations.

3 Results and Discussion

In Fig. 1 we show the variation in the total energy per atom for the globally optimized structures together with that of the icosahedral Au_{13} cluster (for which the total energy could be lowered upon a local symmetry-breaking relaxation, which is seen as the two triangles in Fig. 1, with the

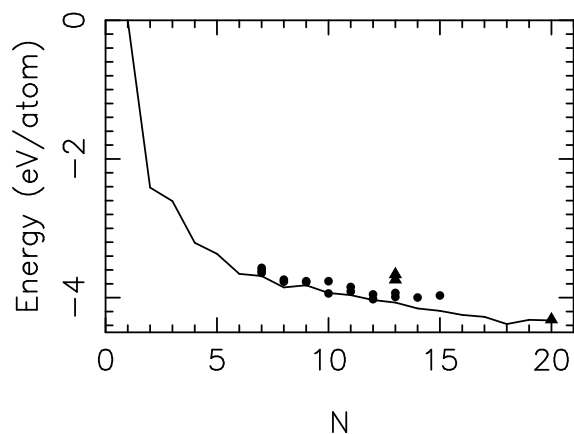


Figure 1: The variation in the total energy per atom (relative to that of the isolated atom) for the optimized Au_N clusters (solid curve) together with those of planar structures (dark circles) and those of icosahedral Au_{13} and tetragonal Au_{20} clusters (dark triangles).

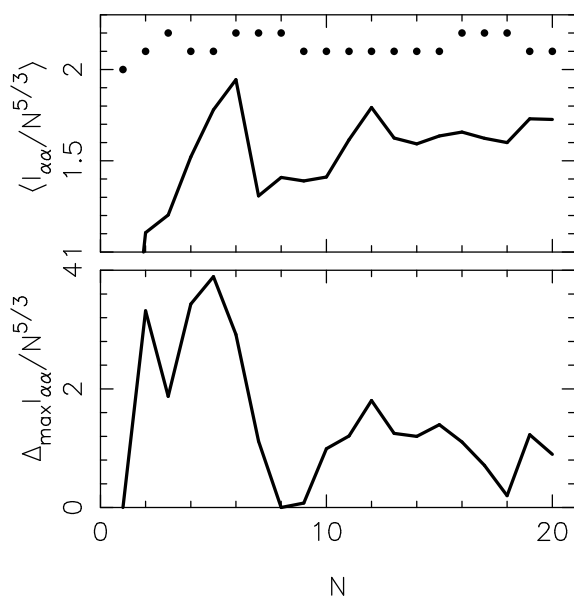


Figure 2: Properties related to the eigenvalues $I_{\alpha\alpha}$ of the matrix containing the moments of inertia. The upper panel shows the average value (scaled by $N^{5/3}$) together with marks indicating whether the Au_N cluster is overall spherical (dots in the lowest row), overall cigar-like shape (middle row) or overall lens-like shape (upper row). The lower panel shows the largest difference in the eigenvalues.

lower one corresponding to the lower-symmetry structure), and that of the tetragonal Au_{20} cluster for which the total energy was only marginally higher than that of the globally optimized structure.

In order to obtain additional information on the structure, we first determine the center for each cluster, $\vec{R}_0 = \frac{1}{N} \sum_{i=1}^N \vec{R}_i$, with \vec{R}_i being the position of the i th atom, and then the radial

distance for each atom $r_i = |\vec{R}_i - \vec{R}_0|$. Subsequently, we calculate the 3×3 matrix containing $\sum_i s_i t_i$ (with s and t being x , y , and z), and from the eigenvalues $I_{\alpha\alpha}$ of this we analyse the overall shape of the cluster: three identical eigenvalues suggest a spherical shape, whereas two large and one small value suggest a lens-like shape, and two small and one large value suggest a cigar-like shape. In Fig. 2 we show the average eigenvalue (scaled by $N^{5/3}$, which is the scaling a spherical jellium would possess) together with marks indicating the overall shape. Also the largest difference between the eigenvalues is shown. We see that except for a single atom, no cluster has an overall spherical shape, in agreement with the suggestion that Au_N clusters in general possess a low symmetry.

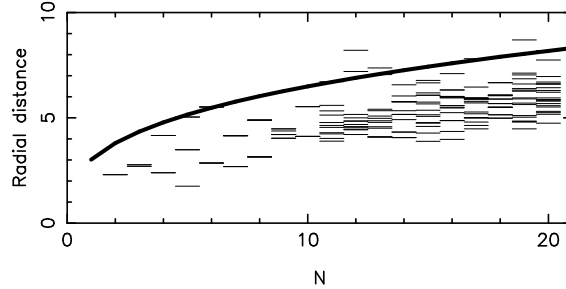


Figure 3: The radial distances of the atoms for the Au_N clusters. For each value of N , a horizontal line indicates that at least one atom has that radial distance. The thicker curve marks the radius of a spherical jellium with the density as that of crystalline gold.

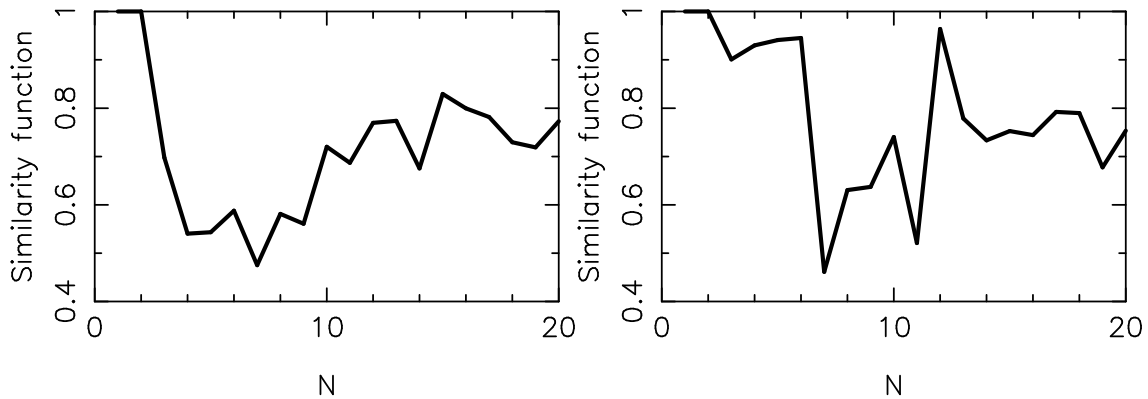


Figure 4: The similarity function quantifying whether the structure of a cluster with N atoms resembles that of the cluster with $N-1$ atoms plus one atom. In the left panel the radial distances, and in the right panel the interatomic distances have been used in quantifying the similarity.

The low symmetry can also be seen in Fig. 3 where we show the radial distances of the atoms as a function of N . The fact that for each value of N we have many different values is an indication of the low symmetry. Interesting is it also to see that for most clusters, the largest radial distance is smaller than the radius of a spherical cut-out of crystalline gold with the same number of atoms, although if, e.g., the atoms are small spheres, the spatial extension of the cluster would be larger than the largest radial distance. Finally, we see a clear shell construction: for $N > 10$ all atoms have fairly large radial distances.

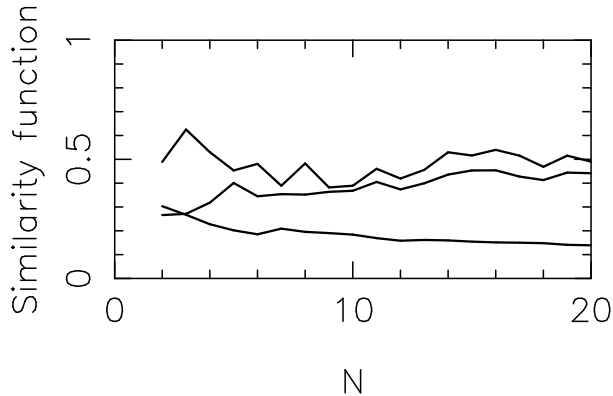


Figure 5: The similarity function quantifying whether the structure of a cluster with N atoms resembles a piece of the fcc crystal. The different curves correspond to different cut-outs of the crystal.

Finally, we shall discuss the similarity of the clusters with different other objects. We consider first two clusters, Au_N and Au_{N-1} . For the former we consider each of the N structures that can be obtained by removing one atom. Subsequently, we compare the radial distances or the interatomic distances for the two structures, $q = \left[\frac{1}{P} \sum_{j=1}^P (x'_i - x_i^0)^2 \right]^{1/2}$ with P being $N-1$ or $(N-1)(N-2)/2$ and with x'_i and x_i^0 being the quantities for the $(N-1)$ -atomic fragment of the Au_N cluster and for the Au_{N-1} cluster, respectively. A similarity function is then defined as $S = \frac{1}{1+q_{\min}/a_0}$, with q_{\min} being the smallest value of q and $a_0 = 1$ a.u. Other similarity functions are constructed by considering the radial distances of an unrelaxed spherical cut-out of the crystalline material (with different values depending on where the center of the cut-out is placed). $S \rightarrow 1$ ($S \rightarrow 0$) if the two structures that are being compared are very similar (very different).

Some examples of such an analysis are shown in Figs. 4 and 5. The fairly small values of S in both figures show that in the size range considered here, the structures do indeed not resemble each other, neither are they close to small fragments of the infinite crystal.

4 Conclusion

We have presented results of our theoretical study on the electronic and structural properties of Au_N clusters. We have used an unbiased approach in optimizing the structure together with a parameterized density-functional method for calculating the total energy and the electronic properties of a given structure.

We found that for clusters with up to 6 atoms, the structure of the lowest total energy was planar. For larger clusters, truly three-dimensional objects are found but for clusters with up to 15 atoms, planar structures were found to lie very close in energy to those found in the unbiased search. We can not exclude that removing inaccuracies in our approach would change the relative ordering of those. Another interesting finding is that the high-symmetry structures for $N = 13$ and $N = 20$ (i.e., an icosahedron and a tetrahedron, respectively) are also comparable in energy with those we optimized (in particularly for $N = 20$ this is the case), but that for $N = 13$, the icosahedron lowers its symmetry through local relaxation. Moreover, in many cases our structures possess a cage-like structure.

The fact that the structures possess a low symmetry was clearly observable in the distribution of the radial distances of the atoms and in the eigenvalues of the matrix with the moments of

inertia. Finally, our similarity functions indicate that the structures of the individual clusters neither resemble each other, nor resemble pieces of the infinite fcc crystal.

Acknowledgements

This work was supported by the DFG (German Research Foundation) through the SFB 277 at the University of Saarland.

References

- [1] F. Baletto and R. Ferrando, *Rev. Mod. Phys.* **77**, 371 (2005).
- [2] F. Furche, R. Ahlrichs, P. Weis, C. Jacob, S. Gilb, T. Bierweiler, and M. M. Kappes, *J. Chem. Phys.* **117**, 6982 (2002).
- [3] S. Gilb, P. Weis, F. Furche, R. Ahlrichs, and M. M. Kappes, *J. Chem. Phys.* **116**, 4094 (2002).
- [4] X. Gu, M. Ji, S. H. Wei, and X. G. Gong. *Phys. Rev. B* **70**, 205401 (2004).
- [5] J. Wang, J. Jellinek, J. Zhao, Z. Chen, R. B. King, and P. von Ragué Schleyer, *J. Phys. Chem. A* **109**, 9265 (2005).
- [6] S. Bulusu, X. Li, L-S. Wang and X-C. Zeng, *PNAS* **103**, 8326 (2006).
- [7] H. Häkkinen, M. Moseler, O. Kostko, N. Morgner, M. A. Hoffmann, and B. v. Issendorff, *Phys. Rev. Lett.* **93**, 093401 (2004).
- [8] D. Porezag, Th. Frauenheim, Th. Köhler, G. Seifert, and R. Kaschner, *Phys. Rev. B* **51**, (1995) 12947.
- [9] G. Seifert, R. Schmidt, *New J. Chem.* **16**, (1992) 1145.
- [10] G. Seifert, D. Porezag and Th. Frauenheim, *Int. J. Quantum Chem.* **58**, (1996) 185.
- [11] J. H. Holland, *Adaption in Natural Algorithms and Artificial systems* (University of Michigan Press, Ann Arbor, MI, 1975).
- [12] D. E. Goldberg, *Genetic Algorithms in Search, Optimization and Machine Learning* (Addison-Wesley, Reading, MA, 1989).

Global Structure Optimization Study on Au_{2-20}

Yi Dong^a and Michael Springborg^b

Physical and Theoretical Chemistry, University of Saarland, D-66123 Saarbrücken, Germany

Received: date / Revised version: date

Abstract. The geometries and electronic properties of the most stable small Au_n clusters with $n = 2$ to 20 are presented. An intensive search for low-energy minima of Au_n clusters was carried through using a density-functional tight-binding method combined with genetic algorithms for an unbiased global structure optimization. The structural and energetic properties of the small gold clusters are compared with those of planar Au_n clusters with $n = 5$ to 15. Also a comparison with results from the spherical jellium model is presented.

PACS. 36.40.-c Atomic and molecular clusters – 61.46.Bc Clusters

1 Introduction

Clusters formed by gold atoms are among the most intensively studied clusters, partly because they can be used in electronic devices [1], as nanomaterials [2], and as catalysts [3–6]. As a consequence, there exist many theoretical studies on the electronic and structural properties of Au_n clusters.

For instance, Häkkinen and Landman investigated neutral and anionic gold clusters Au_{2-10} using the density-functional theory with scalar-relativistic *ab initio* pseudopotentials and a generalized gradient approximation [7]. Wang *et al.* studied lowest-energy gold clusters with size from 2 to 20 [8], whereas Walker [9] performed density functional theory calculations on neutral and cationic gold clusters with up to nine atoms. Small gold clusters show catalytic activity, like Au_8 supported on MgO that can catalyze the oxidation reaction of CO to CO_2 , and Au_{10} is used to catalyze CO oxidation on a TiO_2 support. It has also been suggested that the surface roughening plays an important role in the catalytic activity, since nonplanarity of gold clusters localizes the electron density and thus promotes reactivity.

For an understanding of all the properties of small gold clusters it is mandatory to have a detailed information on the structural and electronic properties of these systems. Although much effort has been invested in this endeavour, there are still many open questions, of which one interesting one is at what size the gold cluster changes from 2D to 3D geometry [10].

Since the number of structural degrees of freedom of an Au_n cluster equals $3n - 6$, since the number of inequivalent (meta-)stable structures grows essentially exponentially with n , and since the computational demands for a

single structure scales as n^k with $k \geq 3$, theoretical studies on Au_n clusters are in one or another way biased. Either many structures are studied with less accurate methods, or few, selected, structures are studied with more accurate methods.

As a typical example we mention the studies of Garzón *et al.* [11] and of Michaelian *et al.* [12] who used global optimization methods (based on genetic algorithms) combined with the simple Gupta potential for the description of interatomic interactions. The optimized structures were subsequently studied further using density functional calculations.

In the present work, we apply a parameterized density-functional tight-binding method combined with an unbiased global minimum search to determine the lowest energy structures of gold clusters with from 2 to 20 atoms. In contrast to previous unbiased structure optimizations, our total-energy method includes electronic degrees of freedom, making it, we believe, more accurate. Because of the recent interest in planar gold clusters [13–15], we also included such ones in our study, together with the icosahedral Au_{13} and tetragonal Au_{20} clusters.

2 Computational Method

By using a parameterized tight-binding density-functional method combined with genetic algorithms we have determined the global total-energy-minimum structures for gold clusters containing up to 20 atoms. The planar gold clusters with 5–15 and the icosahedral Au_{13} and tetragonal Au_{20} clusters were relaxed locally.

The density-functional tight-binding method [16–18] is based on the density functional theory of Hohenberg and Kohn in the formulation of Kohn and Sham. Moreover, the Kohn-Sham orbitals ψ_i of the system of interest are

^a Corresponding author; *e-mail*: y.dong@mx.uni-saarland.de

^b *e-mail*: m.springborg@mx.uni-saarland.de

expanded in terms of atom-centered basis functions $\{\phi_j\}$,

$$\psi_i(\mathbf{r}) = \sum_j c_{ij} \phi_j(\mathbf{r}). \quad (1)$$

This gives the secular equations

$$\sum_m c_{im} (h_{mn} - \epsilon_i S_{mn}) = 0, \quad (2)$$

where the matrix elements of Hamiltonian h_{mn} and the overlap matrix elements S_{mn} are defined as

$$\begin{aligned} h_{mn} &= \langle \phi_m | \hat{h} | \phi_n \rangle \\ S_{mn} &= \langle \phi_m | \phi_n \rangle \end{aligned} \quad (3)$$

and the Hamiltonian is defined as

$$\hat{h} = \hat{t} + V_{\text{eff}}(\mathbf{r}) \quad (4)$$

with \hat{t} being the kinetic-energy operator and $V_{\text{eff}}(\mathbf{r})$ being the effective Kohn-Sham potential which is approximated as a simple superposition of the potentials of the neutral atoms

$$V_{\text{eff}}(\mathbf{r}) = \sum_j V_j^0(|\mathbf{r} - \mathbf{R}_j|). \quad (5)$$

In the present method, all three-center terms are ignored, but all two-center terms are calculated exactly.

From the Kohn-Sham eigenvalues $\{\epsilon_i\}$ of the system of interest and those of the isolated atoms, $\{\epsilon_{jm}\}$ (with m being an atom index and j an orbital index), we can arrive at an approximate total energy of the system of interest relative to that of the non-interacting atoms,

$$E_r \simeq \sum_i \epsilon_i - \sum_j \sum_m \epsilon_{jm} + \frac{1}{2} \sum_{j \neq j'} U_{jj'}(|\mathbf{R}_j - \mathbf{R}_{j'}|). \quad (6)$$

The last term is a set of short-ranged, repulsive pair potentials. These are obtained by requiring that the total energy of two-atomic systems (in our case, on Au₂) as a function of interatomic distance is accurately reproduced.

Finally, in the present study only the $5d$ and $6s$ electrons of the Au atom are explicitly included in the calculations, whereas the rest are treated within a frozen-core approximation.

Ultimately, we checked the accuracy of our approach by calculating the lattice constant of crystalline Au. The result is within 0.3% of the experimental value.

In optimizing the structures of gold clusters, we have used genetic algorithms. As we have shown in our studies on (HAIO)_{*n*} clusters [19,20], this approach gives accurate results.

The genetic algorithms are based on the principles of natural evolution and are, therefore, also called evolutionary algorithms [21,22]. They provide an efficient tool for global geometry optimizations. Our version of the genetic algorithms is as follows. Suppose that we have optimized the structure of the cluster with $n - 1$ atoms. From this structure we construct a first generation consisting of M independent clusters for the n -atom system by randomly

adding one Au atom and letting each of these structures relax to its nearest total-energy minimum. Subsequently, a new set of clusters is constructed by cutting each of the original ones randomly into two parts that are interchanged (under the constraints that any atom should not be too close to any other atom or too far from all the other ones) and, afterwards, let relax. Out of the total set of $2M$ structures, the M ones of the lowest total energy are kept for the next generation. This procedure is repeated until the lowest total energy is unchanged for a large number of generations.

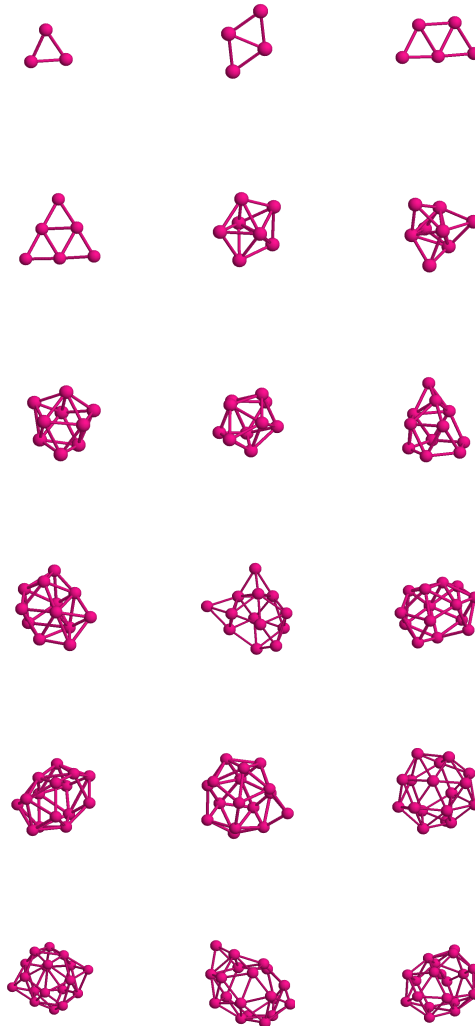


Fig. 1. The structures of the Au_{*n*} clusters from the global structure optimization. n goes from 3 in the upper left corner to 20 in the lower right corner.

3 Results and Discussion

In Fig. 1 we show the structures that our global structure optimization has produced for Au_{*n*} with $3 \leq n \leq 20$.

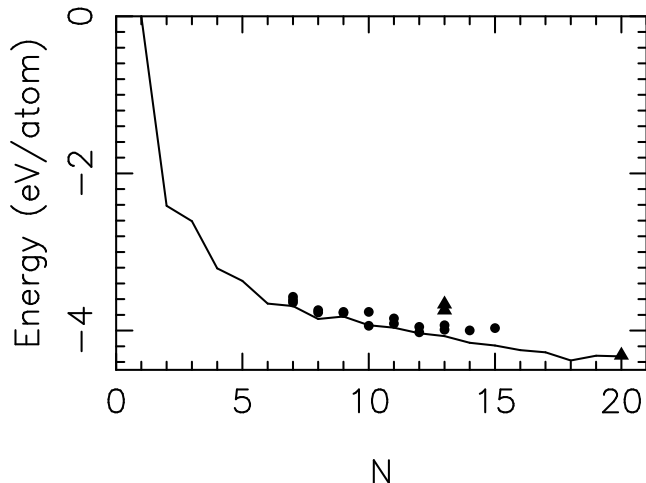


Fig. 2. The variation in the total energy per atom (relative to that of the isolated atom) for the optimized Au_n clusters (solid curve) together with those of planar structures (dark circles) and those of icosahedral Au₁₃ and tetragonal Au₂₀ clusters (dark triangles).

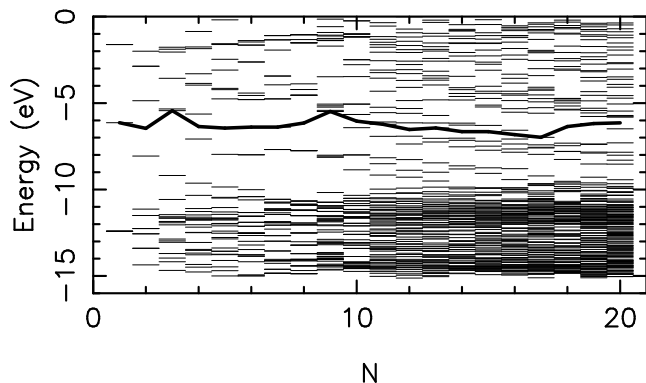


Fig. 3. The orbital energies for Au_n clusters as a function of *n*. Each line for a given *n* marks at least one orbital with that energy, and the thicker curve shows the Fermi energy.

It is seen that up to $n = 6$ the clusters are planar, but above that the structures are truly three-dimensional ones. Nevertheless, as Fig. 2 shows, the total energy per atom for the planar structures with up to 15 atoms is only slightly higher than that of the structures of Fig. 1. It is therefore possible that a more accurate method would predict that the planar ones have a lower total energy.

For most planar clusters we considered more different structures, resulting in more different total energies, as seen in the figure. In one single case ($n = 10$) the planar geometry even resulted in a total energy that was lower than that of the global optimization, indicating that despite the high reliability of the genetic algorithms, also they may at cases fail. For the icosahedral Au₁₃ cluster, the total energy could be lowered upon a local symmetry-lowering relaxation, which is seen as the two triangles in Fig. 2 (with the lower one corresponding to the lower-symmetry structure), whereas for the tetragonal Au₂₀ clus-

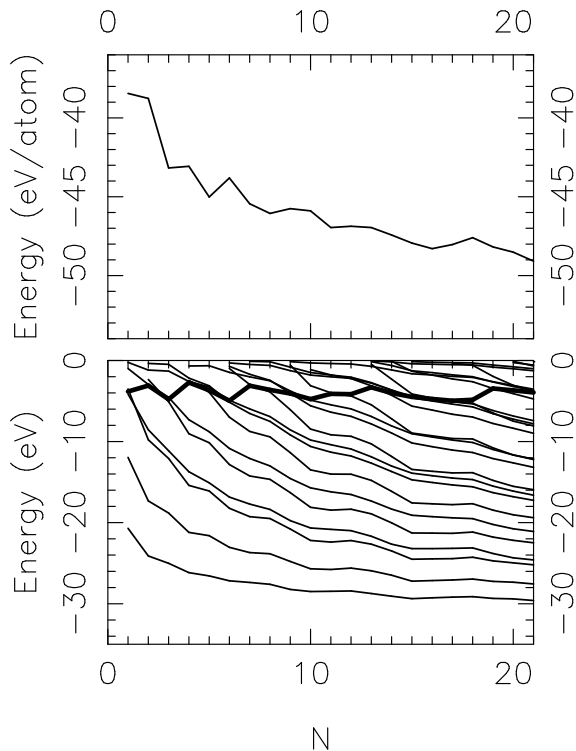


Fig. 4. Results from calculations using the spherical jellium model and assuming that each atom contributes with 11 electrons. The upper panel shows the variation in the total energy per atom, and the lower one the orbital energies with the thicker curve marking the Fermi energy.

ter the total energy was only marginally higher than that of the globally optimized structure.

It is interesting to compare the results of Fig. 2 with those of Fig. 3. In the latter figure we show the orbital energies for the different Au_n clusters. Here, the Fermi energy possesses a locally maximum for $n = 3, 9$, and 20 , which, with $n = 20$ partly being an exception, also are systems of low stability. Moreover, for the two former, the removal of a single electron would move the Fermi energy into a large energy gap, suggesting that Au₃⁺ and Au₉⁺ are particularly stable. Finally, Fig. 3 shows how a deep-lying broad band of orbitals from the $5d$ functions is formed for the larger systems.

Often the spherical jellium model is used in obtaining a simple description of the stability and the orbitals of metal clusters. Assuming that one atom contributes with only one electron, one would obtain particularly stable clusters for those with 2, 8, 18, and 20 atoms. However, when assuming that each atom contributes with 11 electrons, the situation will change. This is shown in Fig. 4 where results from a spherical-jellium study are shown. The variation in the total energy is clearly much stronger than that of Fig. 2. One reason could indeed be that the $5d$ electrons of Au only partly are so delocalized that they feel the spatial extensions of the clusters. This is confirmed by the orbital energies, shown in the lower panel, that do not at all resemble those of Fig. 3.

Table 1. Symmetry of gold clusters from 3 to 20 atoms

Size	Symmetry	Size	Symmetry	Size	Symmetry
3	D_2	9	D_{2v}/D_2	15	C_1
4	D_{2h}	10	D_2	16	C_s
5	C_{2v}	11	C_1	17	C_1
6	D_{3h}	12	C_1	18	C_2
7	D_{5h}	13	C_s	19	C_1
8	T_d	14	C_s	20	C_1

As may be seen from Fig. 1, the structures we find in our global optimization are fairly irregular. This can also be extracted from the results of Table 1 that lists the symmetry groups of the structures. These are indeed all of low symmetry. Finally, a recent study of Bulusu *et al.* [23] finds that hollow gold cages exist for Au_{*n*} with $n = 16-18$, both according to experimental and theoretical results. In Fig. 1 we see that our study finds many Au_{*n*} clusters with $n = 7 - 20$ to have cage-like structures.

4 Conclusion

In this work we have presented results of our theoretical study on the electronic and structural properties of Au_{*n*} clusters. We have used an unbiased approach in optimizing the structure together with a parameterized density-functional method for calculating the total energy and the electronic properties of a given structure.

We found that for clusters with up to 6 atoms, the structure of the lowest total energy was planar. For larger clusters, truly three-dimensional objects are found but for clusters with up to 15 atoms, planar structures were found to lie very close in energy to those found in the unbiased search. We can not exclude that removing inaccuracies in our approach would change the relative ordering of those. Another interesting finding is that the high-symmetry structures for $n = 13$ and $n = 20$ (i.e., an icosahedron and a tetrahedron, respectively) are comparable in energy with those we optimized (in particular for $n = 20$ this is the case), but that for $n = 13$, the icosahedron lowers its symmetry through local relaxation. Moreover, in many cases our structures possess a cage-like structure.

Indeed, the observation of low-symmetry structures was a general finding of our calculations. Thus, these clusters are far spherical. Thus, as we also explicitly demonstrated, the spherical jellium model does not at all provide an accurate description of the properties of the small Au_{*n*} clusters. Instead, an explicit description of the 5*d* and 6*s* orbitals is needed, suggesting also that methods based on pair potentials but without an explicit description of the orbital interactions may provide inaccurate results for those small systems.

Acknowledgements

This work was supported by the DFG (German Research Foundation) through the SFB 277 at the University of Saarland.

References

1. M. Dorogi, J. Gomez, R. Osifichin, R. P. Andres, and R. Reifenberger, *Phys. Rev. B* **52**, (1995) 9071.
2. R. L. Whetten, M. N. Shafiqullin, J. T. Khoury, T. G. Schaaff, I. Vezmar, M. M. Alvarez, and A. Wilkinson, *Acc. Chem. Res.* **32**, (1999) 397.
3. B. Yoon, H. Häkkinen, U. Landman, A. S. Wörz, J.-M. Antonietti, S. Abbet, K. Judai, and U. Heiz, *Science* **37**, (2005) 403.
4. A. Sanchez, S. Abbet, U. Heiz, W.-D. Schneider, H. Häkkinen, R. N. Barnett, and U. Landman, *J. Phys. Chem. A* **103**, (1999) 9573.
5. M. Neumaier, F. Weigend, O. Hampe, and M. M. Kappes, *J. Chem. Phys.* **122**, (2005) 104702.
6. N. Lopez and J. K. Nørskov, *J. Am. Chem. Soc.* **124**, (2002) 11263.
7. H. Häkkinen and U. Landman, *Phys. Rev. B* **62**, (2000) R2287.
8. J.-L. Wang, G.-H. Wang and J.-J. Zhao, *Phys. Rev. B* **66**, (2002) 035418.
9. A. V. Walker, *J. Chem. Phys.* **122**, (2005) 094310.
10. R. M. Olson, S. Varganov, M. S. Gordon, H. Metiu, S. Chretien, P. Piecuch, K. Kowalski, S. A. Kucharski, and M. Musial, *J. Am. Chem. Soc.* **127**, (2005) 1049.
11. I. L. Garzón, M. R. Beltrán, G. Gonzalez, I. Gutierrez-Gonzalez, K. Michaelian, J. A. Reyes-Nava, and J. I. Rodriguez-Hernandez, *Eur. Phys. J. D* **24**, (2003) 105
12. K. Michaelian, N. Rendón, and I. L. Garzón, *Phys. Rev. B* **60**, (1999) 2000.
13. S. Gilb, P. Weis, F. Furche, R. Ahlrichs, and M. M. Kappes, *J. Chem. Phys.* **116**, (2002) 4094.
14. H. Häkkinen, B. Yoon, U. Landman, X. Li, H.-J. Zhai, and L.-S. Wang, *J. Phys. Chem. A* **107**, (2003) 6168.
15. V. Bonačić-Koutecký, J. Burda, R. Mitrić, M. Ge, G. Zampella, and P. Fantucci, *J. Chem. Phys.* **117**, (2002) 3120.
16. D. Porezag, Th. Frauenheim, Th. Köhler, G. Seifert, and R. Kaschner, *Phys. Rev. B* **51**, (1995) 12947.
17. G. Seifert, R. Schmidt, *New J. Chem.* **16**, (1992) 1145.
18. G. Seifert, D. Porezag and Th. Frauenheim, *Int. J. Quantum Chem.* **58**, (1996) 185.
19. Y. Dong and M. Springborg, *In Proceedings of 3rd International Conference "Computational Modeling and Simulation of Materials"* (Vincezini, P. et al., Eds.: Techna Group Publishers: Faenza, Italy, 2004) 167.
20. Y. Dong, M. Burkhart, M. Veith, and M. Springborg, *J. Phys. Chem. B* **109**, (2005) 22820.
21. J. H. Holland, *Adaption in Natural Algorithms and Artificial systems* (University of Michigan Press, Ann Arbor, MI, 1975).
22. D. E. Goldberg, *Genetic Algorithms in Search, Optimization and Machine Learning* (Addison-Wesley, Reading, MA, 1989).
23. S. Bulusu, X. Li, L.-S. Wang and X.-C. Zeng, *PNAS* **103**, (2006) 8326.

Unbiased determination of structural and electronic properties of gold clusters with up to 58 atoms

Yi Dong[†] and Michael Springborg[‡]

*Physical and Theoretical Chemistry,
University of Saarland, 66123 Saarbrücken, Germany*

(Dated: September 19, 2006)

Abstract

Isolated neutral Au_N clusters are studied using a parameterized density-functional tight-binding method combined with genetic algorithms for N from 2 up to 58. Various descriptors are used in analysing the results, including stability, shape, and similarity functions, as well as radial distances of the atoms and the orbital energies, all as functions of N . Also dissociation patterns and the symmetry of the clusters are analysed. By comparing with results of jellium calculations and with those of earlier embedded-atom studies, it is demonstrated that for gold clusters, electronic effects are very important, leading to a partly suppression of the occurrence of magic numbers, as well as to low-symmetry and only partly compact clusters. Also shell-like structures are found.

[†]e-mail: y.dong@mx.uni-saarland.de

[‡]e-mail: m.springborg@mx.uni-saarland.de

I. INTRODUCTION

It is well known that materials properties depend sensitively on their structure and composition, and actually most technological products are to a large extent a consequence of our capability to exploit this fact, although precise prediction of the materials properties for a given system not yet has become possible. During the last quarter of a century another approach for controlling and varying materials properties has been intensively studied and partly also exploited in practical applications. Thus, when the materials dimensions are reduced to the nm range, their properties change markedly from those of their macroscopic counterparts.

One class of such systems is provided by clusters that typically contain between some 10s and some 100 000s of atoms and most often only a few type of atoms (with, however, the possible exception of surfactants that saturate dangling bonds on the surface of the clusters). Quantum-size effects combined with the fact that the number of surface atoms relative to the total number of atoms is far from vanishing may be held responsible for the unique, size-dependent properties of those materials and they have, accordingly, been the subject of many experimental and theoretical studies (see, e.g., [1]). The precise determination of the relation between size and property is, however, not easy for clusters. In experimental studies the clusters are rarely isolated, but instead they often interact with some other medium like a solvent or a supporting surface, possess surfactants, or their precise size is only approximately known. On the other hand, theoretical studies most often deal with isolated clusters of a well-defined size and often without ligands for which it is overwhelmingly complicated to determine the structure. Without any further information the identification of the structure of the lowest total energy for a cluster of N atoms requires searching in a geometry space of $3N - 6$ dimensions, which for any but the smallest values of N hardly is possible.

A special case is that of gold clusters. They have attracted much attention over the last 20 years, partly due to applications in, for example, catalysis, biology, and nanotechnology,²⁻⁴ and partly because gold clusters can be a useful model system for theoretical studies. On the other hand, it has turned out to be particularly difficult to determine the structures of

these clusters. When attempting to perform an unbiased structure optimization of a larger range of cluster sizes, parameter-free electronic-structure methods cannot be applied due to the large computational needs and, instead, more or less accurate approximate methods have to be applied. And then it has turned out that in particular for gold clusters, the resulting structures depend very sensitively on the applied method (see, e.g., [1]), which is to a much lesser extent the case for clusters of most other elements.

Various electronic-structure methods have been applied for gold clusters with up to around 20 atoms with the special emphasis on identifying the size at which the clusters change from two- to three-dimensional.⁵⁻¹⁵ Slightly larger Au_N clusters (with N up to 26) were studied by Fa *et al.*¹⁶ using parameter-free density-functional calculations, but for even larger clusters there exists only few electronic-structure studies for selected sizes and/or structures (see, e.g., [17,18]). Instead, unbiased studies of the structures of gold clusters for larger N are all based on more or less empirical interaction potentials, like the embedded-atom, the Sutton-Chen, the Murrell-Mottram, and the Gupta potential (see, e.g., [1,19,20]), which, however, turn out to lead to markedly different results depending on the potential.

As a step towards a more accurate, but unbiased, study of the properties of gold clusters for also larger values of N we shall here report results of a study that explicitly includes a description of the electronic degrees of freedom. Using a parameterized density-functional method in combination with genetic algorithms for the structure determination we have optimized the structures for Au_N clusters with N up to 58. The computational approach shall be described in Sec. II and the results in Sec. III. We shall put special emphasis on analysing our findings through some few key descriptors and also compare them with those of two extreme situations: the results of the above-mentioned empirical calculations that do not include electronic degrees of freedom, and those of jellium calculations that exclude structural degrees of freedom. Finally, Sec. IV summarizes our findings.

II. THE COMPUTATIONAL METHOD

In order to calculate the electronic properties and total energy of a given structure we have used the parameterized density-functional tight-binding (DFTB) method of Seifert *et al.*²¹⁻²³ For the determination of the structure of the lowest total energy we have combined this method with genetic algorithms.

The density-functional tight-binding method is based on the density functional theory of Hohenberg and Kohn in the formulation of Kohn and Sham. Then, the Kohn-Sham orbitals Ψ_i of the system of interest are expanded in terms of atom-centered localized basis functions χ_m ,

$$\Psi_i(\mathbf{r}) = \sum_m c_{im} \chi_m(\mathbf{r} - \mathbf{R}_j). \quad (1)$$

The Kohn-Sham single-particle operator is approximated as

$$\hat{h} = \hat{t} + V_{\text{eff}}(\mathbf{r}) = \hat{t} + \sum_j V_j^0(|\mathbf{r} - \mathbf{R}_j|), \quad (2)$$

with \hat{t} being the kinetic-energy operator and $V_{\text{eff}}(\mathbf{r})$ being the effective Kohn-Sham potential which is approximated as a simple superposition of the potentials of the neutral atoms. Furthermore, we assume that the matrix elements $\langle \chi_m | V_j^0 | \chi_n \rangle$ vanish unless at least one of the two basis functions is centered at atom j . Finally, all remaining matrix elements are calculated accurately.

From the Kohn-Sham eigenvalues of the isolated atoms and of the system of interest we calculate the total energy (relative to that of the isolated atoms) according to

$$E_B \approx \sum_i^{\text{occ}} \epsilon_i - \sum_j \sum_m \epsilon_{jm} + \frac{1}{2} \sum_{j \neq j'} U_{jj'}(|\mathbf{R}_j - \mathbf{R}_{j'}|) \quad (3)$$

(with m being an atom index and j an orbital index). Here, U_{jk} is a short-range pair potential between atoms j and k that is so adjusted that results from parameter-free density-functional calculations on two-atomic systems as a function of the interatomic distance are accurately reproduced.

Finally in this study only the $5d$ and $6s$ electrons were explicitly included in the calculations, whereas the others were treated within a frozen-core approximation.

Since the approach is based on extrapolating results from the two-atomic systems to larger systems, we tested it by calculating the lattice constant of crystalline Au. We found 7.73 a.u., which is in excellent agreement with the experimental value of 7.71 a.u.²⁴ Subsequently, we assume that the properties of the finite Au_N clusters are accurately described, too, although this is an approximation.

In optimizing the structures of gold clusters, we have used a method based on genetic algorithms that we earlier have used in optimizing the structures of $(\text{HAIO})_N$ clusters.^{25,26} The genetic algorithms are based on the principles of natural evolution and are, therefore, also called evolutionary algorithms^{27,28} and have been found to provide an efficient tool for global geometry optimizations. Our version of the genetic algorithms is as follows. Suppose that we have optimized the structure of the cluster with $N - 1$ atoms. From this structure we construct a so-called generation consisting of M independent clusters for the N -atom system by randomly adding one Au atom and letting each of these M structures relax to its nearest total-energy minima. Subsequently, a new set of clusters is constructed by cutting each of the original ones randomly into two parts that are interchanged (under the constraint that no atom should become too close to any other atom or too far from all the other ones) and, afterwards, allowed to relax. Out of the total set of $2M$ structures, the M ones of the lowest total energy are kept as the next generation. This procedure is repeated until the lowest total energy is unchanged for a large number of generations.

In addition to these calculations we also considered the spherical jellium model. Here, it was assumed that all but the 11 $5d$ and $6s$ valence electrons per gold atom as well as the nuclei were smeared out to a spherical medium (jellium) with a constant density inside which the valence electrons were moving. The density of the jellium was taken to be the same as in crystalline Au, and a local-density approximation within density-functional theory was assumed valid for the valence electrons. The resulting one-dimensional, single-particle equations were solved numerically and self-consistently.

Finally, throughout the paper we shall use a.u. as length unit and eV as energy unit. Moreover, brief accounts of our results for clusters with $N \leq 20$ have been presented elsewhere.^{29,30}

III. RESULTS AND DISCUSSION

From the DFTB calculations we extract the total energy as a function of size of the cluster, $E_B(N)$. In Fig. 1 we show $E_B(N)/N$ as a function of N for the globally optimized structures together with the value of the icosahedral Au_{13} cluster (for which the total energy could be lowered upon a local symmetry-breaking relaxation, which is seen as the two triangles in Fig. 1, with the lower one corresponding to the lower-symmetry structure), and that of the tetragonal Au_{20} cluster for which the total energy was only marginally higher than that of the globally optimized structure. In the figure we also show results for planar clusters with $N \leq 15$. The figure shows that for clusters with up to 6 atoms, the structure of the lowest total energy is planar. For larger clusters, truly three-dimensional objects are found but for clusters with up to 15 atoms, planar structures lie very close in energy to those found in the unbiased search. We can not exclude that removing inaccuracies in our approach would change the relative ordering of those. On the other hand, Koskinen *et al.*³¹ found also that the DFTB method predicts a transition from 2- to 3-dimensional structures for a relatively low value of N . Finally, the experimentally observed tetragonal Au_{20} cluster³² is indeed a structure of a very low total energy.

In Fig. 1 we see that the total energy per atom is an overall decreasing function of N until $N \simeq 20$ after which value the function instead oscillates around values within roughly 10% of that of the infinite crystal. When approximating the interatomic interactions so that the electronic degrees of freedom are not directly included, structure optimizations often tend to produce structures that are characterized by closed packing whereby as many atoms as possible obtain a high coordination. In that case, the total energy per atom is overall decaying as function of cluster size (see, e.g., [20]). However, already the existence of planar gold clusters suggests that such a description is inaccurate for gold. Therefore, the structure of gold clusters is not only determined by a condition of minimizing the surface area, but also electronic interactions between nearest neighbors are important, meaning ultimately that the total energy per atom not will be a simple, and slowly, decaying function of N but will possess a rather different functional behavior, as seen in the figure. As we shall see

below, these properties of gold clusters manifest themselves at many different places.

In order to identify particularly stable clusters we consider the stability function,

$$\Delta_2 E_B(N) = E_B(N + 1) + E_B(N - 1) - 2E_B(N), \quad (4)$$

that has maxima (minima) for particularly (un)stable structures. This function is shown in Fig. 2. Due to the above-mentioned change in $E_B(N)$ for $N \simeq 20$ the stability function is much more smooth for $N < 20$ than for $N > 20$. For $N \leq 20$ our results confirm those of Wang *et al.*¹¹ who predicted a clear even-odd oscillatory pattern, i.e., clusters with even N were stabler than those with odd N . On the other hand, the most pronounced maxima, at $N = 24, 33, 40, 42, 51,$ and 54 do not follow this even-odd pattern, and are only marginally in agreement with the results of the embedded-atom calculations,²⁰ that do not explicitly include electronic degrees of freedom.

In order to analyse the origin of the particularly stable clusters (i.e., magic numbers), we first consider the effects of electronic degrees of freedom. In Fig. 3 we show the stability function as obtained from the jellium calculations. It is clear that this stability function takes somewhat larger, positive or negative values than that of the DFTB calculations, suggesting that the fact that the DFTB calculations also allow for structural relaxations leads to an overall damping of the stability of the clusters as a function of their size. Moreover, the two curves show only a marginal agreement. In fact, embedded-atom calculations²⁰ lead to even smaller absolute values of the stability, suggesting that ‘stability’ is dictated by a complicated interplay between structural and electronic degrees of freedom.

Whether the jellium model is adequate can, e.g., be studied by looking at the orbital energies. In Fig. 4 we show the orbital energies for the jellium model as a function of cluster size. Since the spherical symmetry is assumed for all clusters, it is trivial to separate the orbitals according to their symmetry properties and, subsequently, to plot their energies as continuous curves. In contrast, Fig. 5 shows the results from the DFTB calculations. A comparison shows first of all that in the DFTB calculations a narrower, deep-lying band (below -10 eV) exists that is formed by the $5d$ functions. Thus, around the Fermi level, orbitals formed mainly by the $6s$ functions are found. This could suggest that in the jellium

calculations one should treat not 11 but only 1 valence electron per atom. This would, however, lead to magic numbers at 2, 8, 18, 20, 34, and 58, which hardly is in agreement with the results of the DFTB calculations. A further result of a comparison between Figs. 4 and 5 is that for each value of N the cluster has a lower symmetry in the DFTB calculations than assumed in the jellium calculations. Therefore, the orbitals have much lower degeneracies in the DFTB calculations leading to many more, different orbital energies. A remarkable exception is $N = 33$ that has only few different orbital energies and, in addition, is particularly stable (see Fig. 2).

Before leaving the discussion of electronic effects we present one result that indicates that the electronic degrees of freedom have some impact on the stability of the clusters. In the DFTB calculations we do not allow for a spin-polarization. Therefore, the gap E_g between the highest occupied and lowest unoccupied orbital (HOMO and LUMO) vanishes for odd N . However, for odd N we may consider two other gaps, one between the single-occupied orbital and the lowest completely empty orbital, $E_{g,1}$, and one between the highest completely filled orbital and the single-occupied one, $E_{g,2}$. In Fig. 6 we show E_g for even N and $E_{g,1}$ and $E_{g,2}$ for odd N . The maxima for N around 6, 8, 18, and 34 (E_g) and 9, 19, 23, 33, and 35 ($E_{g,1}$) correlate fairly well with some of the maxima in Fig. 2. These results are only marginally in agreement with those of Wang *et al.*¹¹ who, however, found that many of the clusters in the range $2 \leq N \leq 20$ were planar, which most likely is the case in that size range, pointing to some limitations of the present approach.

As indirectly indicated in Fig. 5, the optimized structures of the Au_N clusters possess a low symmetry. This is further illustrated in Table I, where the point groups of the optimized structures from the DFTB calculations are listed. It is obvious that most clusters have a low symmetry. A similar tendency is also found in embedded-atom calculations²⁰ where electronic degrees of freedom are not included directly, indicating that the occurrence of the low symmetry is not only an electronic effect like a Jahn-Teller distortion. In their first-principles, density-functional study on Au_N clusters for N up to 20, Wang *et al.*¹¹ found that many clusters have a planar structure, which in some sense also is a low-symmetry structure. Moreover, Häkkinen *et al.*¹⁷ found that for $53 \leq N \leq 58$, low-symmetry, ‘amorphous’

structures are found, which they ascribed to strong relativistic effects. In our calculations, relativistic effects are only partly included, but similar results are nevertheless found. Quite different structures were found by Fa *et al.*¹⁶ whose first-principles, density-functional calculations indicated that for N up to 26, structures with a close resemblance to fragments of the crystal for some values of N as well as tubelike structures for other N were found. This is in remarkable contrast to our findings, as we shall discuss further below.

In order to obtain additional information on the structure, we first determine the center for each cluster,

$$\vec{R}_0 = \frac{1}{N} \sum_{i=1}^N \vec{R}_i, \quad (5)$$

with \vec{R}_i being the position of the i th atom, and then the radial distance for each atom

$$r_i = |\vec{R}_i - \vec{R}_0|. \quad (6)$$

Subsequently, we calculate the 3×3 matrix containing $\sum_i s_i t_i$ (with s and t being x , y , and z), and from the eigenvalues $I_{\alpha\alpha}$ of this we analyse the overall shape of the cluster: three identical eigenvalues suggest a spherical shape, whereas two large and one small value suggest a lens-like shape, and two small and one large value suggest a cigar-like shape. In Fig. 7 we show the average eigenvalue (scaled by $N^{5/3}$, which is the scaling a spherical jellium would possess) together with marks indicating the overall shape. Also the largest difference between the eigenvalues is shown.

We see that except for a single atom, no cluster has an overall spherical shape, in agreement with the results of Table I. However, the largest difference of the eigenvalues takes particularly low values for $N = 8, 9, 18, 25$, and 33 . Some of these values correspond to particularly stable clusters, for which the stability accordingly may be related to a roughly spherical structure, whereas other values occur for clusters with just some few extra atoms on the surface of a compact core.

This is confirmed by Fig. 8 that shows the radial distances for the different Au_N clusters. For N up to around 10 all atoms have a relatively large, but in many case quite scattered distance to the center, suggesting structures of very low symmetry. For $8 \leq N \leq 24$ all radial distances take quite large values suggesting that the structure of these clusters resembles

a hollow cage, The existence of such structures was actually predicted recently.³³ Also the results of density-functional calculations by Gu *et al.*³⁴ on Au_N clusters with $32 \leq N \leq 35$ point to the existence of cage-like structures, which, however, here only marginally is supported in this size range.

For several clusters one or more of the largest radial distances are significantly larger than the radius of the spherical jellium for the same cluster size. The reason is that these clusters have a particularly low symmetry and are very far from being spherical (this can also be seen in the lower part of Fig. 7 as clusters with large maximal differences). Such clusters often possess atoms on the surface that are bonded to only one or two nearest neighbors. That such structural elements exist have also been seen in the density-functional study of Remacle and Kryachko on smaller clusters.¹³ Fig. 8 confirms that the cluster for $N = 33$ is particularly symmetric.

As mentioned above, Fa *et al.*¹⁶ suggested the occurrence of structures related to either fragments of the crystal or to tube-like structures. Our results of Figs. 7 and 8 do not support the latter suggestion. In order to address the first suggestion in more details we use two different approaches. In the first we use so-called similarity functions defined as follows. For a given N we sort all the radial distances. Simultaneously, we construct a spherical fragment of the crystal (with a fixed choice of the center) and sort its radial distances, $\{r_i^{\text{fcc}}\}$. From

$$q = \left[\frac{1}{N} \sum_{i=1}^N (r_i - r_i^{\text{fcc}})^2 \right]^{1/2}, \quad (7)$$

the similarity function is defined as

$$S = \frac{1}{1 + q/u_l} \quad (8)$$

($u_l = 1$ a.u.), which approaches 1 (0) if the two structures are very similar (different). This function is shown in Fig. 9, where we also compare with the structure of an icosahedron. Here, we have compared the radial distances of the Au_N cluster with those of an icosahedral Au_{147} cluster in the same way as above. Our experience for other systems^{35,36} suggests that only when the similarity function is well above 0.8 the two structures that are compared are structurally related to each other. Thus, the results of the present study do not at all confirm the suggestions of Fa *et al.*¹⁶

Alternatively, we may use the common-neighbor analysis.³⁷ A cut-off distance is defined (we use the average of the nearest- and next-nearest-neighbor distances in the fcc crystal) and to each pair of two atoms, three indices, (i, j, k) , are defined. i is the number of common neighbors, j is the number of bonds between those, and k is the number of bonds in the longest unbroken sequence of bonds among those. For an infinite fcc crystal, the three sets $(2, 1, 1)$, $(4, 2, 1)$, and $(4, 4, 4)$ occur with a relative occurrence of $4 : 2 : 1$. In Fig. 10 we show the results of this analysis. We recognize very many other sets of indices than those of the fcc crystal and with relative occurrence comparable with the ones of the indices of the fcc crystal. Thus, also this analysis does not at all suggest that fragments of the crystal are found.

An interesting cluster is the Au_{55} cluster which has been the subject of numerous experimental and theoretical studies (see, e.g., [17]). As seen in Table I, we find that it has a relatively low symmetry (and not an icosahedral, cuboctahedral, or dodecahedral symmetry, as often assumed) with one atom at the center of a slightly distorted high-symmetric structure. Accordingly, this as well as other structures that according to Table I have a low symmetry, appear as being close to high-symmetric upon visual inspection as shown for the Au_{13} , Au_{18} , Au_{33} , and Au_{55} clusters in Fig. 11.

The radial distances of Fig. 8 suggest that certain structural motifs develop as a function of cluster size, i.e., that the cluster with N atoms is similar to that with $N - 1$ atoms plus an extra atom. Some deviations may be found for the smallest values of N as well for $N = 33$. In order to quantify this suggestion we consider similarity functions that are obtained by comparing the cluster with $N - 1$ atoms with each of the N fragments with $N - 1$ atoms of the cluster with N atoms. Both for the Au_{N-1} cluster and for each of the fragments we calculate and sort either the radial distances or the interatomic distances and calculate subsequently a q value analogous to that above. The smallest value of the N q values is used in defining the similarity function S . The result is shown in Fig. 12. It is obvious that the two descriptors give somewhat different results, but also that hardly any of the clusters can be related to the one of one atom less. Thus, here indeed ‘each atom counts!’ In particular, the figure shows that the Au_{33} cluster is exceptional and different from the other ones.

Finally, we have seen that the total energy per atom is almost constant for N above around 20. This has as a further consequence that when considering the dissociation processes, $\text{Au}_N \rightarrow \text{Au}_{N-K} + \text{Au}_K$, and seeking that value of $K \neq 0$ that requires the smallest energy, we find quite scattered values, cf. Fig. 13. Thus, whereas $K = 1$ or $K = 2$ for $N \leq 20$, K takes much larger values for larger N , implying that many of the larger clusters may preferably split into two not too different parts.

IV. CONCLUSIONS

Using an unbiased structure-optimization method (based on genetic algorithms) in combination with a parameterized density-functional method we have studied electronic and structural properties for the whole series of Au_N clusters with $N \leq 58$. This study represents the first such one where also electronic degrees of freedom explicitly are included, which indeed turns out to be important.

Most other related studies have been carried through using simpler descriptions for the interatomic interactions without explicitly including electronic-orbital interactions. Since the latter are those being responsible for directional interactions, it may not surprise that most, previous studies have found structures characterized by close packing. This includes the finding of particularly stable, highly symmetric clusters (i.e., magic numbers).

When including orbital interactions, not only packing but also directional interactions determine the optimal structure and, therefore, in most cases our optimized structures do not have a very high symmetry, i.e., atoms bonded to just one or two neighbors are often found. In this respect, gold seems to be special. For other metals, packing effects are often dominating, whereas for covalently bonded elements, the effects due to directional bonds are dominating. We suggest that for gold there is a competition between the two leading to the low-symmetry, although often quite compact structures of the Au_N clusters.

Admittedly, by using a parameterized (and not first-principles) method, our results may be connected with some uncertainty. Thus, the fact that we find the transition from planar to three-dimensional structures for a much too small N may be explained from this. On the

other hand, low-symmetry structures have been found in other, more accurate studies on selected clusters, as discussed above.

The fact that electronic effects are important was indicated by the results of the calculations for the spherical-jellium model. In particular the stability function from these calculations had a somewhat larger amplitude than was the case for the DFTB results. Once again, the lowering of the symmetry is one reason for this difference. Furthermore, in some cases we could correlate the occurrence of particularly stable clusters with large gaps of the electronic orbitals around the Fermi level.

In agreement with recent results, we found that the most stable structures for $10 \leq N \leq 20$ correspond to shell-like structures. Moreover, we predict that Au_{33} should be particularly stable. Surprisingly, for $N > 20$ the total energy per atom changes only little, which as a consequence means that the energetically favored dissociation channels for these clusters often are those where the cluster splits into two larger fragments.

Moreover, the structures showed hardly any resemblance with fragments of either crystalline gold or an icosahedron. Nevertheless, the structures did show some regular patterns like the building up of atomic shells for clusters larger than around 20 atoms.

In total, we hope to have demonstrated that the properties of gold clusters are surprising and that they can only be understood in details if incorporating explicitly electronic effects. Whether also an accurate description of relativistic effects is necessary, we will leave as an open question.

ACKNOWLEDGMENTS

This work was supported by the SFB 277 at the University of Saarland. The authors are very grateful to the Fonds der Chemischen Industrie for generous support.

REFERENCES

- ¹ F. Baletto and R. Ferrando, *Rev. Mod. Phys.* **77**, 371 (2005).

- ² B. Yoon, H. Häkkinen, U. Landman, A. S. Wörz, J.-M. Antonietti, S. Abbet, K. Judai, and U. Heiz. *Science*. **307**, 403 (2005).
- ³ J. Guzman and B. C. Gates. *J. Am. Chem. Soc.* **126**, 2672 (2004).
- ⁴ A. Sachenz, S. Abbet, U. Heiz, W. D. Schneider, H. Häkkinen, R. N. Barneet, and U. Landman. *J. Phys. Chem. A*. **103**, 9573 (1999).
- ⁵ H. Häkkinen, B. Yoon, U. Landman, X. Li, H.-J. Zhai, and L.-S. Wang, *J. Phys. Chem. A* **107**, 6168 (2003).
- ⁶ S. Gilb, P. Weis, F. Furche, R. Ahlrichs, and M. M. Kappes, *J. Chem. Phys* **116**, 4094 (2002).
- ⁷ M. Neumaier, F. Weigend, O. Hampe, and M. M. Kappes, *J. Chem. Phys.* **122**, 104702 (2005).
- ⁸ G. Bravo-Pérez, I. L. Garzón, and O. Novaro, *J. Mol. Struc. (Theochem)* **493**, 225 (1999).
- ⁹ H. Grönbeck and W. Andreoni, *Chem. Phys.* **262**, 1 (2000).
- ¹⁰ H. Häkkinen and U. Landman, *Phys. Rev. B* **62**, 2287 (2000).
- ¹¹ J. Wang, G. Wang, and J. Zhao, *Phys. Rev. B* **66**, 035418 (2002).
- ¹² A. V. Walker, *J. Chem. Phys.* **122**, 094310 (2005).
- ¹³ F. Remacle and E. S. Kryachko, *J. Chem. Phys.* **122**, 044304 (2005).
- ¹⁴ J. P. K. Doye and D. J. Wales, *New J. Chem.* **22**, 733 (1998).
- ¹⁵ N. T. Wilson and R. L. Johnston, *Eur. Phys. J. D* **12**, 161 (2000).
- ¹⁶ W. Fa, C. Luo, and J. Dong, *Phys. Rev. B* **72**, 205428 (2005).
- ¹⁷ H. Häkkinen, M. Moseler, O. Kostko, N. Morgner, M. A. Hoffmann, and B. v. Issendorff, *Phys. Rev. Lett.* **93**, 093401 (2004).
- ¹⁸ L. Xiao, B. Tollberg, X. Hu, and L. Wang, *J. Chem. Phys.* **124**, 114309 (2006).
- ¹⁹ D. Alamanova, Y. Dong, H. u. Rehman, M. Springborg, and V. G. Grigoryan, *Comp. Lett.* **1**, 319 (2005).
- ²⁰ D. Alamanova, V. G. Grigoryan, and M. Springborg, *Z. Phys. Chem.* **220**, 811 (2006).
- ²¹ D. Porezag, Th. Frauenheim, Th. Köhler, G. Seifert, and R. Kaschner, *Phys. Rev. B* **51**, 12947 (1995).
- ²² G. Seifert and R. Schmidt, *New J. Chem.* **16**, 1145 (1992).

- ²³ G. Seifert, D. Porezag, and Th. Frauenheim, *Int. J. Quant. Chem.* **58**, 185 (1996).
- ²⁴ C. Kittel, *Introduction to Solid State Physics* (John Wiley & Sons, New York, 1976).
- ²⁵ Y. Dong and M. Springborg, in *Proceedings of 3rd International Conference "Computational Modeling and Simulation of Materials"*, P. Vincenzini and F. Zerbetto, Eds., (Techna Group Publishers, Faenza, Italy, 2004) 167.
- ²⁶ Y. Dong, M. Burkhardt, M. Veith, and M. Springborg, *J. Phys. Chem. B* **109**, 22820 (2005).
- ²⁷ J. H. Holland, *Adaption in Natural Algorithms and Artificial systems* (University of Michigan Press, Ann Arbor, USA, 1975).
- ²⁸ D. E. Goldberg, *Genetic Algorithms in Search, Optimization and Machine Learning* (Addison-Wesley, Reading, USA, 1989).
- ²⁹ Y. Dong and M. Springborg, *Adv. Comp. Methods Sci. Eng.* (in press).
- ³⁰ Y. Dong and M. Springborg, *Eur. Phys. J. D* (submitted).
- ³¹ P. Koskinen, H. Häkkinen, G. Seifert, S. Sanna, Th. Frauenheim, and M. Moseler, *New J. Phys.* **8**, 9 (2006).
- ³² J. Li, X. Li, H.-J. Zhai, and L.-S. Wang, *Science* **299**, 864 (2003).
- ³³ S. Bulusu, X. Li, L.-S. Wang, and X. C. Zeng, *Proc. Natl. Acad. Sci.* **103**, 8326 (2006).
- ³⁴ X. Gu, M. Ji, S. H. Wei, and X. G. Gong, *Phys. Rev. B* **70**, 205401 (2004).
- ³⁵ V. G. Grigoryan and M. Springborg, *Phys. Rev. B* **70**, 205415 (2004).
- ³⁶ V. G. Grigoryan, D. Alamanova, and M. Springborg, *Phys. Rev. B* **73**, 115415 (2006).
- ³⁷ D. Faken and H. Jonsson, *Comp. Mat. Sci.* **2**, 279 (1994).

TABLE I: Point groups (PG) of the optimized Au_N clusters from the DFTB calculations as function of *N*.

<i>N</i>	PG	<i>N</i>	PG	<i>N</i>	PG	<i>N</i>	PG	<i>N</i>	PG	<i>N</i>	PG	<i>N</i>	PG	<i>N</i>	PG
3	<i>C</i> _{2v}	10	<i>C</i> _{4d}	17	<i>C</i> ₁	24	<i>C</i> ₁	31	<i>C</i> ₁	38	<i>C</i> ₁	45	<i>C</i> ₁	52	<i>C</i> ₁
4	<i>D</i> _{2h}	11	<i>C</i> _{2v}	18	<i>C</i> _{5v}	25	<i>C</i> ₁	32	<i>C</i> ₁	39	<i>C</i> ₁	46	<i>C</i> ₁	53	<i>C</i> ₁
5	<i>C</i> _s	12	<i>C</i> _{5v}	19	<i>D</i> _{5h}	26	<i>C</i> ₁	33	<i>D</i> ₂	40	<i>C</i> ₁	47	<i>C</i> ₁	54	<i>C</i> ₁
6	<i>D</i> _{3d}	13	<i>D</i> _{2h}	20	<i>C</i> _{2v}	27	<i>C</i> ₁	34	<i>C</i> ₁	41	<i>C</i> ₁	48	<i>C</i> ₁	55	<i>C</i> ₁
7	<i>D</i> _{5h}	14	<i>C</i> ₂	21	<i>C</i> ₁	28	<i>C</i> ₁	35	<i>C</i> ₁	42	<i>C</i> ₁	49	<i>C</i> ₁	56	<i>C</i> ₁
8	<i>D</i> _{2d}	15	<i>D</i> _{2d}	22	<i>C</i> ₁	29	<i>C</i> ₁	36	<i>C</i> ₁	43	<i>C</i> ₁	50	<i>C</i> ₁	57	<i>C</i> ₁
9	<i>C</i> _{2v}	16	<i>D</i> ₂	23	<i>C</i> ₁	30	<i>C</i> ₁	37	<i>C</i> ₁	44	<i>C</i> ₁	51	<i>C</i> ₁	58	<i>C</i> ₁

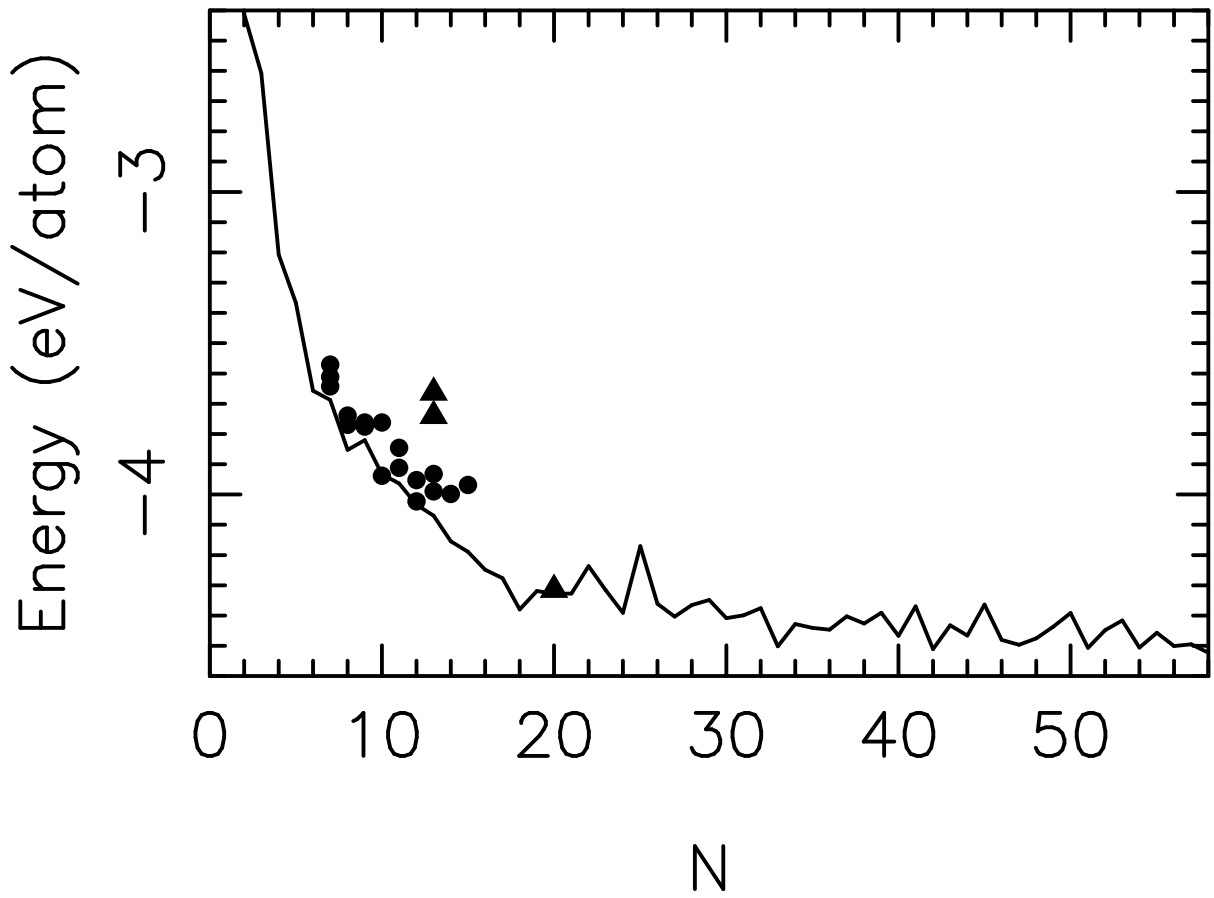


FIG. 1: The variation in the total energy per atom (relative to that of the isolated atom) for the optimized Au_N clusters (solid curve) together with those of planar structures (dark circles) and those of icosahedral Au_{13} and tetragonal Au_{20} clusters (dark triangles).

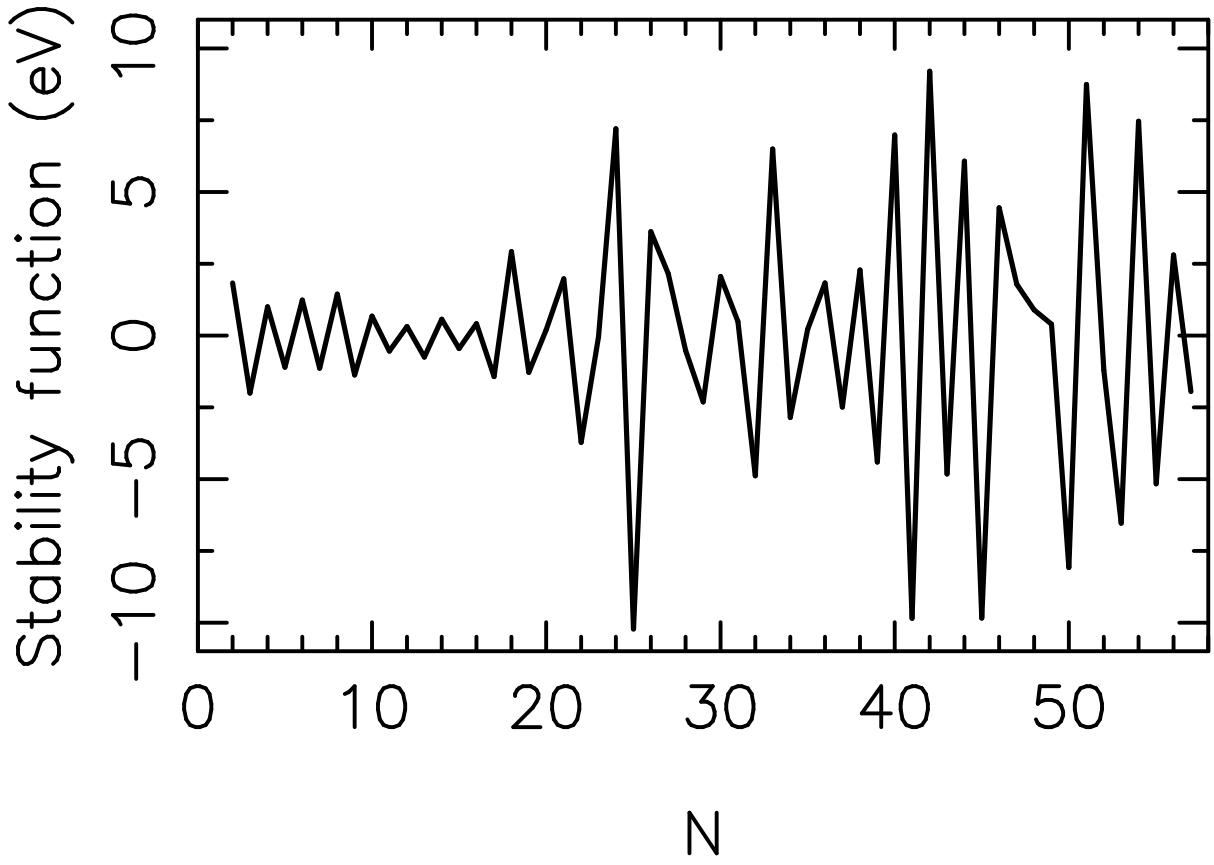


FIG. 2: The stability function which has local maxima (minima) for particularly (un)stable structures.

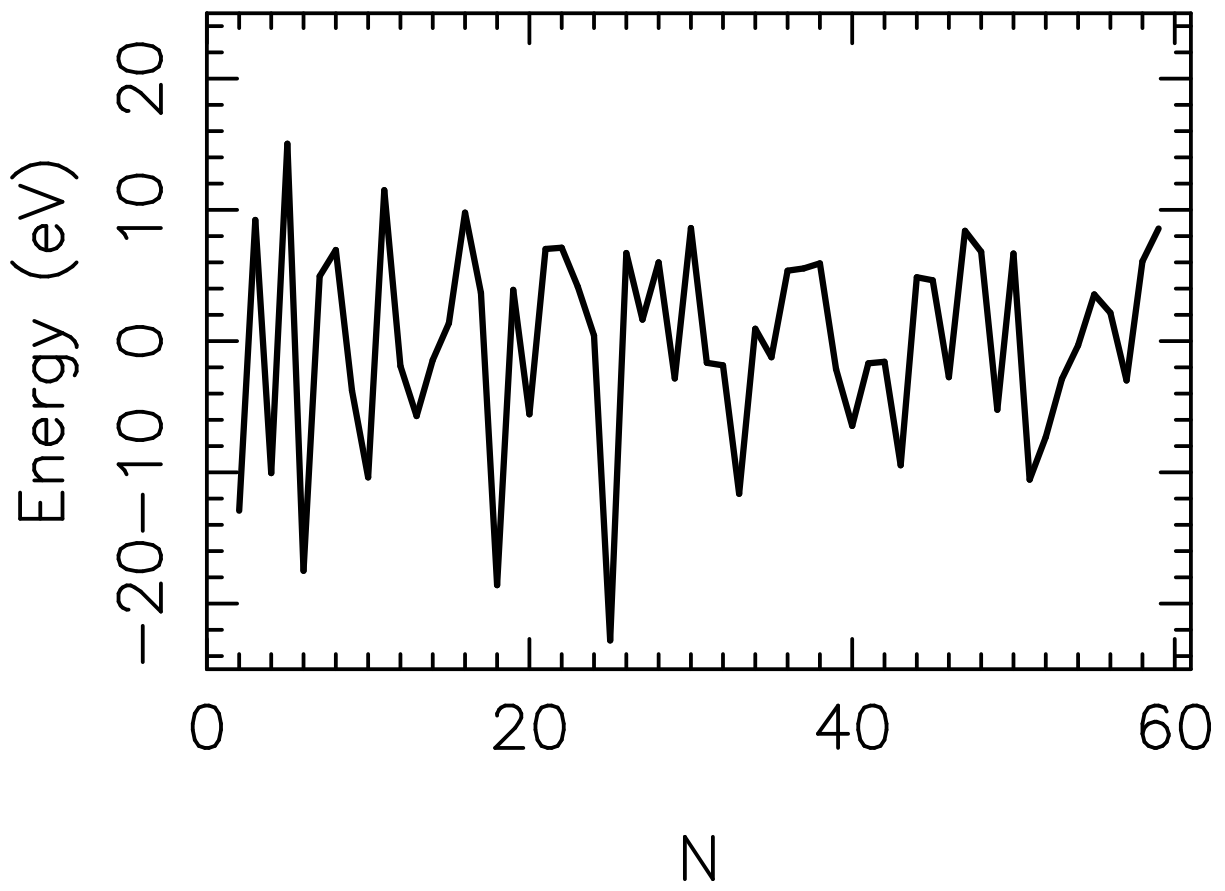


FIG. 3: As Fig. 2, but for the jellium model.

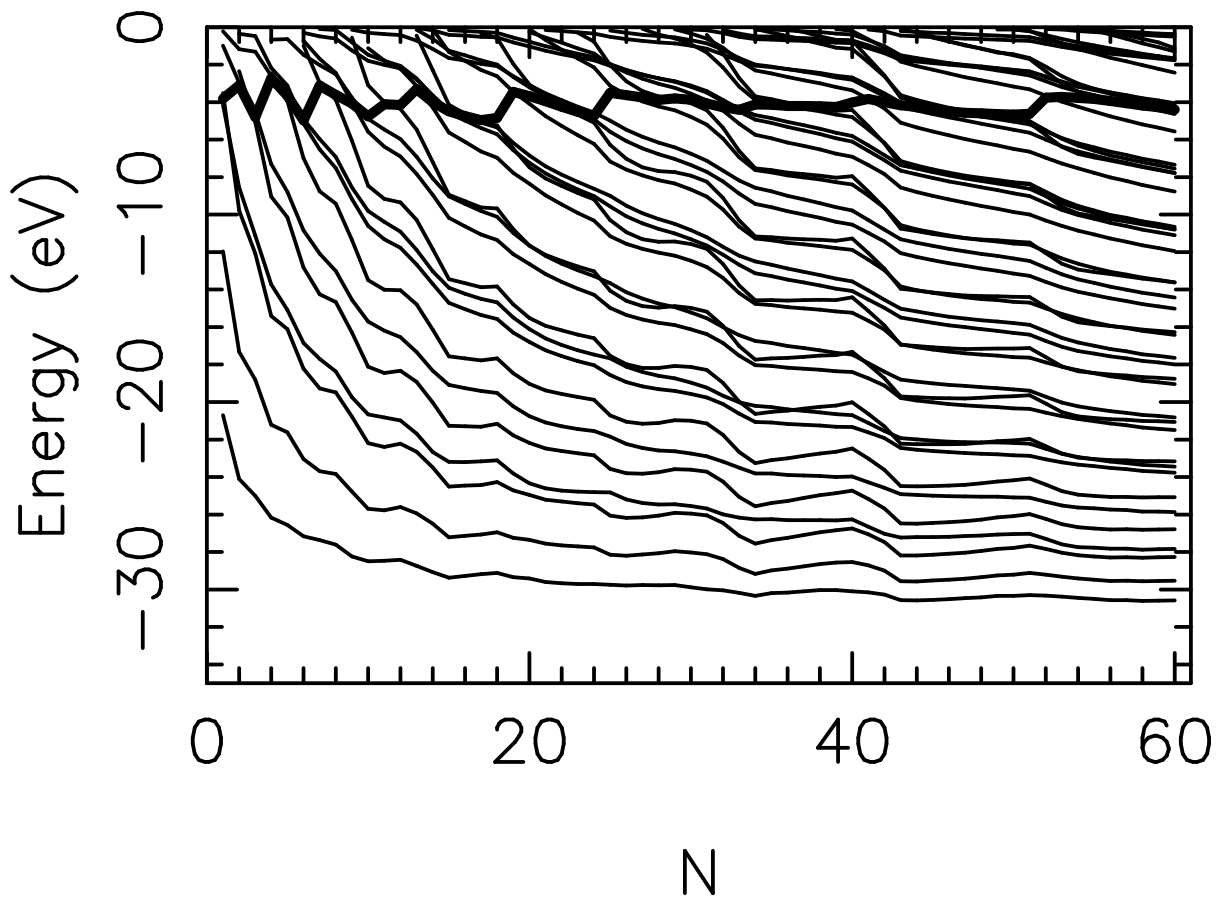


FIG. 4: The orbital energies as a function of cluster size from the jellium calculations. The thicker curve shows the energy of the highest occupied orbital.

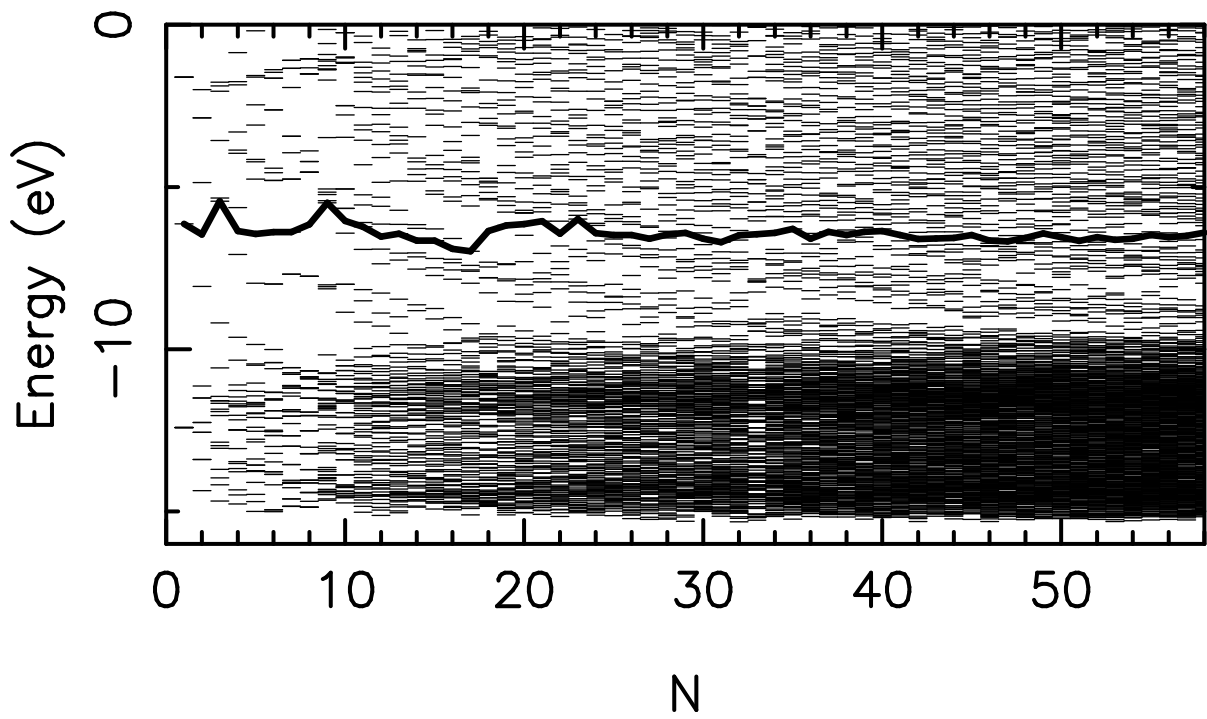


FIG. 5: As Fig. 4 but from the DFTB calculations.

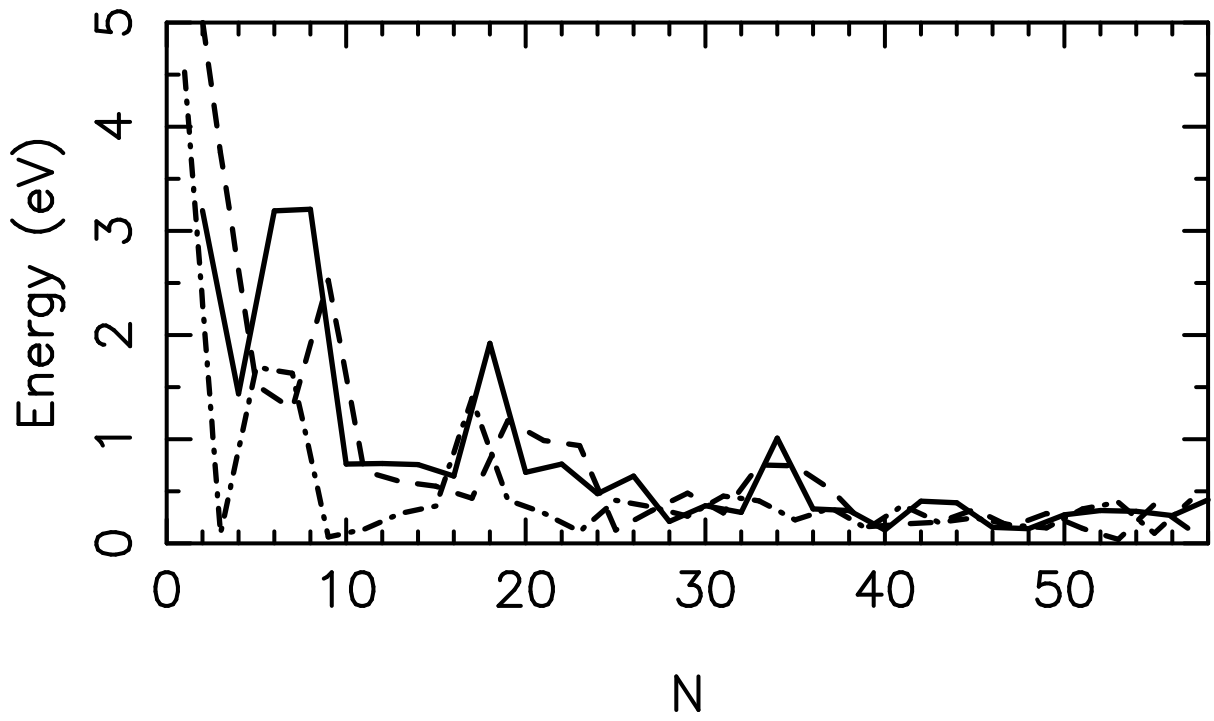


FIG. 6: The three energy gaps, E_g (solid curve) for even N as well as $E_{g,1}$ (dashed curve) and $E_{g,2}$ (dash-dotted curve) for odd N , as a function of N .

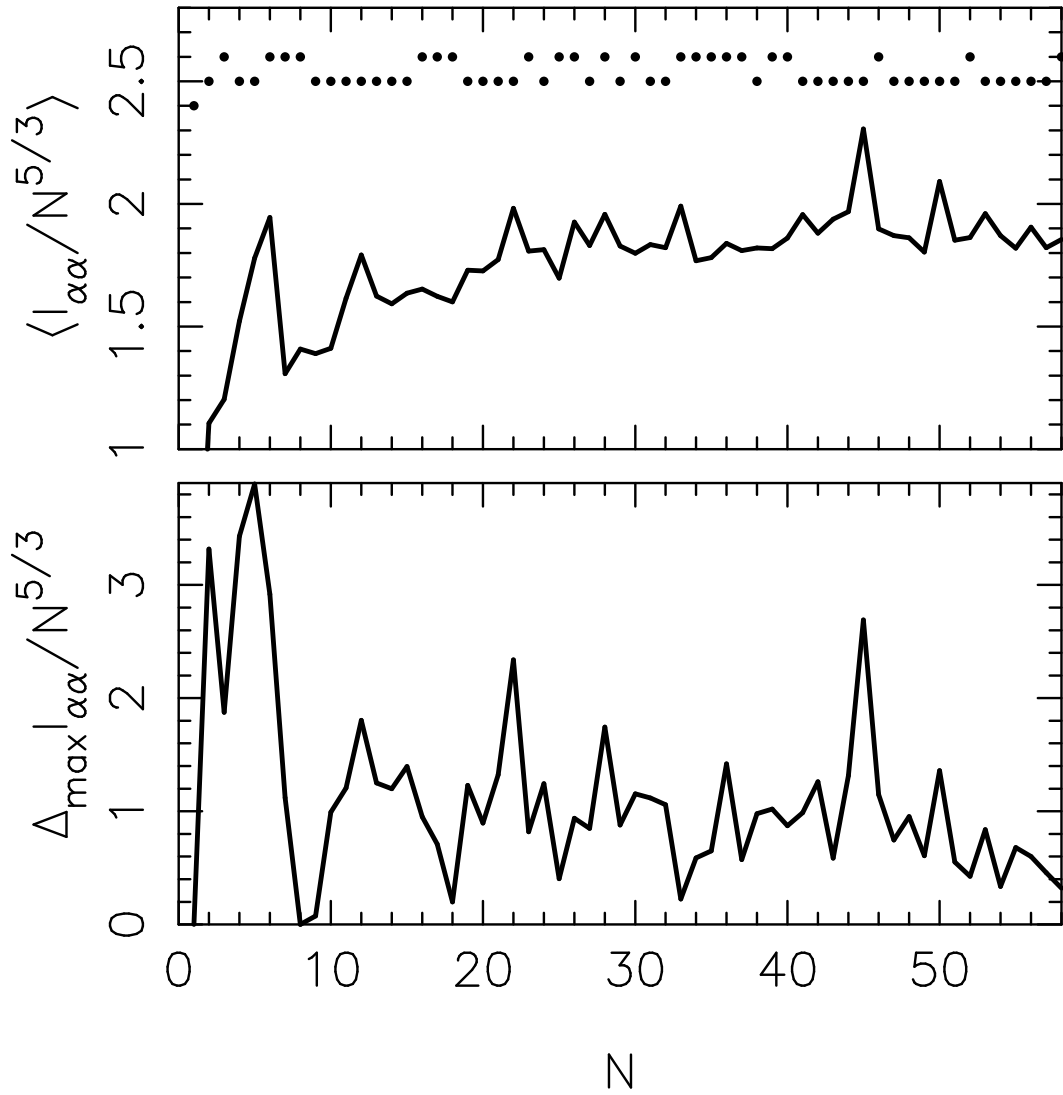


FIG. 7: Properties related to the eigenvalues $I_{\alpha\alpha}$ of the matrix containing the moments of inertia. The upper panel shows the average value (scaled by $N^{5/3}$) together with marks indicating whether the Au_N cluster is overall spherical (dots in the lowest row), overall cigar-like shape (middle row) or overall lens-like shape (upper row). The lower panel shows the largest difference in the eigenvalues.

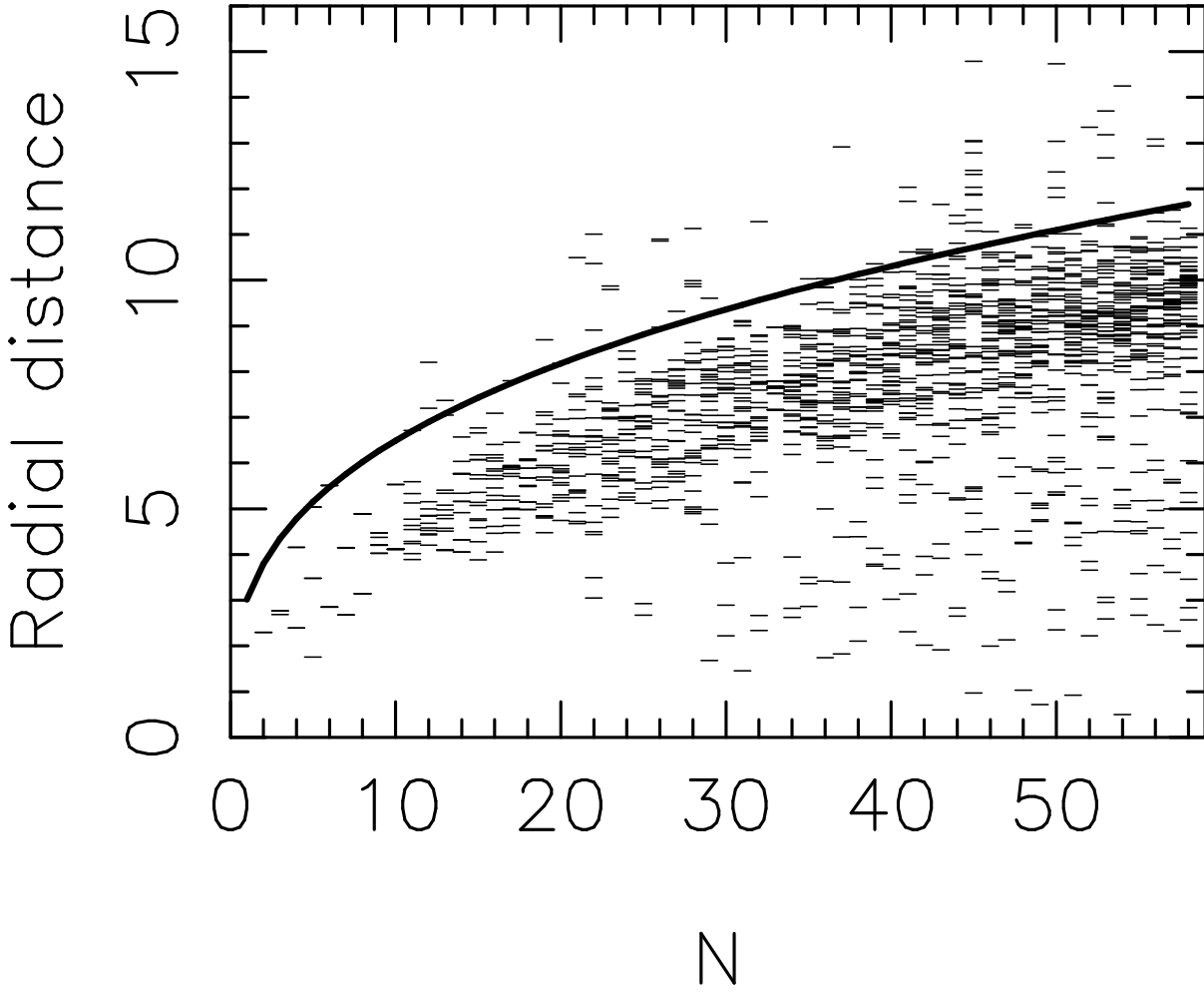


FIG. 8: The radial distances as a function of cluster size, i.e., each small line represents (at least) one atom with that radial distance. The curve shows the radius of the spherical jellium with a density as in the crystal.

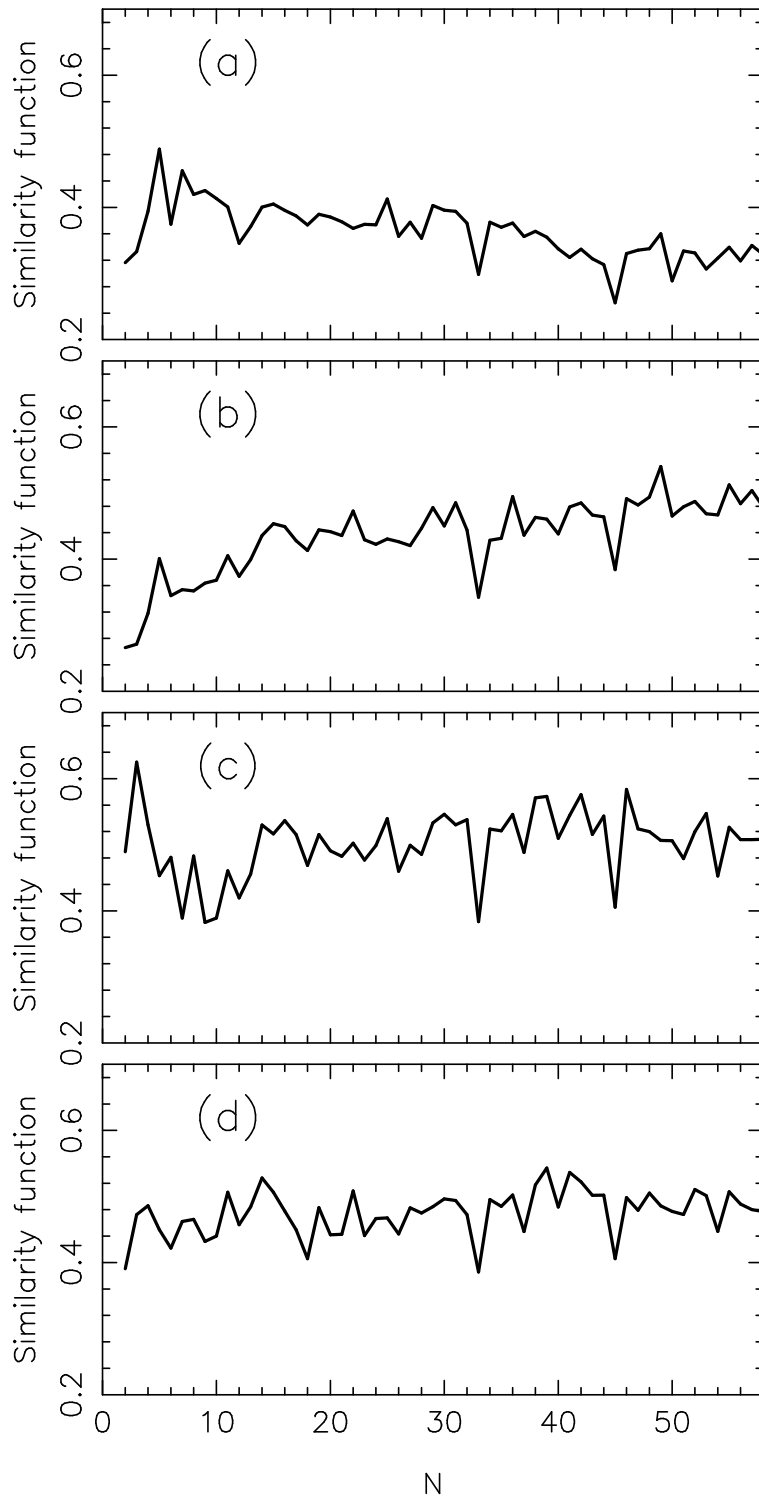


FIG. 9: Each panel shows the similarity function for the Au_N clusters when comparing with (a) an icosahedral cluster, and (b–d) a spherical fragment of the fcc crystal when the center of the fragment is placed at (b) the position of an atom, (c) the middle of a nearest-neighbor bond, and (d) the center of the cube, respectively.

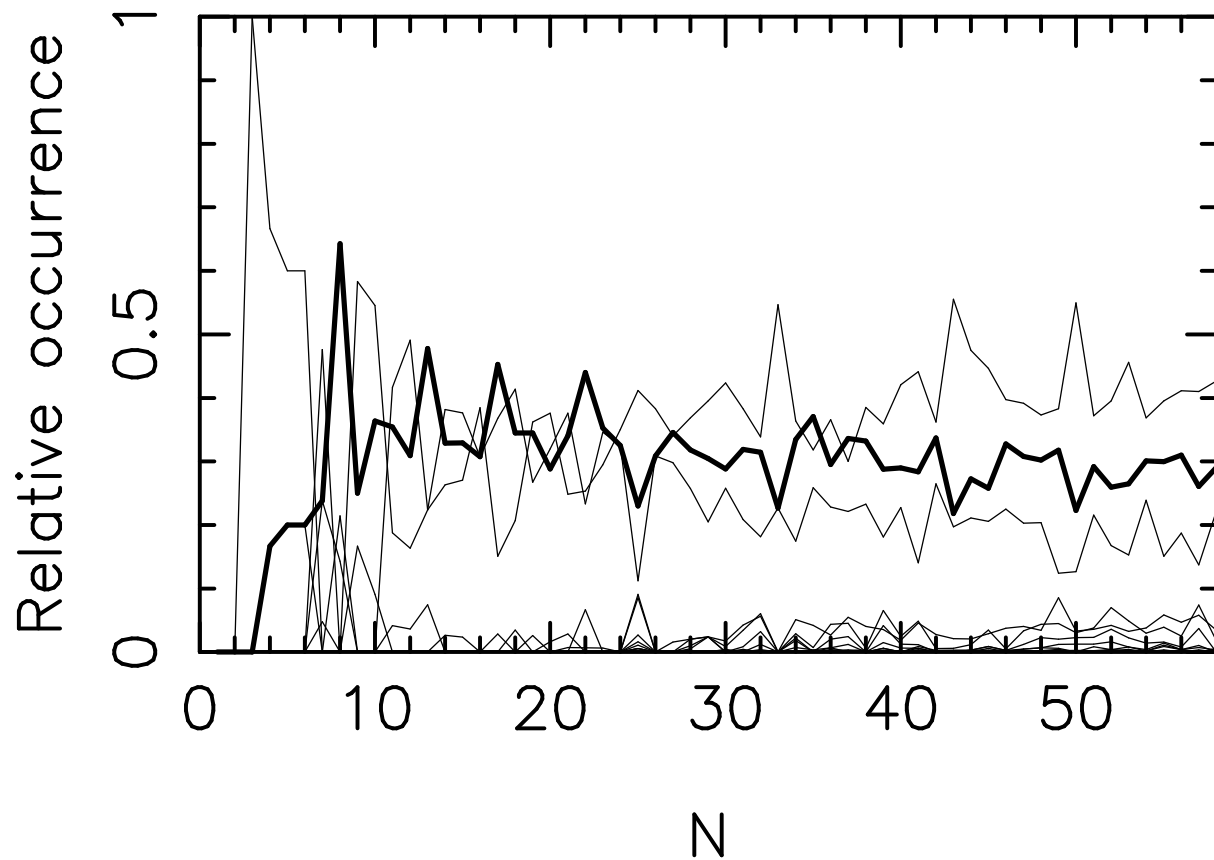


FIG. 10: Results of a common-neighbor analysis. Each curve shows the relative occurrence of a certain set of indices (i, j, k) (described in the text), when excluding $(i, j, k) = (0, 0, 0)$, and the two thicker curves show the occurrence for $(i, j, k) = (2, 1, 1)$. $(i, j, k) = (4, 1, 1)$ and $(i, j, k) = (4, 4, 4)$ are not found in this size range.

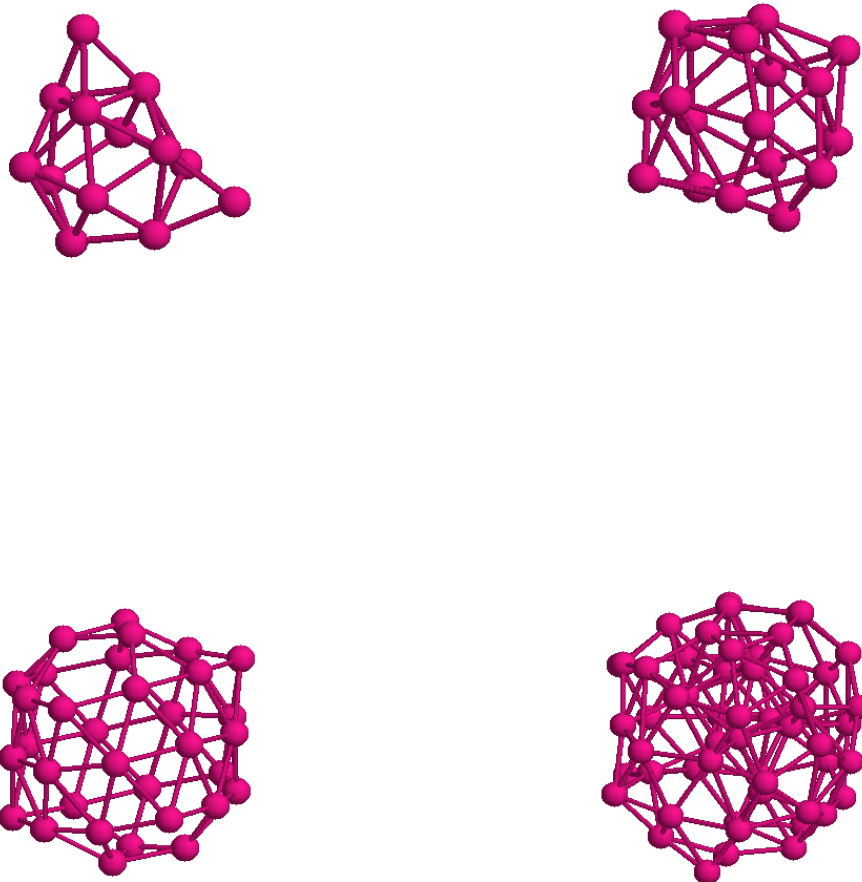


FIG. 11: The optimized structure of Au_N clusters with $N = 13$ (top, left), $N = 18$ (top, right), $N = 33$ (bottom, left), and $N = 55$ (bottom, right).

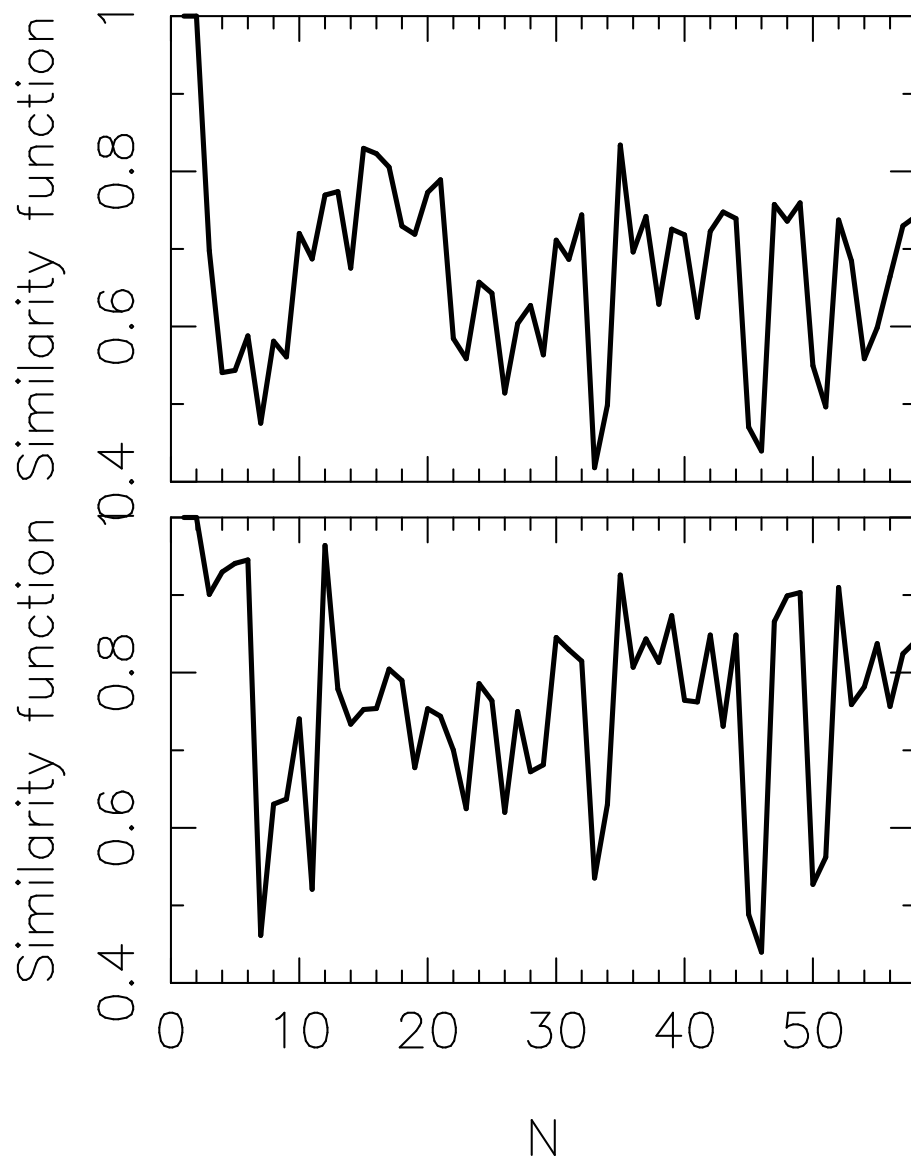


FIG. 12: The similarity function quantifying whether the structure of a cluster with N atoms resembles that of the cluster with $N - 1$ atoms plus one atom. In the upper panel the radial distances, and in the lower panel the interatomic distances have been used in quantifying the similarity.

